REACTIVITY CONTROL OF A PWR 19X19 URANIUM SILICIDE FUEL ASSEMBLY

A Thesis
Presented to
The Academic Faculty

by

Joseph Raymond Burns

In Partial Fulfillment
of the Requirements for the Degree
Masters of Science in the
School of Mechanical Engineering, Nuclear Engineering Program

Georgia Institute of Technology
August 2015

REACTIVITY CONTROL OF A PWR 19X19

URANIUM SILICIDE FUEL ASSEMBLY

Approved by:

Dr. Bojan Petrovic, Advisor
School of Mechanical Engineering,
Nuclear Engineering Program
Georgia Institute of Technology

Dr. Weston Stacey
School of Mechanical Engineering,
Nuclear Engineering Program
Georgia Institute of Technology

Dr. Paolo Ferroni
Westinghouse Electric Company

Date Approved: 7/23/2015

To my parents, Ray Burns and Carol Bruce.

ACKNOWLEDGEMENTS

I must first give sincere thanks to my advisor, Dr. Bojan Petrovic. I have been working with Dr. Petrovic since my undergraduate studies at Georgia Tech, and his guidance and support have taught me a tremendous amount. I would also like to thank the rest of my reading committee. I have had the pleasure of working with Dr. Weston Stacey, whose kindness and support I greatly appreciate. Dr. Paolo Ferroni has provided valuable commentary from the industry viewpoint, and his assistance with this project is greatly appreciated as well. I would not be where I am today without all of the wonderful teachers I have had throughout my education, so I would like to express my appreciation to the entirety of the Nuclear Engineering faculty and staff at Georgia Tech.

I also wish to express my appreciation to my fellow students in the Nuclear Engineering department for their friendship and encouragement. I am deeply grateful to the Davy family as well for taking me in as one of their own, and showing me all of their love and support during my time in Atlanta. As for my own family, I wish to first remember my uncle, the late Danny Bruce. Each year around Thanksgiving when classes were out, it was too far for me to travel home, but my uncle was always more than happy to take me in for some family time. Finally I give thanks from the bottom of my heart to my parents for their unending love and support. My father, Ray Burns, who is my biggest fan, has always been there for encouragement when I was stressed. And last but by no means least, my mother, Carol Bruce, without whom I never would have achieved all that I have. Whenever I've felt overwhelmed by my work, I've always reminded myself of what Mom always told me: "You can do hard things."

This research was performed using funding received from the DOE Office of Nuclear Energy's Nuclear Energy University Programs.

TABLE OF CONTENTS

LIST OF TABLES

LIST OF FIGURES

1. INTRODUCTION

1.1. Problem Definition

In the midst of growing concern over climate change and recent changes to energy policy in the United States, many vendors of advanced nuclear reactors have boosted their licensing efforts over the past several years with the intent of commercial deployment. The Department of Energy (DOE) has provided considerable financial support for the development of small modular reactor (SMR) designs, which promise enhanced safety performance due to integral reactor vessel design and passive safety systems. However, such designs have come under criticism with respect to various uncertainties; one factor which has seemed to particularly decelerate public reception of SMRs is uncertainty regarding the economic competitiveness of these untested, first-of-a-kind designs. The concept of the Integral Inherently Safe Light Water Reactor, or I^2S-LWR, was born from the objective of applying safety-promoting design features found in SMRs to a large pressurized water reactor (PWR) of 1000 MWe, thereby providing an option for a passively safe LWR to markets which would find greater economic benefit in a large reactor.

Pushing the compact core of an integral reactor to a thermal power of 3000 MW necessitates novel design features to allow achievement of a power density that is considerably higher than that of traditional PWRs (16). Several design innovations impact the neutronic behavior of the I^2S-LWR core, chief among them a 19x19 fuel lattice with uranium silicide (U_3Si_2) fuel. Such design features demand a thorough investigation of reactivity control options, including control rods and integral burnable absorbers (BAs). The goal of the present research is therefore to develop feasible I^2S-LWR fuel assembly design options with optimized or near-optimized reactivity control by exploring combinations of various rod cluster control assembly (RCCA) layouts, control rod absorber materials, BA types, BA concentrations, and BA layouts.

Viable fuel assembly designs must provide satisfactory reactivity hold-down, power peaking, and cycle length while meeting constraints on core safety (i.e. moderator temperature coefficient, or MTC) and fuel performance (i.e. fuel rod internal pressure, or RIP). Key characteristics of common multi-objective optimization algorithms shall be followed at a high level in order to guide the progression of design iterations in a logical and organized manner, and lattice physics calculations shall be carried out to assess of the quality of each design iteration. Optimized fuel assembly designs which are produced in this process may then later be used for core loading pattern (LP) design.

The design space for this problem is summarized in Table 1-1. RCCA configuration options will be considered for 24, 28, and 32 control rod guide tubes per assembly so that an anticipated increase in the required control rod reactivity worth (due to under-moderation of the unique I^2S-LWR fuel assembly base design) may be adequately assessed. The geometry of these layouts will be developed so as to maintain octant symmetry within the fuel assembly and to provide optimal rod worth and shutdown margin. The control rod absorber materials to be considered are silver-indium-cadmium (AIC), boron carbide (B_4C), and hafnium (Hf); operational experience is available for each of these. The BA design options are gadolinia (Gd_2O_3) and Westinghouse's Integral Fuel Burnable Absorber (IFBA). Both of these BA types may be implemented with varying amounts of the primary absorbing isotopes to allow for local control of the neutron absorption rate. The concentration and placement of the BAs in an assembly may be chosen to yield a desired reactivity offset and intra-assembly power shape, so that several locally-optimized fuel assembly designs with differing reactivity characteristics can be developed to provide sufficient flexibility in fresh fuel options for the core LP design task.

Table 1-1. Design Space

Design Variable	Options
Enrichment	4.95 w/o ^{235}U
RCCA layout	24, 28, 32 guide tubes per assembly
Control rod absorber material	AIC, B_4C, Hf
BA type	Gd_2O_3, IFBA
BA concentration	Gd_2O_3: 4 and 8 w/o; IFBA: 2.5 mg/in ^{10}B
BA layout	Gd2O3: 8 and 16 poisoned rods per assembly; IFBA: 80 and 160 poisoned rods per assembly

The constraints for the fuel assembly design problem are summarized in Table 1-2. For the RCCA design task, the reactivity worth of each RCCA configuration shall be compared to a reference case which consists of a standard 17x17 UO_2-fuelled assembly with 24 AIC control rods, thus approximating existing Westinghouse-type PWR assembly designs currently in operation. The RCCA design should provide reactivity worth that is at least equal to that of this reference case. Although multiple fuel assembly designs with various reactivity characteristics will be developed, reactivity hold-down is included as a constraint because the BA loading of any practical design must allow a sufficiently low soluble boron concentration to keep the core MTC negative. Previous fuel cycle analyses carried out by Westinghouse have indicated economically feasible cycle lengths of 12 and 18 months (8); RCCA and BA designs should therefore yield fuel assembly design options with cycle lengths of at least 12 months, but designs with at least 18-month lifetimes must be realized as well. The cycle length achievable with a given fuel assembly design is heavily dependent on how completely the BAs are depleted. Incomplete BA depletion yields a residual reactivity penalty later in the cycle, thereby reducing cycle length. This reactivity penalty will therefore be assessed for each design iteration. Finally, the RIP limit guards against clad ballooning and other modes of fuel failure, which can obstruct coolant flow and challenge thermal safety margins. This limit may be challenged if excessive

helium is released by $^{10}B(n,\alpha)^{7}Li$ reactions in IFBA-poisoned lattices. A detailed analysis of the determination of this RIP limit and its implications is given in Appendix D.

Table 1-2. Constraints

Variable	Requirements
Control rod worth	Greater than or equal to that of reference case
Reactivity hold-down	Sufficiently negative MTC
Cycle length	At least 12 months; 18 months must be achievable as well
RIP	< 36.2 MPa

Assessment of the fuel assembly neutronic performance is carried out using the T-NEWT and T-DEPL sequences in the SCALE code suite. For each design iteration, two-dimensional models of the I^2S-LWR fuel assembly in $1/4^{th}$ geometry are built with reflective boundary conditions imposed on all edges, thereby approximating an infinite lattice in all three spatial dimensions; a layout of a sample fuel assembly model is given in Figure 1-1. Following the transport and depletion calculations for each assembly design, relevant performance parameters are extracted from the SCALE output and passed into a post-processing code. The static control rod reactivity worth is used as the key metric for RCCA design assessment; BA design evaluation requires several metrics, including reactivity hold-down, power peaking, poison depletion, cycle length, soluble boron reactivity worth, and MTC. The methodology employed throughout the RCCA and BA design process is discussed in greater detail in Chapter 3.

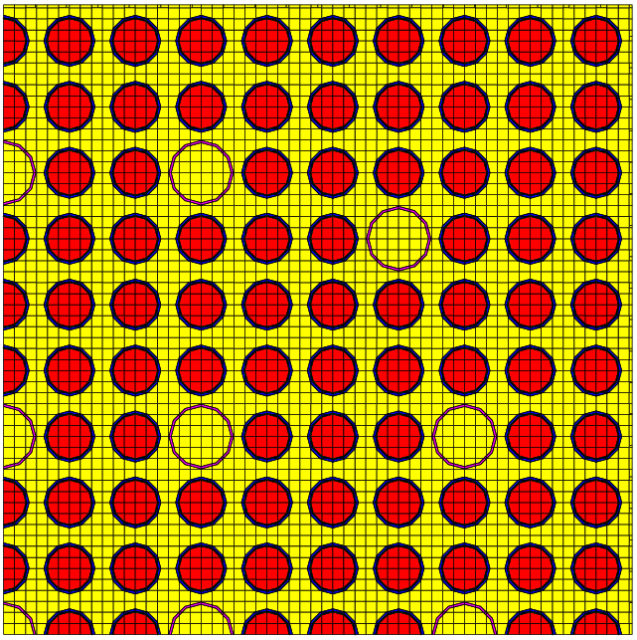

Figure 1-1. Sample Fuel Assembly Model

1.2. Overview of the I^{2}S-LWR

The I^{2}S-LWR design development effort is a DOE Nuclear Energy University Programs (NEUP) Integrated Research Project (IRP) led by Georgia Tech, in collaboration with the University of Michigan, Virginia Tech, the University of Tennessee, the University of Idaho, Florida Tech, Morehouse College, Brigham Young University, Idaho National Laboratory, Southern Nuclear, Westinghouse, the University of Zagreb, the University of Cambridge, and Politecnico di Milano. Realization of the core design goal of high power density presents several design challenges that require innovative solutions.

A two-dimensional view of the I^{2}S-LWR core and primary circuit components is reproduced from (18) in Figure 1-2. The core consists of 121 fuel assemblies with an active height of 12 ft, which is the same as the active height of many other Westinghouse-type PWRs. The space between the core barrel and the inner vessel wall is occupied by several primary heat exchanger and decay heat exchanger units. The primary heat exchanger design chosen is a micro-channel heat exchanger which enables a high volumetric heat transfer rate from the

primary side to the secondary side. The fuel assemblies themselves take on a 19x19 square lattice with reduced fuel rod dimensions (relative to a standard 17x17 Westinghouse-type fuel assembly), thereby providing increased heat transfer surface area to remain well within thermal safety margins (16).

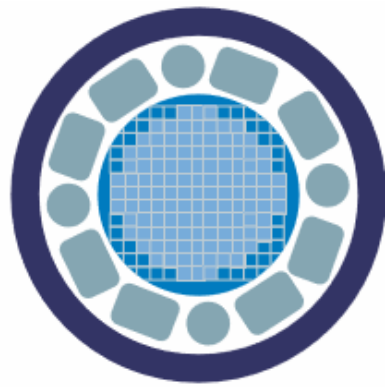

Figure 1-2. I^2S-LWR Vessel Layout (18)

The choice of fuel form and cladding for the I^2S-LWR has not yet been finalized. Studies have indicated that traditional uranium oxide (UO_2) fuel with Zircaloy cladding performs satisfactorily in the high power density core (8). These findings, in conjunction with the wide operational experience basis and current ubiquitous use of UO_2 fuel, make oxide fuel an attractive option for the initial deployment of the I^2S-LWR. However, it is envisioned that once the performance and safety of the I^2S-LWR can be demonstrated in operation, the fuel form should be changed to U_3Si_2. Silicide fuel presents a significant improvement in thermal conductivity compared to oxide fuel. In addition to having a higher conductivity at room temperature, silicide fuel becomes more conductive with increasing temperature, while oxide fuel becomes less conductive with increasing temperature until a minimum around 2000 K (5). The unirradiated thermal conductivity trends with temperature for oxide and silicide fuel forms are given in Figure 1-3. In addition to improving thermal conductivity, silicide fuel also has a greater heavy metal density than oxide fuel, thus allowing significant improvements in cycle

length and potential reduction in fuel cycle cost. A drawback to silicide fuel is uncertainty regarding its irradiation swelling behavior. There is some variation in results of U_3Si_2 irradiation experiments, but generally it appears that silicide fuel exhibits greater volumetric swelling than oxide fuel (5). Additional investigation into the swelling of silicide fuel is necessary and should be carried out under conditions comparable to those that would be found in the operation of the I^2S-LWR.

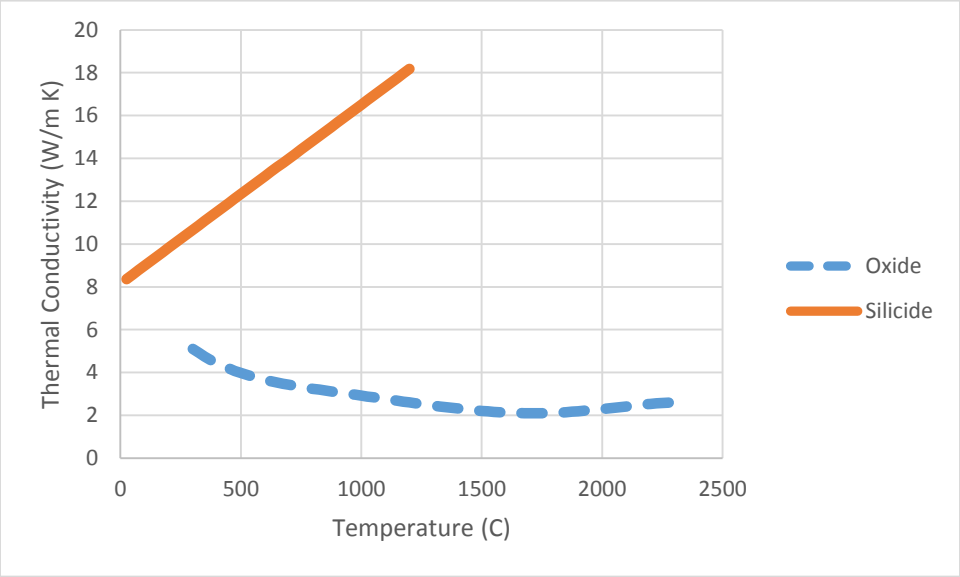

Figure 1-3. Termperature-Dependent Thermal Conductivity of UO_2 and U_3Si_2

Some key design parameters of the I^2S-LWR are compared with those of other typical PWRs in Table 1-3 below.

Table 1-3. Key I^2S-LWR Design Parameters

	I^2S	**Traditional PWR**
Core power density (MW/m^3)	~120	~100
Fuel assembly	19x19	17x17
Fuel material	U_3Si_2	UO_2
Fuel thermal conductivity at 500 °C (W/m K)	15	3.6
Fuel total density (g/cm^3)	12.2	10.97
Fuel heavy metal density (g/cm^3)	11.29	9.67
Clad material	Ferritic steel (FeCrAl)	Zircaloy-4 or ZIRLO©

1.3. Organization

In Chapter 2, some background is provided on the reactivity control requirements set by the Nuclear Regulatory Commission (NRC), and an overview of key characteristics of and operational experience with various control rod and BA designs is presented. Popular optimization methods used in core and fuel assembly design processes are discussed as well.

Chapter 3 details the methodology employed for the design problems to be explored. The SCALE code suite and its use in developing fuel assembly models for neutronics calculations is discussed. The fuel assembly models themselves used for RCCA and BA design are detailed as well, and the modeling nuances specific to each problem are highlighted.

In Chapter 4, the results of the RCCA and BA design calculations are presented; these results are used to select optimal and/or near-optimal designs as detailed in Chapter 5.

Finally, Chapter 6 concludes the thesis and suggests design recommendations based on the calculations and analysis given in Chapters 4 and 5.

2. BACKGROUND

2.1. Licensing Requirements

In Appendix A of 10 Code of Federal Regulations 50 (10 CFR 50), the NRC outlines high-level design requirements, referred to as General Design Criteria (GDCs), which must be met in order for a nuclear reactor design to be licensed in the United States. Those GDCs that are most directly relevant to reactivity control are as follows (7):

- GDC 11 requires the design to be able to offset reactivity insertion events with "prompt nuclear feedback."
- GDC 26 specifies that two independent reactivity control schemes must be used, one of which must use control rods. The control rods must ensure that reactivity changes throughout normal operation do not cause violation of specified acceptable fuel design limits (SAFDLs) within sufficient margin (i.e. accounting for the highest worth control rod being stuck). The second scheme must control reactivity due to normal changes in power during operation such that SAFDLs are not violated. Further, one of these reactivity control schemes alone must be able to maintain the core in a subcritical state under cold conditions.
- GDC 27 requires that the combination of reactivity control systems ensures that the core can be cooled within sufficient margin under postulated accident conditions.
- GDC 28 requires sufficient reactivity control to prevent damage to the reactor coolant pressure boundary and the vessel internals that would compromise the ability to cool the core during reactivity insertion events.

Of the GDCs listed above, only GDC 26 does not apply to transient scenarios. As the present research does not delve into transient analysis, it must be determined in a separate study whether or not the RCCA and BA designs developed here will satisfy the remaining GDCs.

GDC 26 specifies that two independent reactivity control schemes must be used, but operating PWRs generally use a total of three schemes. Control rods are primarily used to adjust the core thermal power during operation and shut down the reactor when necessary. BAs offset initial excess reactivity at the beginning of a cycle (BOC) and are used to shape the core power and flux distributions with the goal of uniformity to maximize fuel utilization. The third method of reactivity control involves addition of boric acid to the coolant, yielding a negative impact on reactivity due to thermal neutron absorption by ^{10}B. As changing the boron concentration in the coolant is a slow process, this method of reactivity control is appropriate for controlling long-term changes in core reactivity due to depletion. For practical purposes, all three reactivity control schemes must be accounted for in considering satisfaction of GDC 26.

The soluble boron concentration has a heavy impact on MTC. In a PWR core with poisoned coolant, an increase in coolant temperature yields two competing reactivity effects. With an increase in temperature, the coolant density decreases, thereby reducing neutron moderation and hardening the neutron energy spectrum, which yields a negative impact on reactivity. The decrease in coolant density also decreases the boron density, which reduces the rate of neutron absorption by the poison; this can yield a net positive impact on reactivity if the boron concentration is sufficiently high. In order to maintain a negative MTC, the soluble boron concentration must therefore be limited. Achieving this requirement necessitates providing sufficient reactivity control without soluble boron; furthermore, as PWRs generally operate at full power with control rods completely withdrawn, this reactivity control must be provided

entirely by BAs. If the BA loading provides sufficient reactivity control to limit the critical boron concentration (CBC) to a level at which the MTC is negative, a reactivity insertion event can be countered by the reactor's inherent feedback to prevent unacceptable increases in fuel temperature. As SAFDLs are typically given with respect to a peak fuel temperature, it can therefore be assumed that SAFDLs will not be violated and GDC 26 is satisfied if a fuel assembly design at a given iteration provides a reactivity offset sufficient to allow a critical boron concentration (CBC) that does not yield a positive MTC. This provides justification of the reactivity control criterion given in Table 1-2.

2.2. Control Rod Design

From the standpoint of reactivity control, control rods must be designed to provide both fine control of the core thermal power and the ability to scram the reactor, thereby setting the requirement of high absorption cross section for the absorber material. However, a control rod with a high concentration of strongly absorbing material may cause large local depressions in the core flux profile when it is inserted into the core, which can yield undesirable local reactivity perturbations. The absorptive species in such a control rod can also be depleted quickly, reducing its effectiveness as it is used. The control rod design optimization task therefore requires consideration of both black and gray absorber materials; the black absorber yields a large negative reactivity worth, and the gray materials are added to prevent rapid depletion and large local flux depressions when the rod is inserted (11). Other phenomena, such as irradiation-induced swelling of the absorber and mechanical considerations, set additional requirements for control rod design that are beyond the scope of the present work.

The candidate control rod absorber materials for the I^2S-LWR include AIC, B_4C, and Hf. AIC control rods are quite popular in PWRs of Western design. The composition of the AIC

absorber is an alloy of 80 percent silver, 15 percent indium, and 5 percent cadmium by weight. AIC control rods are effective due to the thermal absorption cross section of 20600 barns of ^{113}Cd, and inclusion of silver and indium in the absorber material slows the loss of effectiveness due to cadmium depletion and reduces the flux depression upon insertion. Fabrication of AIC control rods is simple as well. B_4C ceramic control rods are also very common in Western reactor designs, and some reactor vendors have developed RCCA designs which use both AIC and B_4C. B_4C rods also benefit from the large absorption cross section of ^{10}B across a wide range of energies, which reduces local flux depression upon insertion, but they must be designed to account for the pressure buildup from helium accumulation due to the $^{10}B(n,\alpha)^7Li$ reaction. The operational experience base for Hf control rods is minimal, as thus far they have primarily been used in German reactors for submarine propulsion. Hf control rods have desirable neutronic and mechanical properties. Hf absorbs neutrons in both the thermal and epithermal energy ranges, thereby reducing local flux depression upon insertion and granting a great deal of longevity without losing absorption effectiveness. However, fabrication of Hf control rods is challenging and expensive (11). Other absorber materials that are being researched for commercial use include dysprosium titanate, hafnium diboride, gadolinia, and europia (19).

The reactivity worth of any of these designs may be varied via enrichment with the primary absorbing isotopes, but additional analyses are necessary to assess the impact of such a design change on the depletion of the rod as well as the magnitude of the local flux depression upon insertion. Table 2-1 below gives the primary absorptive isotopes for each control rod material discussed above, and Figures 2-1 to 2-4 show the energy-dependent reaction cross sections of each of these isotopes. These cross sections are taken from the ENDF/B-VII library (12).

Table 2-1. Control Rod Absorber Primary Absorptive Isotopes

Material	Primary Absorptive Isotopes
AIC	^{113}Cd
B_4C	^{10}B
Hf	^{174}Hf
	^{177}Hf

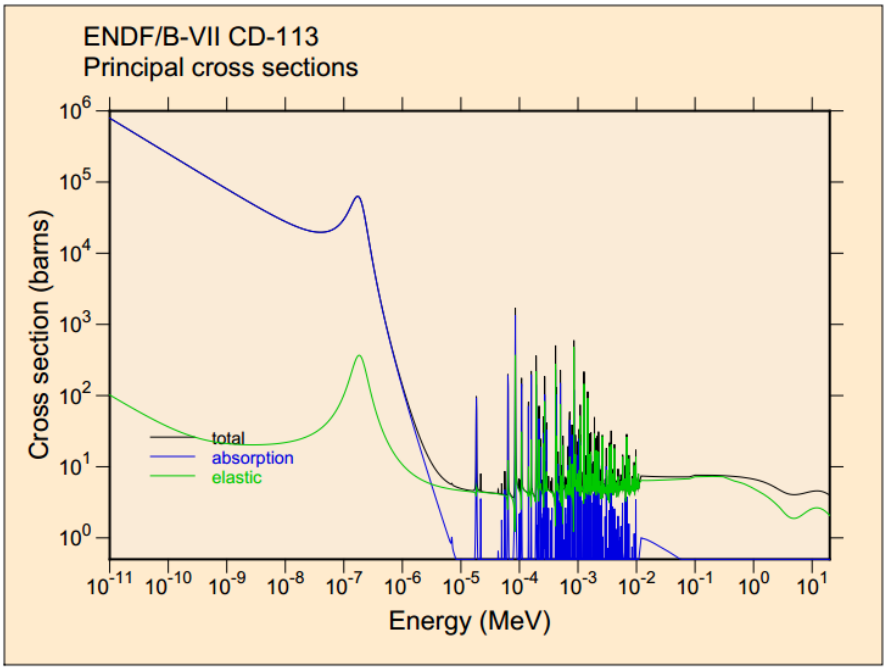

Figure 2-1. ^{113}Cd Cross Sections (12)

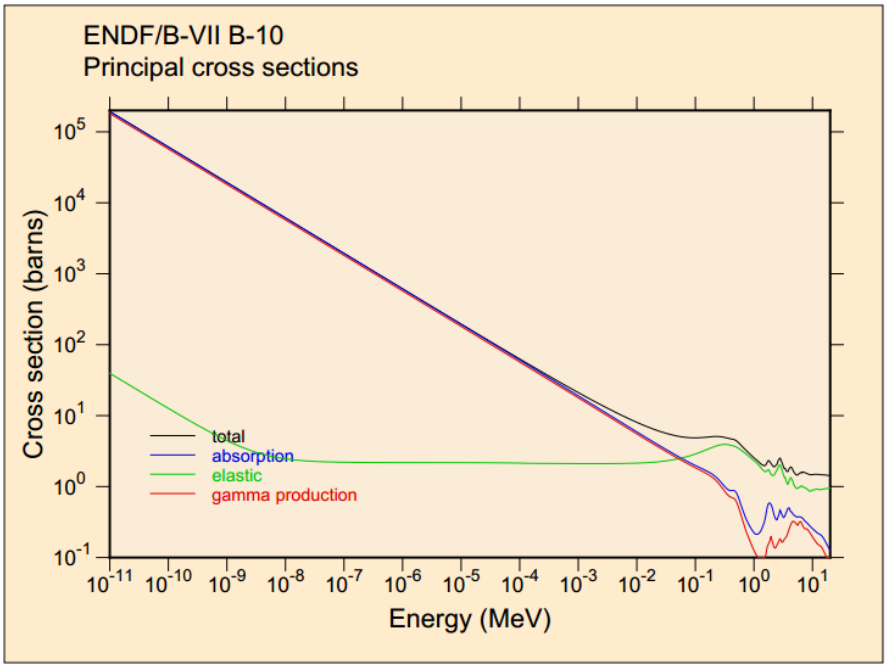

Figure 2-2. ^{10}B Cross Sections (12)

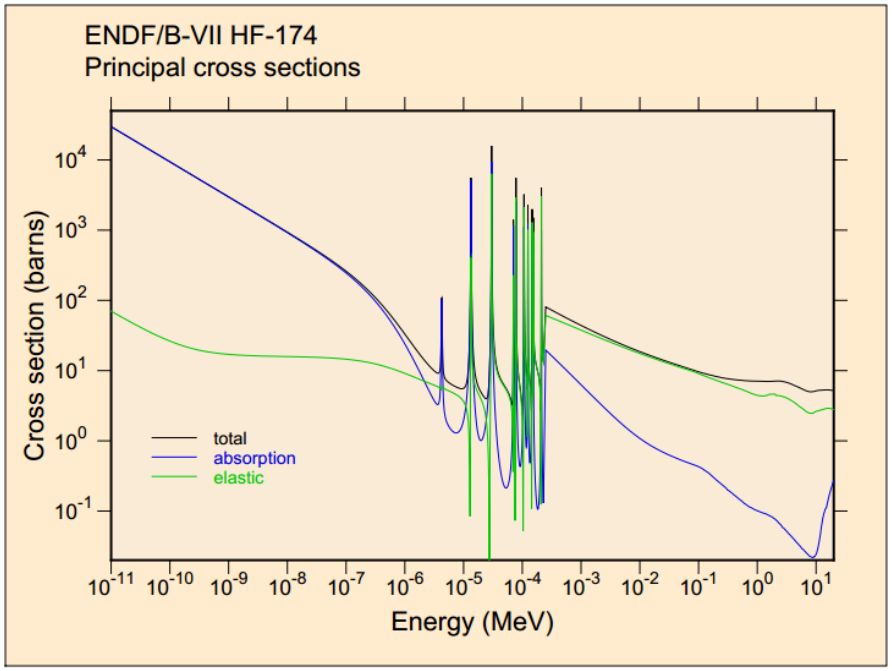

Figure 2-3. ^{174}Hf Cross Sections (12)

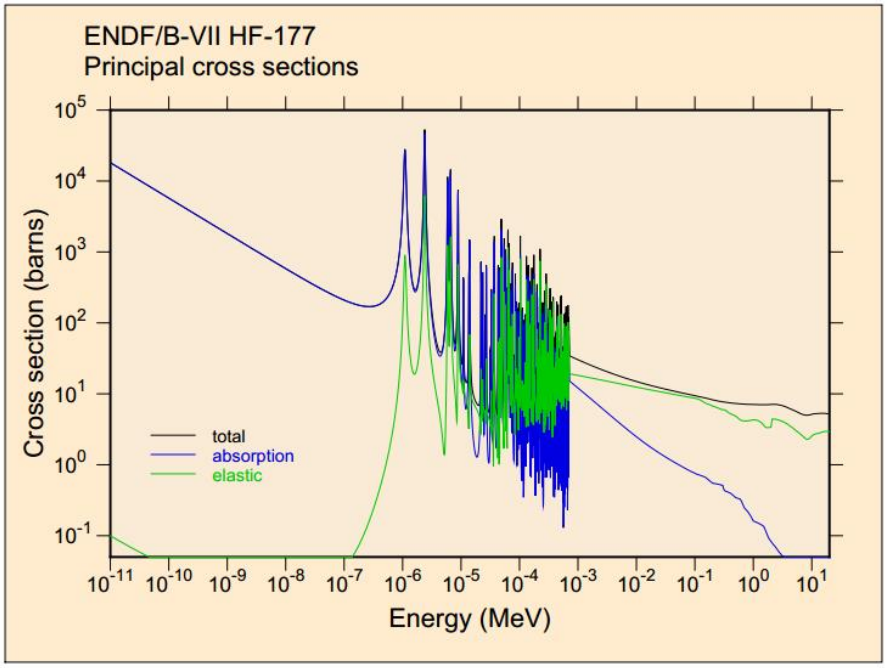

Figure 2-4. ^{177}Hf Cross Sections (12)

Control rod design evaluation requires three-dimensional full-core model analyses, as the reactivity characteristics of a control rod depend very strongly on its location in the core. The RCCAs in a core design are typically grouped into two or more "banks" based on their reactivity characteristics and the symmetry of the core (3). All rods in a particular bank move together. The bank with the largest negative reactivity worth, often referred to as the safety bank, is reserved for scramming the reactor and remains fully withdrawn during normal operation. The other banks, called regulating banks, are used for adjusting the core power production and may be inserted and withdrawn as needed during normal operation and startup. The control rods used to bring the core to full power operation from cold shutdown are called shim rods. Positioning the RCCAs in the core is typically done in a checkerboard-like pattern to maximize control for a limited amount of space available in the upper portion of the reactor vessel for control rod drive mechanisms (CRDMs); this space is especially limited in integral reactor designs such as the I^2S-

LWR. Figure 2-5 shows a sample RCCA arrangement in a small PWR core. Each cell in the figure represents a fuel assembly, and those that are shaded represent RCCA locations.

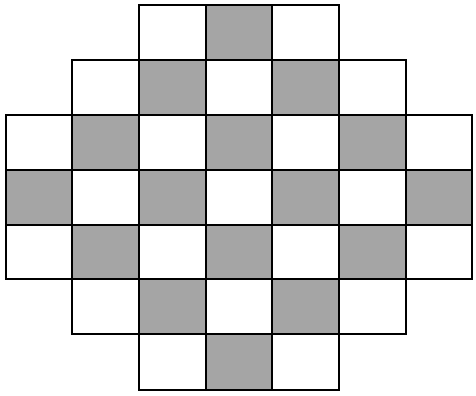

Figure 2-5. Sample RCCA Layout in a Small PWR Core

2.3. Burnable Absorber Design

As mentioned in Section 2.1, BAs are particularly useful for achieving a desired core power shape. In an uncontrolled fuel lattice of uniform enrichment at BOC, the flux distribution tends to peak in the center of the lattice, yielding a greater depletion rate in this region relative to the rest of the lattice. As fuel is depleted more quickly in the center of the lattice, the local reactivity is diminished, which then causes the flux distribution to become more uniform throughout the cycle. BAs are placed so as to reduce the large BOC flux peaking and ideally achieve a uniform depletion rate over the entire core throughout the cycle. Additionally, the reactivity control provided by BAs reduces the burden on soluble boron and therefore reduces the likelihood of a positive MTC. For heavily poisoned assemblies, as the BA in a poisoned assembly is depleted, the assembly reactivity will initially increase from its BOC value as the poison available for neutron absorption is reduced. The assembly reactivity reaches a peak approximately one third of the way through the cycle, at which point the reactivity reduction due to fuel depletion offsets the increase in reactivity due to poison depletion. After this point the

reactivity decreases in an approximately linear fashion for the remainder of the cycle. Figure 2-5 below shows a comparison of a representative reactivity trend of poisoned and unpoisoned assemblies throughout a cycle.

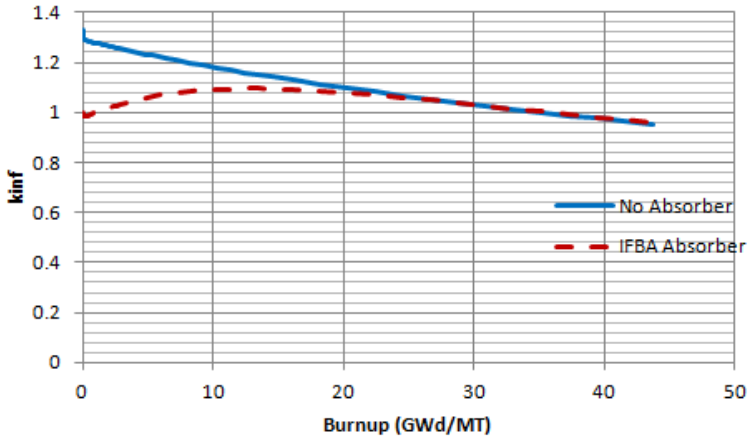

Figure 2-5. Reactivity of Poisoned and Unpoisoned Assemblies

Early BAs were discrete in design and were placed in guide tubes in fuel assemblies without control rods so that they were entirely separated from the fuel material itself. These designs included Pyrex, a borosilicate glass, and the burnable poison rod assembly (BPRA), a mixture of alumina and boron carbide. Westinghouse also developed a discrete BA known as the Wet Annular Burnable Absorber (WABA) rod. This design consists of an annular rod of a mixture of alumina and boron carbide with Zircaloy inner and outer cladding. The central region is filled with water to allow for internal moderation and more complete absorber depletion (23).

In the 1970's, core designs began to utilize integral BAs in the form of gadolinia (Gd_2O_3) mixed uniformly with the fuel material. The advent of integral BAs provided significant core design improvements with respect to power peaking and cycle length, as the constraints associated with the fuel management task were greatly relaxed with the allowance of loading poisoned fuel assemblies into RCCA locations (24). Gadolinia was chosen for the thermal absorption cross section of 61100 barns for ^{155}Gd and 259000 barns for ^{157}Gd. Erbia (Er_2O_3) has

also been considered as an integral BA due to its resonance absorption characteristics (which improve MTC), and it has been employed in Combustion Engineering core designs. In the 1980's, Westinghouse developed the Integral Fuel Burnable Absorber, a thin coating of ZrB_2 around the fuel pellet in select locations within a fuel assembly (23).

The primary absorptive isotopes of each of these BA designs are given in Table 2-2 below. The cross sections of the primary gadolinium and erbium absorptive species are given in Figures 2-6 to 2-8 as well; these are again taken from the ENDF/B-VII library (12) (the ^{10}B cross sections were presented in Section 2.2).

Table 2-2. BA Primary Absorptive Isotopes

Burnable Absorber	Absorptive Isotopes
Pyrex	^{10}B
BPRA	^{10}B
Gd_2O_3	^{155}Gd
	^{157}Gd
Er_2O_3	^{167}Er
IFBA (ZrB_2)	^{10}B

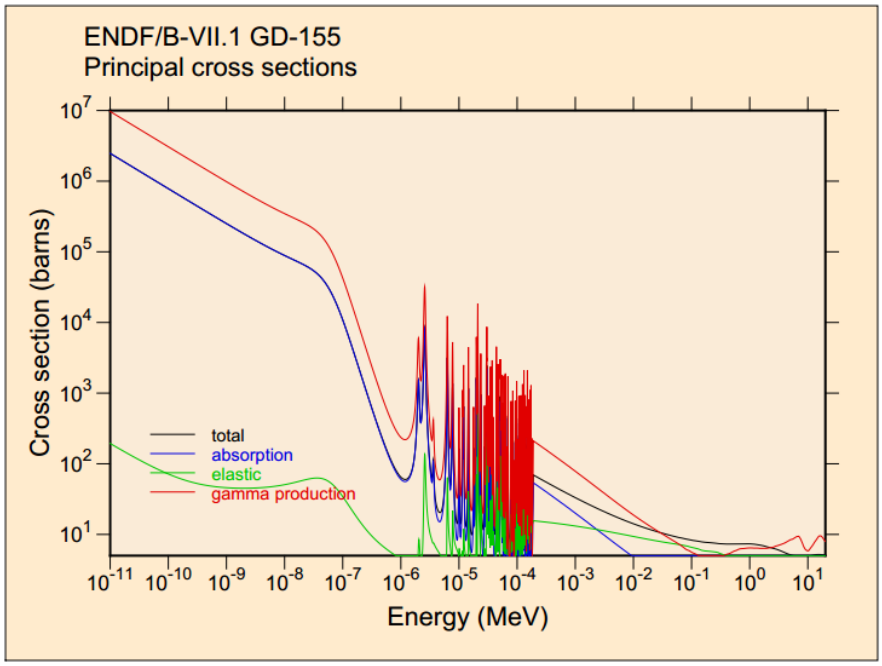

Figure 2-6. ^{155}Gd Cross Sections (12)

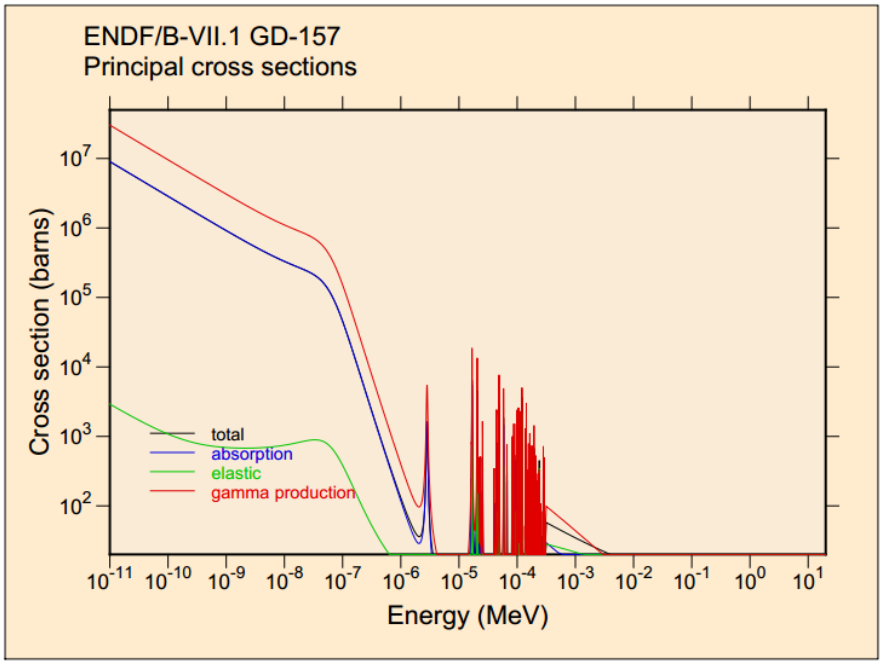

Figure 2-7. ^{157}Gd Cross Sections (12)

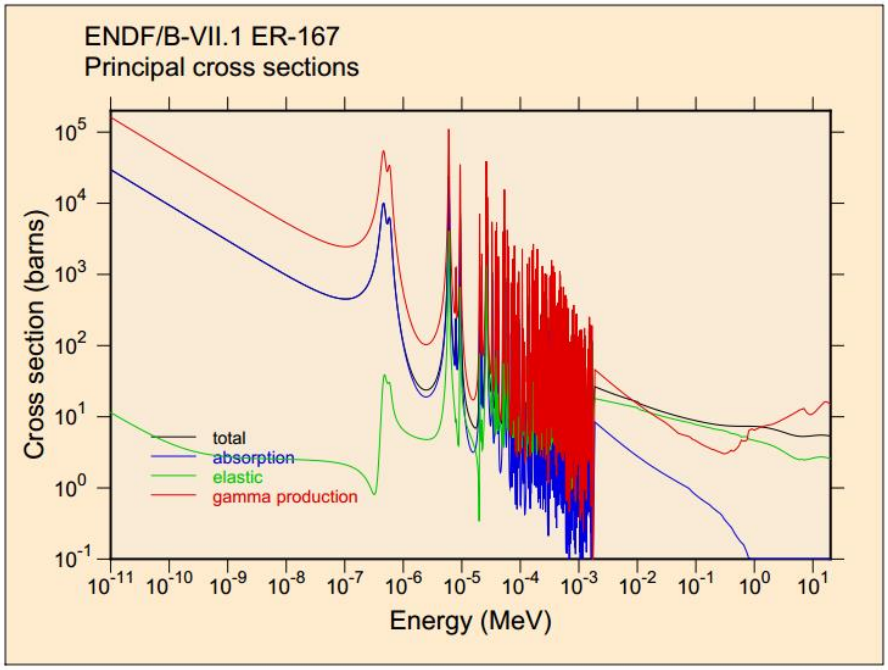

Figure 2-8. ^{167}Er Cross Sections (12)

The candidate burnable absorber designs for the I^{2}S-LWR are gadolinia and IFBA; these designs yield very different reactivity effects when used in a fuel assembly. Gadolinia is mixed uniformly in the fuel material and therefore displaces fuel, imposing a reduction in cycle length.

Additionally, gadolinia is not completely depleted during a cycle, yielding a residual reactivity penalty at the end of a cycle (EOC) that further challenges cycle length. As IFBA is applied as a coating on the fuel pellet outer surface, no fuel is displaced, and it is virtually completely depleted during a cycle; therefore no penalty to cycle length is incurred with IFBA. Both BA designs absorb neutrons of thermal energies and therefore tend to harden the core neutron energy spectrum. The hardened spectrum then promotes increased breeding of ^{239}Pu in a uranium-fuelled core, thereby increasing reactivity and cycle length. However, in gadolinia-poisoned assemblies, this effect is offset by the residual reactivity penalty. Therefore, in comparing an uncontrolled assembly with assemblies poisoned with IFBA and gadolinia, the EOC reactivity of the IFBA assembly is greatest of the three, and that of the gadolinia assembly is the least of the three (22).

Selection of the fuel rods to be poisoned in an assembly should be carried out to minimize intra-assembly power peaking. Poisoned rods therefore appear in symmetric locations in a fuel assembly. Additionally, IFBA-poisoned rods must be chosen so that cooling channels are not obstructed if He buildup causes clad ballooning in several neighboring fuel rods. The reactivity offset of the applied BAs can be varied by adjusting the amount of poison used; specifically, the weight percentage of gadolinia in a fuel rod, the thickness of the IFBA coating, and the number of poisoned fuel rods can be chosen to achieve a desired reactivity offset. Gadolinia concentrations are typically found up to a maximum of 8 w/o, while IFBA concentrations (which are usually specified in terms of ^{10}B mass per axial inch along the fuel rod) are typically found at 1.57 mg/in and 2.355 mg/in. Fuel assemblies with up to 32 gadolinia-poisoned rods and up to 156 IFBA-poisoned rods have been used in 17x17 Westinghouse-type

designs. Figures 2-9 to 2-12, reproduced from (22), show the locations of poisoned fuel rods in some sample 17x17 assemblies.

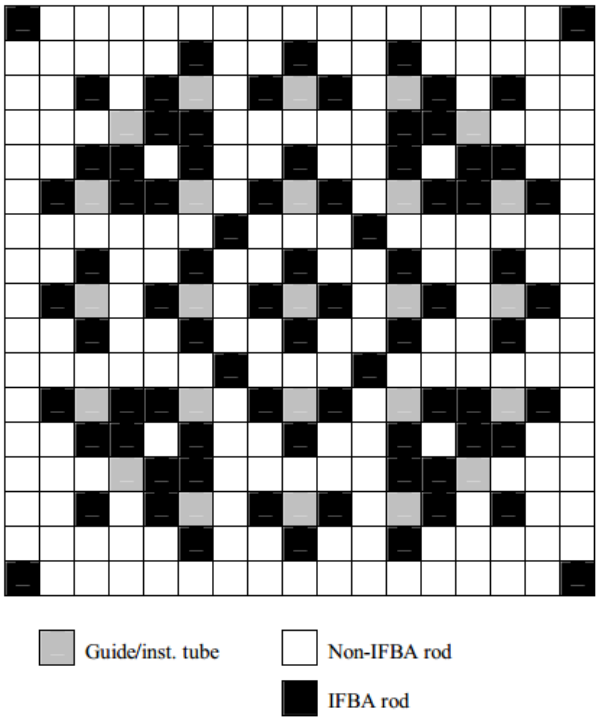

Figure 2-9. Sample 17x17 Fuel Assembly with 80 IFBA Rods (22)

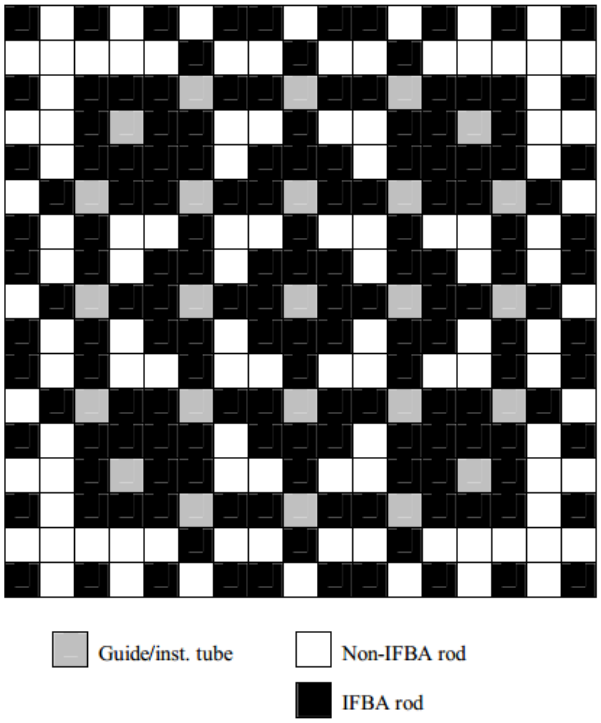

Figure 2-10. Sample 17x17 Fuel Assembly with 156 IFBA Rods (22)

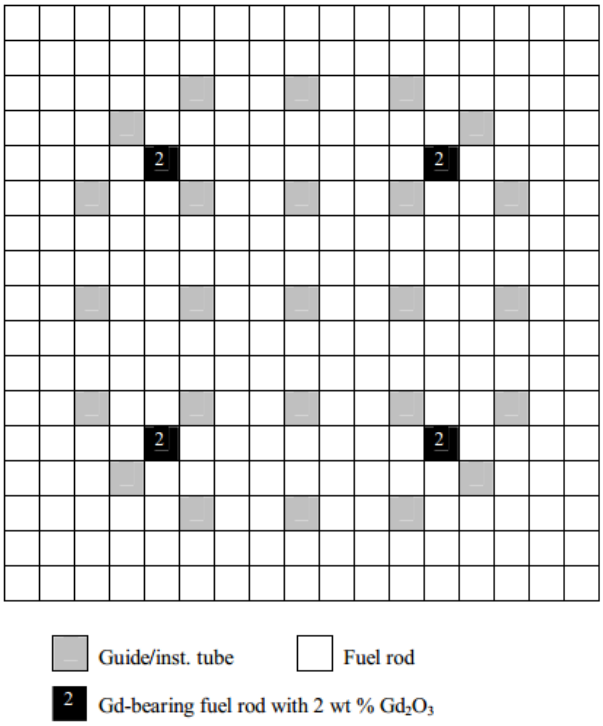

Figure 2-11. Sample 17x17 Fuel Assembly with 4 Gadolinia Rods (22)

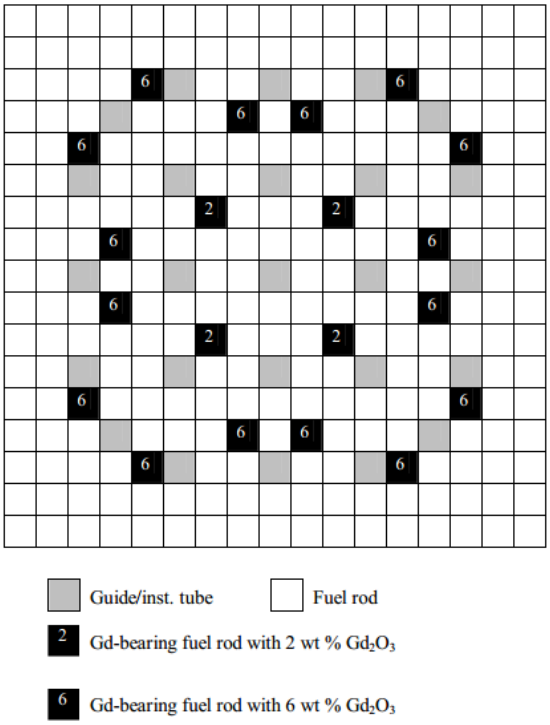

Figure 2-12. Sample 17x17 Fuel Assembly with 20 Gadolinia Rods (22)

2.4. Optimization

The nuclear design optimization task is a difficult and complicated one involving both continuous and discrete variables. In industry, optimization is most commonly considered with respect to core LP design, where after each cycle the design engineer must select which fuel assemblies to discharge, how to shuffle remaining fuel assemblies, where to load fresh fuel assemblies, and what the enrichment of those fresh assemblies should be. An exhaustive deterministic search for the globally-optimized LP at any refueling outage is not at all feasible considering the size of the search space; in the I^2S-LWR, for example, with 121 fuel assembly locations, there are $121! = 8.09 \times 10^{200}$ possible shuffle operations without even considering discharge and loading of fresh fuel. Stochastic optimization methods which handle subsets of the solution space are very popular in nuclear design optimization for this reason.

Optimization problems can generally be defined as the minimization of a function (or an equivalent maximization) subject to specified constraints. The function to be minimized is referred to as the objective function, and its definition must account for all parameters which need to be simultaneously optimized. In the fuel assembly design task, these parameters can include enrichment, poison concentration, intra-assembly power peaking, reactivity, and cycle length. Specifically, the goal is to maximize the cycle length while minimizing enrichment, poison concentration, power peaking, and reactivity; a fuel assembly design with these optimized parameters would theoretically attain the best possible fuel cycle cost with the most efficient use of the fuel and poison materials. In this application, the objective function must therefore be constructed such that its extrema correspond to an ideal set of parameters, i.e. a completely flat power distribution, longest possible cycle length, and so on.

Deterministic optimization methods use specific rules to proceed in a well-defined manner in a search of a solution space. Examples include gradient-based methods (such as the method of steepest descent/ascent) and bracketing methods (such as the bisection method of root solving). In such methods, an initial guess of the solution is taken as a starting point, and the value of the objective function is calculated at this point. Rules are then applied to select the next solution point for evaluation; for example, in the method of steepest descent/ascent, the gradient of the objective function is estimated, and the next iteration is taken at a point a specified path length along the direction of the gradient. The value of the objective function is then calculated at this new point, and the process is repeated until no further improvements to the objective function are realized and an optimum is found (14).

While deterministic optimization methods are useful for reliably obtaining optima from well-behaved objective functions, they are impractical for use with complicated objective

functions with dependence on the design variables that is not readily quantifiable (such is the case with fuel assembly design, where determining the dependence of reactivity and power peaking on BA placement requires a great deal of computational effort). Stochastic optimization methods take the approach of choosing a population of potential solutions as a starting point, calculating the corresponding values of the objective function, and applying a stochastic process to choose the subsequent solutions for evaluation. Selection criteria are applied to determine suitable solutions to propagate into further iterations. Solutions with the best objective function values in each population are retained, and the process is repeated until a stop criterion is met. Examples of stochastic optimization methods include genetic algorithms (GAs) and simulated annealing (SA) (14). As an example of the stochastic process of populating later iterations, in a GA, the best solutions (those with the best objective function values) from one population are used as a basis to produce "genetically" similar solutions for the subsequent population; i.e. these new solutions have similar characteristics to the best solutions in the previous population. In the fuel assembly design task, genetically similar fuel assemblies may have only slight differences in BA layouts.

Methods such as those listed above have been used extensively in industry and research. Espinosa-Paredes and Guzman (2011) developed a simple deterministic process for optimizing the BA loading for the Laguna Verde reactor core by iterating between assembly enrichment and BA content (4). Yilmaz et al (2006) applied a GA with multiple fitness functions to accelerate convergence of BA optimization in a fixed LP (26). Haibach and Feltus (1997) used a GA-based code for core LP optimization using deterministically-developed poisoned fuel assembly designs (10). Application of such processes is beyond the scope of the present study; however, their characteristics shall be qualitatively mimicked at a high level so as to guide judgment in each

step of the fuel assembly design process. In this work, fuel assembly designs are constructed heuristically at each iteration, and their evolution as iterations progress is guided by a GA-like approach wherein the previous population of designs informs construction of subsequent designs.

3. METHODOLOGY

The reactivity control characteristics of the I^2S-LWR fuel assembly designs to be developed are assessed using the SCALE code package for transport and depletion calculations. RCCA designs are characterized by the static reactivity worth of control rod insertion, to be determined by calculating the difference in the fuel assembly reactivity when the control rods are inserted and withdrawn. The BA design process is a more involved high-level optimization exercise requiring depletion calculations for each fuel assembly design. These fuel assembly designs will span several iterations, and relevant performance parameters are calculated at each step to assess each design.

The SCALE suite consists of a number of control modules for reactor simulation and analysis; those pertinent to the present research are included in the T-NEWT and T-DEPL sequences of TRITON (Transport Rigor Implemented with Time-Dependent Operation for Neutronic Depletion). The major modules used in these sequences are CENTRM (Continuous Energy Transport Module) and PMC (Produce Multigroup Cross Sections) for cross section calculations, NEWT (New ESC-Based Weighting Transport Code) for discrete ordinates transport calculations, and COUPLE and ORIGEN (Oak Ridge Isotope Generation Code) for isotopic depletion. Control rod evaluation is carried out using a fresh assembly model, and therefore only the T-NEWT sequence is necessary for cross section generation and transport calculations. Depletion calculations are necessary for BA evaluation, and thus the T-DEPL sequence is used. The T-DEPL sequence employs a predictor-corrector method of depletion by processing cross sections at the beginning of a depletion step, using these cross sections to deplete to the middle of the depletion step, recalculating cross sections at this point in the

depletion step, and then using the updated cross sections to calculate the entire depletion step. This process is repeated for all depletion intervals.

3.1. Control Rod Reactivity Worth

Estimation of the static control rod reactivity worth is made as the key metric for RCCA design assessment. Reactivity worth calculations are performed using two-dimensional models of a single quarter assembly and four adjacent quarter assemblies. Reflective boundary conditions are imposed on all boundaries, thereby approximating an infinite lattice. The T-NEWT sequence of SCALE is used to calculate the fuel assembly reactivity for rodded and unrodded cases in both geometries. As infinite lattices have been approximated due to imposing reflective boundary conditions, rod insertion in the single quarter assembly cases effectively implies that control rods are inserted in all assemblies in the core. However, this is not an accurate representation of the true core design; RCCA locations are expected to take on a checkerboard-like pattern in the final core design. Therefore, in the four quarter assembly cases, control rods are inserted in only two of the four assemblies diagonally across from each other to better represent the true RCCA layout.

Control rod worth is determined as:

$$Worth\ (pcm) = 10^5\,\frac{k_{out} - k_{in}}{k_{out}} \tag{1}$$

where k_{out} is the neutron multiplication eigenvalue of the unrodded core and k_{in} is that of the rodded core. An alternative worth definition that has been used in industry is:

$$Worth\ (pcm) = 10^5 \ln\frac{k_{out}}{k_{in}} \tag{2}$$

These worth calculations are performed for assemblies with and without soluble boron so as to assess the loss in control rod worth due to competition with additional absorbers. Since BAs are

not included in these fuel assembly models, the boron concentration is set at the critical boron concentration (CBC) so as to yield a neutron energy spectrum which approximates that of a real operating PWR core. The CBC is determined by running T-NEWT transport calculations for each fuel assembly configuration to obtain the reactivity over a range of soluble boron concentrations with control rods withdrawn; the CBC is then interpolated from these results.

3.1.1. Case Matrix

Models of the 19x19 uranium silicide fuel assembly are constructed in configurations of 24, 28, and 32 control rod guide tubes per assembly. The RCCA configurations are constructed such that octant symmetry is maintained within the assembly with reasonable spacing between guide tubes so as to avoid asymmetric flux tilts and large flux depressions upon control rod insertion. Additionally, a reference case consisting of a 17x17 uranium oxide fuel assembly with 24 guide tubes is constructed for comparison; the design of this reference assembly is selected to match a typical traditional Westinghouse-type PWR, thus providing a realistic baseline for comparing control rod reactivity worth. One central instrumentation tube is included in each case. These models in single quarter assembly and four quarter assembly geometry are shown in Figures 3-1 to 3-8 below. The circles present in the four-quarter models indicate those assemblies in which control rods are inserted for these cases estimating reactivity worth with two of four assemblies rodded.

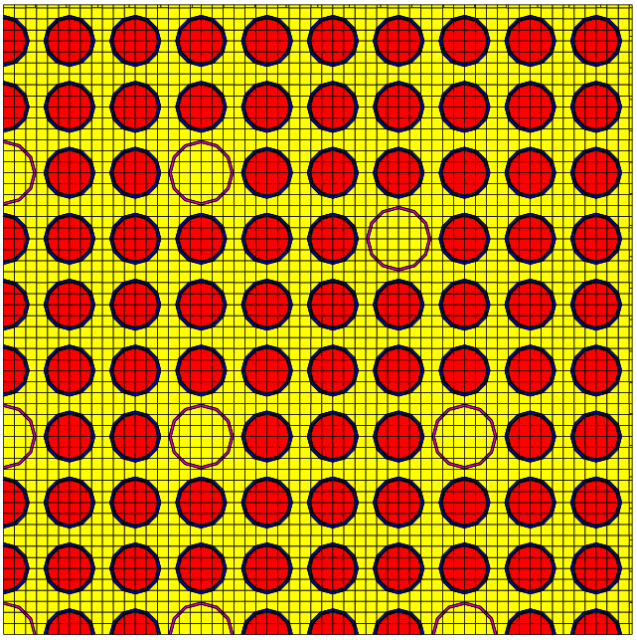

Figure 3-1. Single Quarter 19x19 Assembly with 24 Control Rods

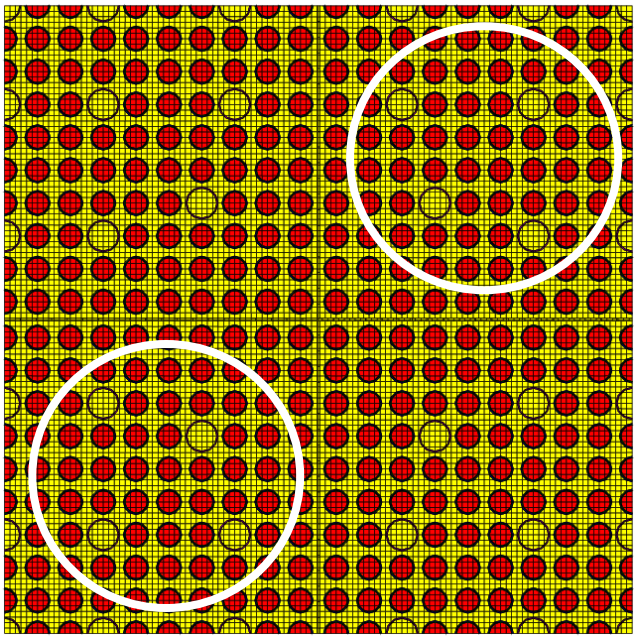

Figure 3-2. Four Quarter 19x19 Assemblies with 24 Control Rods

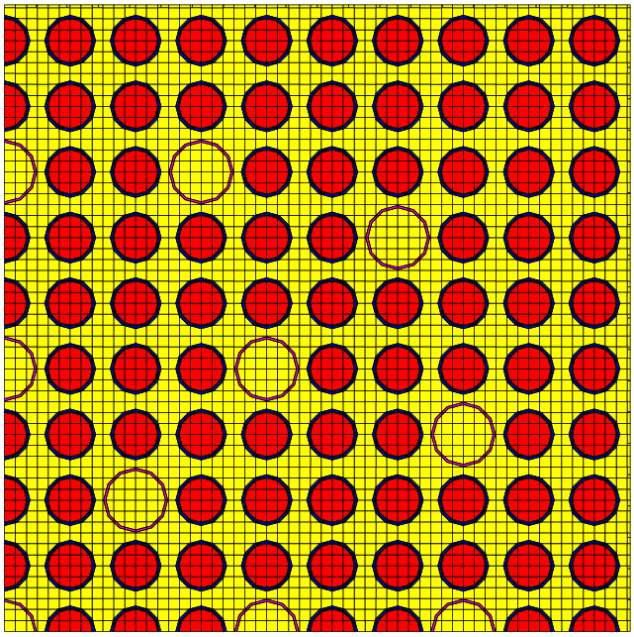

Figure 3-3. Single Quarter 19x19 Assembly with 28 Control Rods

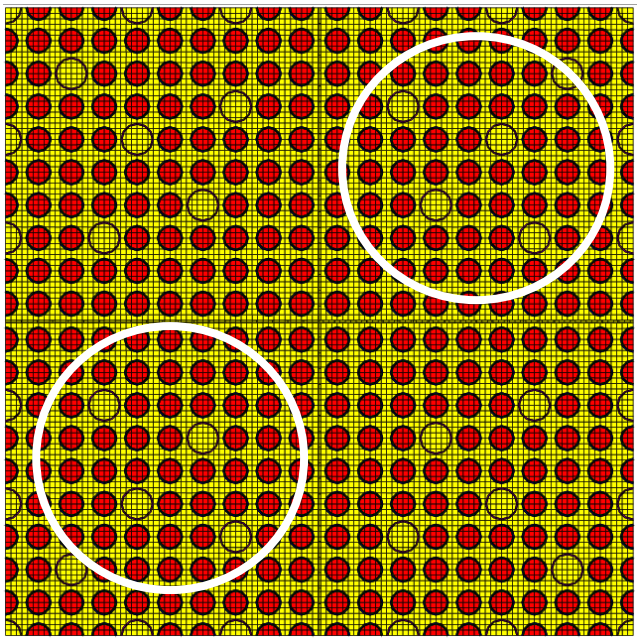

Figure 3-4. Four Quarter 19x19 Assemblies with 28 Control Rods

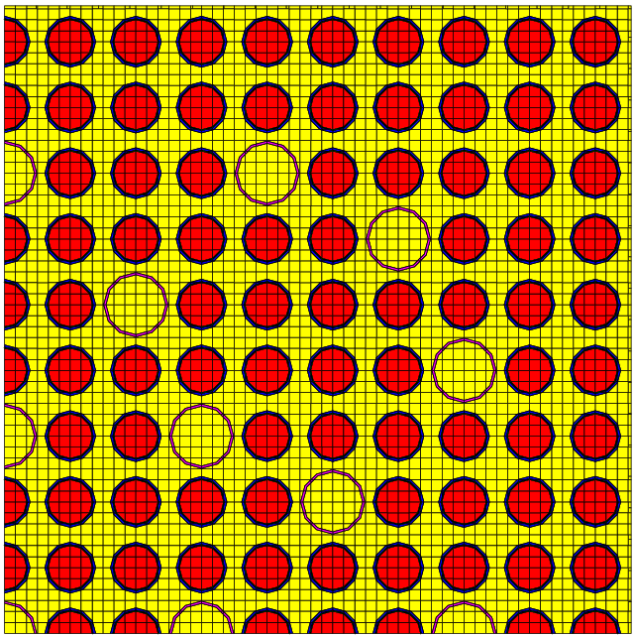

Figure 3-5. Single Quarter 19x19 Assembly with 32 Control Rods

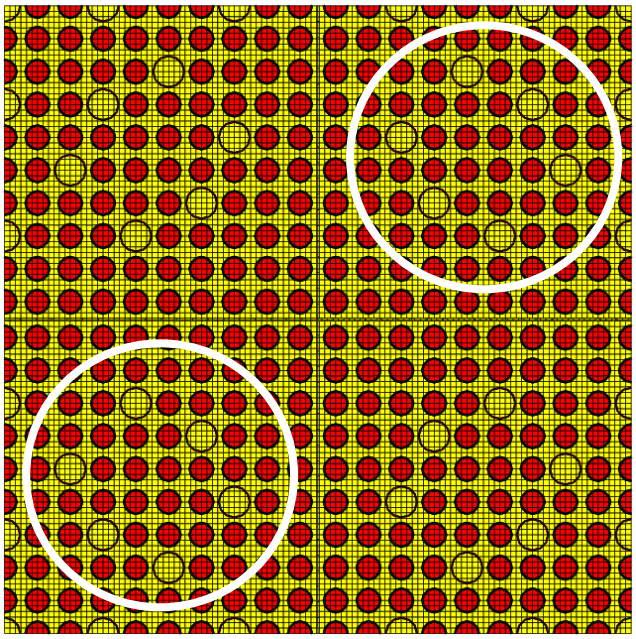

Figure 3-6. Four Quarter 19x19 Assemblies with 32 Control Rods

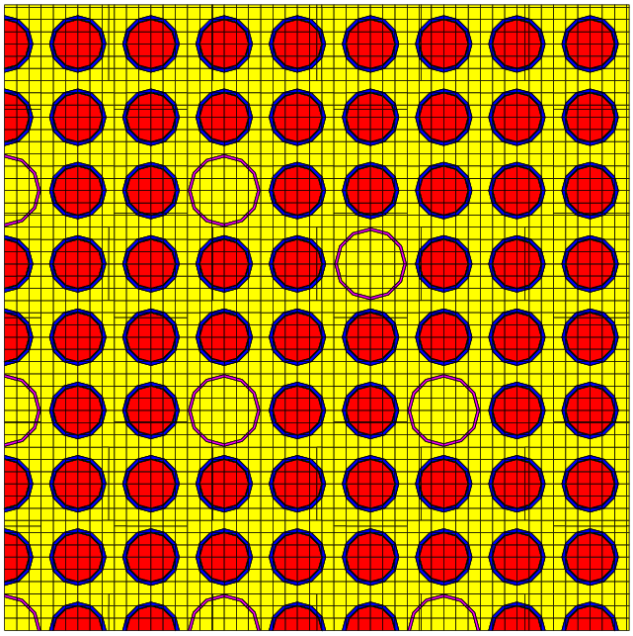

Figure 3-7. Single Quarter 17x17 Assembly with 24 Control Rods

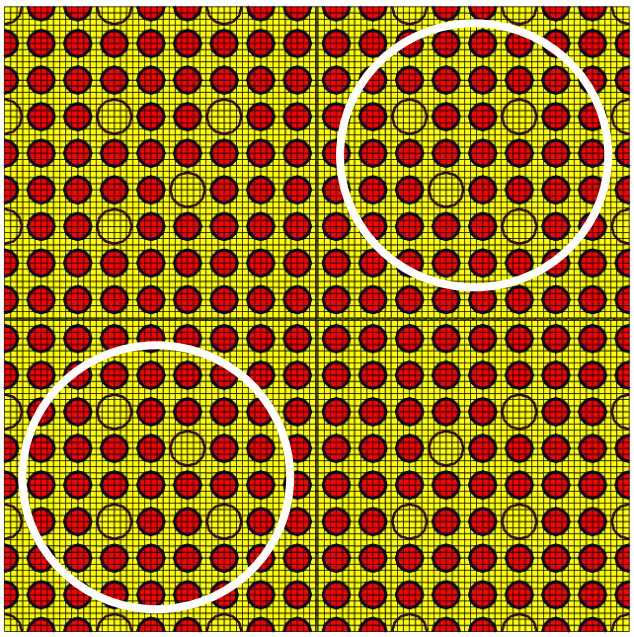

Figure 3-8. Four Quarter 17x17 Assemblies with 24 Control Rods

To determine CBC, transport calculations are performed for each of the above unrodded models with boron concentrations of 0, 2000, 3000, 4000, 5000, 6000, 7000, and 8000 ppm to determine the dependence of the neutron multiplication eigenvalue on boron concentration (the SCALE default natural boron composition is used – see Appendix A). This information is then

used to interpolate the CBC for each assembly configuration. Rodded models are then constructed with AIC, B_4C, and Hf control rods with no boron and at the CBC (the SCALE default natural isotopics are assumed for all elements in these absorbers; these are given in Appendix A as well). Transport calculations are carried out for each case to obtain rodded neutron multiplication eigenvalues, which are then compared with the corresponding unrodded cases; the control rod reactivity worth is then calculated using Equation 1. For the sake of clarity, the progression of calculations to be performed is shown in Table 3-1.

Table 3-1. Control Rod Design Case Matrix

Calculation	Core	Rods	Geometry	Boron
CBC	19x19 silicide assembly with 24 control rods	Out	Quarter assembly and four quarter assemblies	0-8000 ppm boron
	19x19 silicide assembly with 28 control rods	Out	Quarter assembly and four quarter assemblies	0-8000 ppm boron
	19x19 silicide assembly with 32 control rods	Out	Quarter assembly and four quarter assemblies	0-8000 ppm boron
	17x17 oxide assembly with 24 control rods	Out	Quarter assembly and four quarter assemblies	0-8000 ppm boron
Rod worth	19x19 silicide assembly with 24 control rods	AIC, B_4C, Hf inserted and withdrawn	Quarter assembly and four quarter assemblies	No boron and CBC
	19x19 silicide assembly with 28 control rods	AIC, B_4C, Hf inserted and withdrawn	Quarter assembly and four quarter assemblies	No boron and CBC
	19x19 silicide assembly with 32 control rods	AIC, B_4C, Hf inserted and withdrawn	Quarter assembly and four quarter assemblies	No boron and CBC
	17x17 oxide assembly with 24 control rods	AIC, B_4C, Hf inserted and withdrawn	Quarter assembly and four quarter assemblies	No boron and CBC

3.1.2. Limitations

Some limitations of the preceding methodology are immediately apparent. First, transport calculations are carried out in two dimensions; three-dimensional phenomena (which are of utmost significance in control rod design assessment) are therefore lost. Additionally, by approximating an infinite lattice, effects due to RCCA placement are lost and can only be approximated by inserting rods in two diagonally opposite assemblies in cases with four quarter assembly geometry. This also means that shutdown margin cannot be accurately estimated, and therefore the reactivity worth is taken as the key parameter by which to judge the design quality. It is unknown how much accuracy is lost under these simplifications, but the exercise still provides valuable insight into the neutronics of the I^2S-LWR uranium silicide fuel assembly.

3.2. Burnable Absorber Optimization

Burnable absorber layouts are assessed using two-dimensional fuel assembly models as well; models are built in quarter assembly geometry only, and reflective boundary conditions are again imposed on all edges. Each fuel assembly model is depleted using the T-DEPL sequence in SCALE, and key design performance indicators are tracked throughout the cycle. As mentioned previously, BA design evaluation is based on reactivity hold-down, power peaking, poison depletion, cycle length, soluble boron reactivity worth, and MTC. The SCALE output explicitly reports neutron multiplication, power peaking, and poison inventory data, but additional calculations are necessary to estimate the poison reactivity worth, cycle length, boron worth, and MTC. The reactivity worth ρ of the BAs may be calculated from the reported neutron multiplication as:

$$\rho\ (pcm) = 10^5 \frac{k - k_0}{k_0} \tag{3}$$

where k is the poisoned lattice neutron multiplication and k_0 is the uncontrolled lattice neutron multiplication.

The cycle length may be estimated by calculating the assembly discharge burnup; this is taken as the burnup at which the assembly neutron multiplication eigenvalue (k_∞) is equal to 1.03, with the implicit assumption of a 3 percent loss in reactivity due to leakage which is not accounted for in the infinite assembly models. This burnup may be interpolated from the T-DEPL output. The cycle length t may then be calculated as:

$$t = \frac{4 * 121 * BU_d(M/L)H}{P_{th}} \quad (4)$$

where BU_d is the discharge burnup, M/L is the system mass per unit length given in the SCALE output, H is the active core height, and P_{th} is the core thermal power (assumed to be a constant 3000 MW). The factor of 4 expands the quarter assembly model to a full assembly, and the factor of 121 accounts for all fuel assemblies in the core. Thus the cycle length is calculated under the approximation that all fuel assemblies are of the same type; while this is not the case in the true core design, this calculation provides a reasonable measure of how the BA loading impacts the cycle length.

A rigorous calculation of MTC would require a full-core analysis, but the limited models employed in this study may be used to obtain a proxy MTC estimate to glean some understanding of how the fuel assembly BA loading impacts reactivity feedback. To do so, first the CBC is calculated in a manner similar to that used in the control rod study described previously. The assembly neutron energy spectrum at the CBC should approximate that of the full core. Again, T-NEWT calculations are run for several boron concentrations so that the CBC may be interpolated. In order to reduce the size of the case matrix, only ^{10}B is modeled in the moderator (rather than the natural boron composition) at concentrations of 0, 1000, and 2000

ppm; these ^{10}B concentrations may then be converted to a corresponding total B concentration by accounting for the SCALE default natural B composition: 18.43 w/o ^{10}B, 81.57 w/o ^{11}B. Thus the total B concentrations corresponding to the model ^{10}B concentrations of 1000 and 2000 ppm are 5426 and 10852 ppm respectively. This simplification carries the assumption that the ^{11}B does not interact neutronically. This data may then be used to estimate the soluble boron worth W_B of each design:

$$W_B(pcm/ppm) = \frac{10^5}{k}\frac{\Delta k}{\Delta B} \quad (5)$$

where k is the neutron multiplication eigenvalue and B is the soluble (total – that is, both ^{10}B and ^{11}B) boron concentration in ppm. The differences may be taken between concentrations of 0 and 1000 ppm, 1000 and 2000 ppm, or 0 and 2000 ppm ^{10}B. It is anticipated that the boron worth is different for each of these intervals; they would only be identical if the reactivity response to the boron concentration, $\partial k/\partial B$, is linear and independent of the boron concentration. This is likely not the case with integral BAs present, which compete with the soluble boron for neutron absorption.

Models are then constructed with the CBC imposed, and T-NEWT calculations are run for three different water densities; these are selected by perturbing the moderator temperature $\pm$20 ^{o}C from nominal. Appendix A provides greater detail on the material input. These results are used to quantify the change in neutron multiplication with moderator density. MTC is then estimated as:

$$MTC\ (pcm/K) = \frac{10^5}{k_0}\frac{\Delta k}{\Delta \rho_w}\frac{\Delta \rho_w}{\Delta T} \quad (6)$$

where k_0 is the neutron multiplication eigenvalue at the CBC, ρ_w is the moderator density, and T is the moderator temperature. The change in moderator density with temperature is approximated

as a constant -0.002435 g/cm^3 K in the vicinity of the I^{2}S-LWR operating conditions based on data from (15). Similar to the boron worth calculations, the differences may be taken between densities corresponding to T_0 and T_0 + 20 ^{o}C, T_0 and T_0 – 20 ^{o}C, or T_0 – 20 ^{o}C and T_0 + 20 ^{o}C (where T_0 is the nominal moderator temperature) to yield a forward, backward, or center difference approximation, respectively. Each of these calculations may not necessarily yield identical values of the MTC due to nonlinear response of reactivity to the moderator density. This response is similar to the reactivity response to the boron concentration, but with the additional component of varying moderating power with the water density. This moderating component actually counteracts the boron component; an increase in moderator density improves moderation and increases reactivity, but the effective soluble boron concentration increases as well, thereby increasing neutron absorption and decreasing reactivity.

3.2.1. Case Matrix

To develop an initial "population" of BA layouts, depletion of an uncontrolled assembly model is carried out first, and the results are processed to track the criticality and power peaking trends. Based on these results, BAs are then located within the assembly in a heuristic manner with the intent of suppressing the power peaking which naturally occurs in the vicinity of water-filled control rod guide tubes, where the thermal neutron population is greater as a result of increased local moderation. BA layouts are developed for fuel assemblies with 8 and 16 Gd-bearing rods per assembly with concentrations of 4 and 8 percent by weight, and with 80 and 160 IFBA rods per assembly with a concentration of 2.5 mg/in ^{10}B in the axial dimension. This case matrix is presented in Table 3-2 for the sake of clarity. These designs form the first iteration of the BA optimization process.

Table 3-2. Burnable Absorber Design Case Matrix

Poison	Poisoned Rods per Assembly	BA Concentration	Soluble ^{10}B Concentration	Moderator Temperature
Gd_2O_3	8	4 w/o	0-2000 ppm	T_0, $T_0 \pm 20$ ºC
Gd_2O_3	8	8 w/o	0-2000 ppm	T_0, $T_0 \pm 20$ ºC
Gd_2O_3	16	4 w/o	0-2000 ppm	T_0, $T_0 \pm 20$ ºC
Gd_2O_3	16	8 w/o	0-2000 ppm	T_0, $T_0 \pm 20$ ºC
IFBA	80	2.5 mg/in ^{10}B	0-2000 ppm	T_0, $T_0 \pm 20$ ºC
IFBA	160	2.5 mg/in ^{10}B	0-2000 ppm	T_0, $T_0 \pm 20$ ºC

In order to develop subsequent design populations, the results from the previous iteration are used to inform development of the BA layouts for the following iteration. This is done using a heuristic GA-like approach; specifically, BA locations which yield regions of relatively flat power distributions are considered "genetically fit" (that is, these locations are desirable for BA placement), and the remaining BA locations are adjusted to suppress remaining peaking. In this way, the designs of the previous iteration act as the "parents" of the designs of the next iteration, which retain the desirable characteristics of previous designs. The process is repeated to build a pool of assembly designs from which some high-level rules relating design decisions to the relevant performance metrics may be identified.

3.1.2. Limitations

Some of the factors which inhibit the accuracy of the RCCA design process impact the BA optimization task as well. For example, models are again constructed in two dimensions, thereby eliminating information about three-dimensional phenomena which impact the fuel assembly performance (such as axial power peaking). Such issues must be addressed in separate endeavors through axial zoning of the BAs and proper selection of the blanket enrichment. Additionally, these models have been constructed so as to balance high fidelity with computational efficiency. This is achieved by limiting modeling parameters such as the number of radial regions employed in representing Gd-bearing pins, the size of the spatial mesh for

transport calculations, and the energy group structure for calculation of group constants. Incorporation of greater detail in such parameters comes at the cost of greater computational effort, which can have a severe impact on the calculation speed in some cases. Selection of these model settings and their impact on the computation time and solution accuracy is discussed in the next section.

3.3. Modeling Requirements

It is necessary to address the computational models representing the fuel assembly designs under investigation and the accuracy of the solutions they yield. Fuel assemblies containing gadolinia-poisoned fuel rods require particular attention; due to the very large thermal absorption cross sections of ^{155}Gd and ^{157}Gd, the neutron flux in a fresh gadolinia-bearing fuel pin exhibits a significant drop in the radially inward direction. Computationally, this phenomenon must be accounted for so as to capture the change in the neutron spectrum across these pins and yield accurate cross sections. This is done by modeling the fuel region of gadolinia-poisoned rods with multiple radial regions. In addition to the precise number of radial regions employed in modeling these poisoned pins, other calculation parameters used in SCALE which can impact the model fidelity and computation time include the size of the geometric mesh, the P_N scattering order used for various materials, the S_N quadrature order, the energy group structure, and the number of nuclides explicitly tracked. Each of these parameters shall be investigated so as to select the optimal calculation settings that yield acceptable computation time and fidelity for larger calculations in the future.

The remainder of this section contains analyses carried out with a dated fuel assembly model. While these studies were being performed, the I^2S-LWR fuel rods were assumed to be

annular in design. This was later changed in favor of solid fuel. This is the only section which uses models of this fuel design.

3.3.1. Modeling Study Methodology

In order to reduce the complexity and computational effort of the numerous calculations to follow, a simplified fuel assembly model is employed. One quarter of a 5x5 fuel assembly with a single central gadolinia-bearing pin and no guide tubes is constructed as shown in Figure 3-9 below. The pin dimensions (including pitch) and specific power used in the model are identical to that of the I^2S-LWR. The concentration of gadolinia in the poisoned pin is selected arbitrarily as 6 percent by weight. This model was selected so as to approximate the ratio of the number of poisoned pins to the total number of fuel pins that may be expected to be found in a final fuel assembly design for the I^2S-LWR. Specifically, this simplified model contains one poisoned pin out of 25; thus 4 percent of the pins are poisoned. In the 19x19 fuel assembly of the I^2S-LWR, with 25 guide tubes, a loading of 12 poisoned pins out of 336 fuel pins corresponds to 3.57 percent of the fuel pins being poisoned (such a loading may be considered typical based on experience with other PWRs that use gadolinia). Reflective boundary conditions are imposed on all edges so as to approximate an infinite lattice.

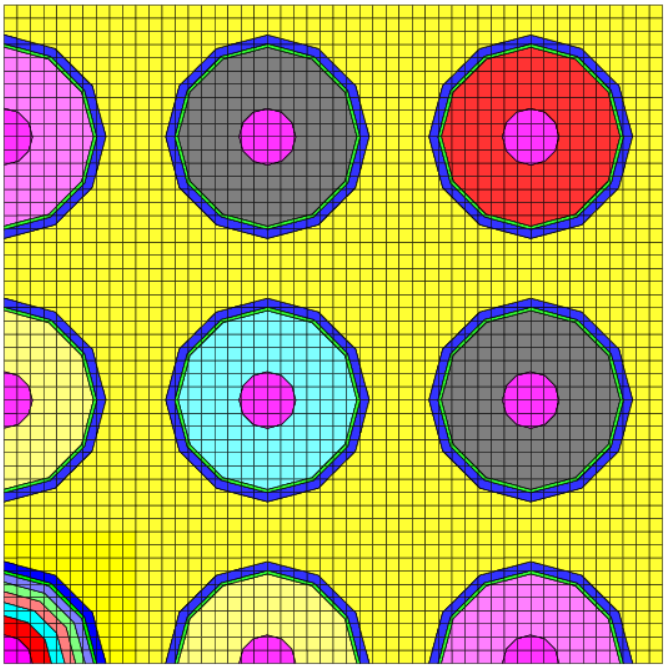

Figure 3-9. Simplified Fuel Assembly Model

Depletion calculations are to be carried out with this fuel assembly model using the T-DEPL sequence in SCALE. The assembly models are depleted to approximately 60 GWd/MT with a fine temporal mesh at the beginning of life, where reactivity is expected to vary most rapidly. Each of the calculation parameters discussed above shall be varied, and the resulting criticality and power peaking trends shall be compared across cases to determine where accuracy may be acceptably sacrificed in favor of improvements in computational effort. The case matrix is summarized in Table 3-3 below, followed by a more detailed description of each parameter.

Table 3-3. Modeling Study Case Matrix

Parameter	Values
Radial Regions in Gd Pin	5, 10, 15
Single Whole Fuel Pin Mesh	4x4, 6x6, 20x20
Quarter Gd Pin Mesh	6x6, 8x8, 10x10
P_N Scattering Order	0, 1, 2 for fuel, as well as “recommended” case
S_N Quadrature Order	12, 16
Energy Groups	44, 49, 238
Nuclides Explicitly Tracked	15, 94, 230, 388

3.3.1.1. Radial Regions in the Poisoned Pin

Including a greater number of radial regions in the gadolinia-bearing fuel pin model allows the variation in the neutron flux and energy spectrum across the fuel region to be more accurately represented, thereby yielding more accurate cross sections. Various calculations involving gadolinia as an IBA found in the literature use between 6 and 10 radial regions (References 2, 3, and 7). The calculations in this study shall consider models with 5, 10, and 15 radial regions.

3.3.1.2. Single Whole Fuel Pin Mesh

The geometric mesh shown in Figure 3-9 above is a 20x20 structure in a single whole fuel pin (the mesh is therefore 10x10 in the quarter pin, and 10x20 or 20x10 in half pins). This shall be compared to cases with much coarser 4x4 and 6x6 structures in a single whole fuel pin. The mesh in the poisoned pin shall be kept constant at 10x10.

3.3.1.3. Poisoned Pin Mesh

The effect of the mesh in the poisoned pin shall be isolated to determine the extent of the impact of the resolution of the radial regions on the depletion results. For these cases, the mesh of the whole fuel pins shall be fixed at 4x4, and the original 10x10 mesh of the quarter poisoned pin shall be compared to structures of 6x6 and 8x8.

3.3.1.4. P_N Scattering Order

In the SCALE input file, P_N scattering order must be specified for all materials present in the model. For maximum fidelity, the scattering order shall initially be fixed at 3 for the light materials (water and helium) and 1 for the clad while that of the fuel is varied from 0 to 2. An additional case shall use the settings recommended in Reference 1; specifically, this consists of scattering orders of 1 for fuel, 0 for helium, 1 for clad, and 2 for water.

3.3.1.5. S_N Quadrature Order

The NEWT module uses a two-dimensional discrete ordinates method for transport calculations, and the SCALE input allows specification of the number of angular directions. Calculations performed in this study shall compare results of cases with S_{12} and S_{16} quadrature structure.

3.3.1.6. Energy Groups

The SCALE system includes a number of cross section libraries available for various depletion sequences. Those that are compatible with the T-DEPL sequence include the ENDF/B-V 238-group library, the ENDF/B-V 44-group library that is collapsed from its 238-group counterpart, the ENDF/B-VI 238-group library, and the ENDF/B-VII 238-group library. Differences between the ENDF releases shall be neglected, and these calculations shall consider the ENDF/B-V 44-group library and the ENDF/B-VII 238-group library. An additional option in the SCALE input (the "weight" parameter) activates a 238-group steady state calculation, the spectrum of which is used to generate a problem-specific 49-group library. This option shall be explored as well.

3.3.1.7. Explicit Nuclide Tracking

The SCALE input allows users to specify how many nuclides should be explicitly tracked during a depletion calculation through the "addnux" parameter. Accounting for a greater number of nuclides, many of which are present only in trace quantities, yields a more accurate estimate of reactivity at the expense of computational effort. Cases shall be compared with 15, 94, 230, and 388 additional nuclides explicitly tracked.

3.3.2. Results

3.3.2.1. Radial Regions in the Poisoned Pin

As previously discussed, cases with 5, 10, and 15 radial regions in the poisoned fuel pin are explored. These regions are constructed so that they have equal area. The other calculation settings for these cases are kept constant and are listed in Table 3-4. These settings are largely arbitrary, but they are expected to be sufficiently rigorous to yield accurate results with a high degree of confidence. The fuel assembly models are visually identical to Figure 3-9 except for the poisoned pin; closer views of the poisoned pin are therefore given in Figures 3-10, 3-11, and 3-12 for each respective case. In these Figures, the two outermost layers represent the clad and gap, while the innermost layer represents the inner fuel pellet void; the remaining layers are the poisoned fuel.

Table 3-4. Calculation Settings for Varying Radial Regions Cases

Parameter	Value
Single Whole Fuel Pin Mesh	20x20
Quarter Poisoned Pin Mesh	10x10
P_N Scattering Order	Fuel: 0 Helium: 3 Clad: 1 Water: 3
S_N Quadrature Order	16
Energy Groups	238
Nuclides Explicitly Tracked	388

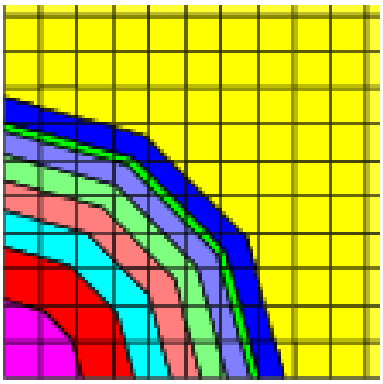

Figure 3-10. Poisoned Pin with 5 Radial Regions

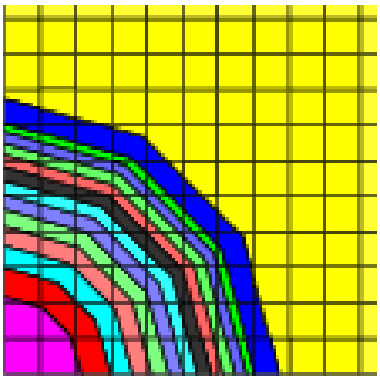

Figure 3-11. Poisoned Pin with 10 Radial Regions

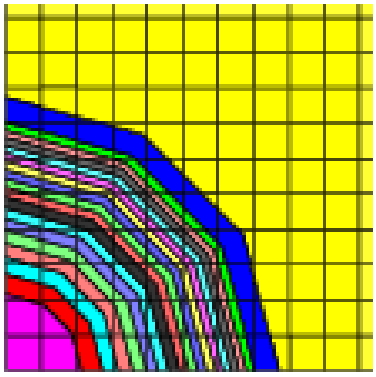

Figure 3-12. Poisoned Pin with 15 Radial Regions

The k_{inf} trend for these cases is given in Figure 3-13, and Figure 3-14 gives the deviation of k_{inf} in pcm of the 5- and 10-region cases from the 15-region case. Additionally, Table 3-5 gives the computation time used by each of these cases. These results indicate that the 5-region case does not deviate from the 15-region case by more than 60 pcm in k_{inf}; indeed, the maximum discrepancy between the 5- and 15-region cases is about 54 pcm in k_{inf}, and nearly 14 hours of computation time are saved. As the difference in the k_{inf} trend between the 5- and 15-region cases is relatively small, the power peaking trend shall be compared only between these two cases. Figure 3-15 gives the deviation in relative pin power between the 5- and 15-region cases at the time where this difference is the largest. The difference in relative pin power is no greater than 0.8 percent. This maximum difference occurs in the poisoned pin, indicating that the number of radial regions employed has the largest impact on the calculation of its own power.

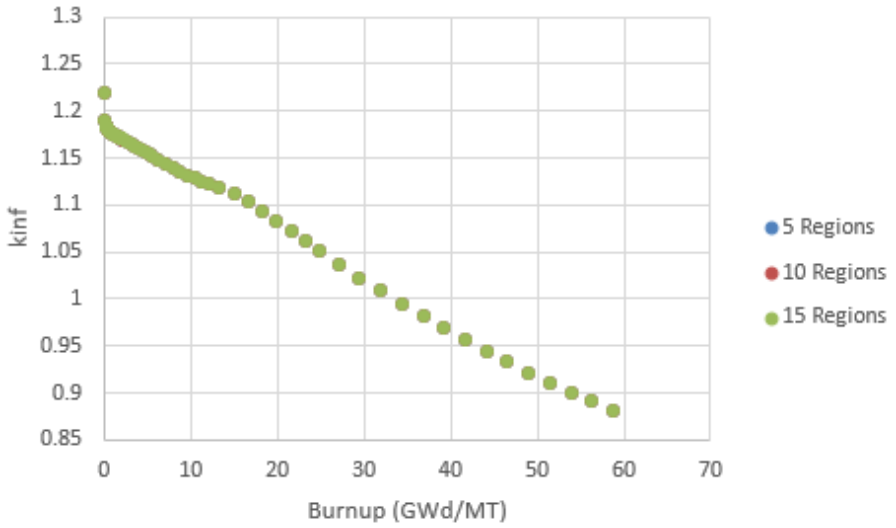

Figure 3-13. Depletion of Varying Radial Regions Cases

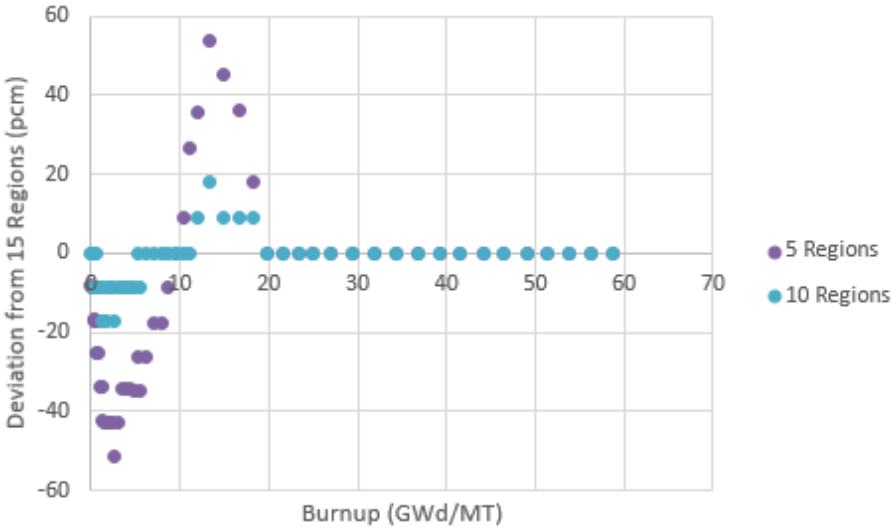

Figure 3-14. Deviation in k_{inf} among Varying Radial Regions Cases

Table 3-5. Computation Time for Varying Radial Regions Cases

Case	Time (hours)
5 Regions	230.66
10 Regions	243.48
15 Regions	244.04

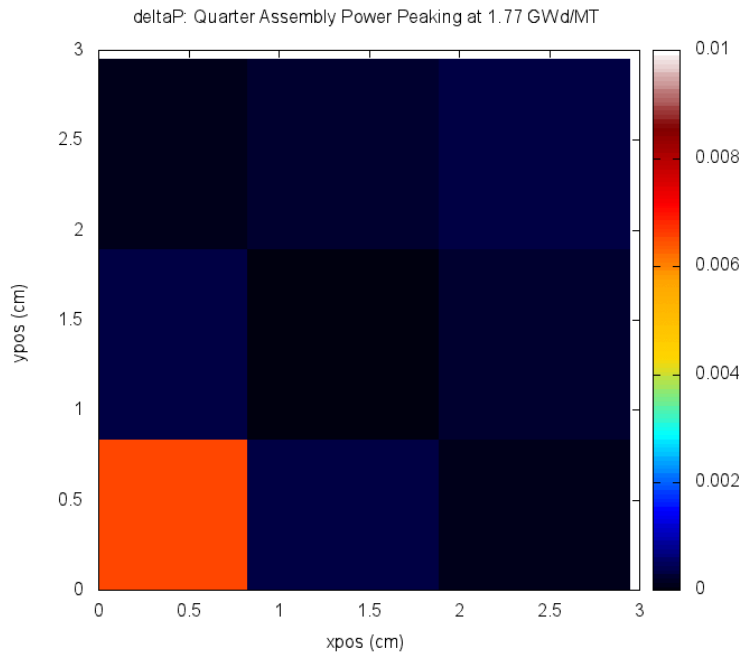

Figure 3-15. Largest Deviation in Relative Pin Power between 5- and 15-Region Cases

3.3.2.2. Single Whole Fuel Pin Mesh

The geometric mesh of a single whole fuel pin is now chosen as 4x4 and 6x6 for comparison against the original 20x20 case. The mesh of the quarter poisoned pin is not varied in these cases, but run time is reduced by performing an S_{12} transport calculation. The calculation settings for these cases are summarized in Table 3-6. Visual representations of the 4x4 and 6x6 cases are given in Figures 3-16 and 3-17, respectively, while that of the 20x20 case is identical to Figure 3-9.

Table 3-6. Calculation Settings for Varying Single Whole Fuel Pin Mesh Cases

Parameter	Value
Radial Regions in Poisoned Pin	5
Quarter Poisoned Pin Mesh	10x10
P_N Scattering Order	Fuel: 0 Helium: 3 Clad: 1 Water: 3
S_N Quadrature Order	12
Energy Groups	238
Nuclides Explicitly Tracked	388

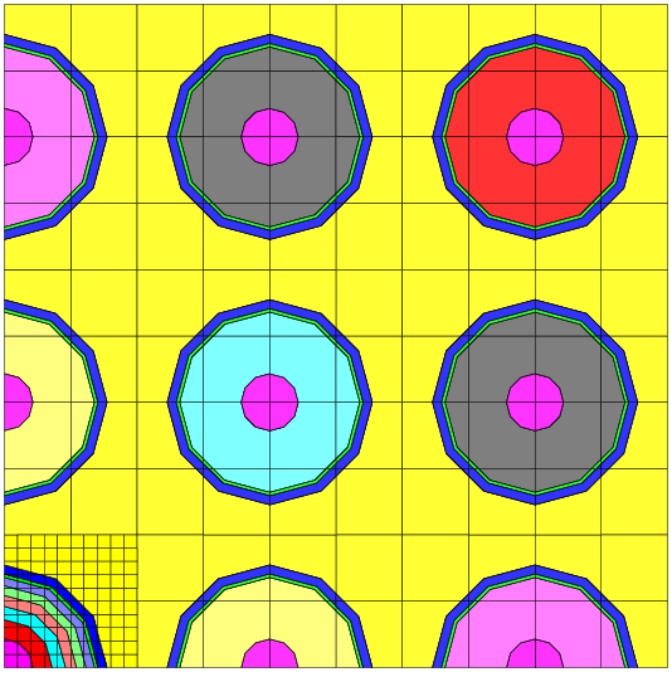

Figure 3-16. Fuel Assembly Model for the 4x4 Single Whole Fuel Pin Mesh Case

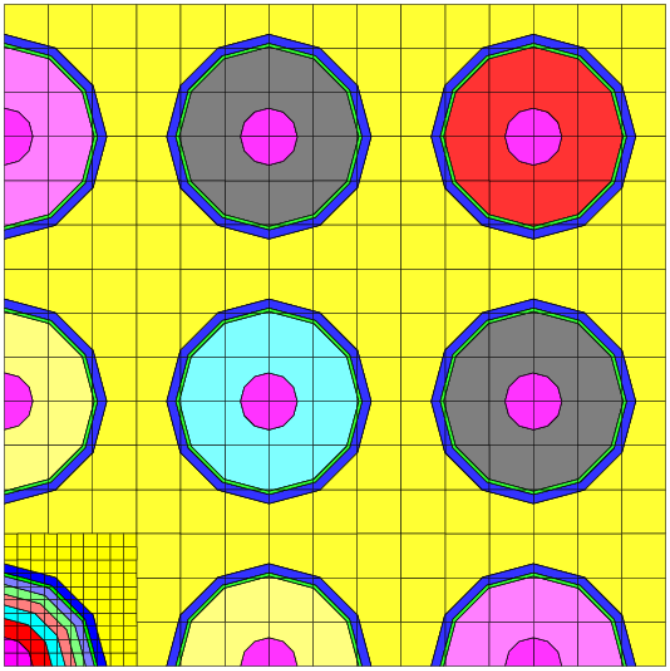

Figure 3-17. Fuel Assembly Model for the 6x6 Single Whole Fuel Pin Mesh Case

Figure 13-18 below shows the kinf trend for each of these cases, and Figure 3-19 gives the deviation of k_{inf} in pcm of the 4x4 and 6x6 cases from the 20x20 case. Table 3-7 gives the computation time used by each case. These results indicate significant reduction in computation

time by using a coarser mesh without prohibitive loss in accuracy. As the 6x6 case deviates less from the 20x20 case in k_{inf}, the power peaking shall be compared between these two cases. Figure 3-20 gives the fractional difference in relative pin power between the 6x6 and 20x20 cases at the time where this difference is the largest. This difference is well under 0.4 percent, and again occurs in the poisoned pin.

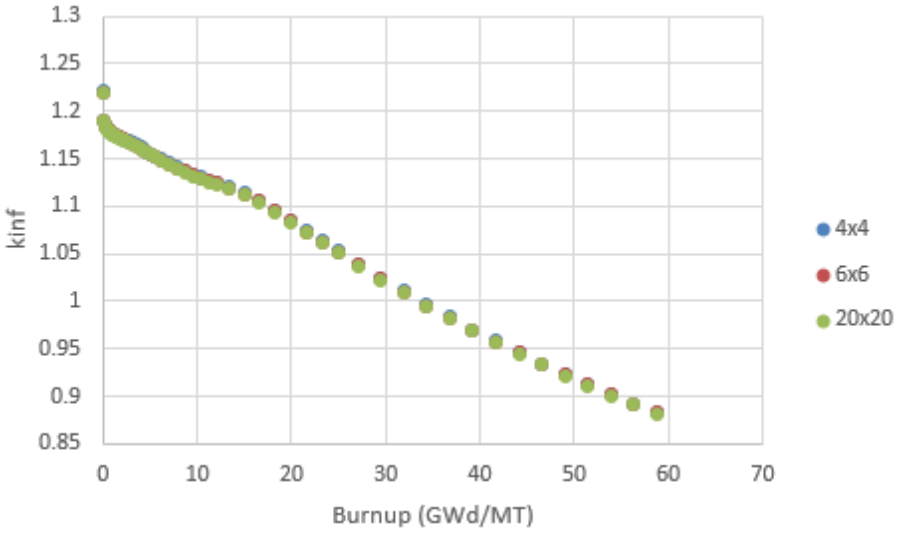

Figure 3-18. Depletion of Varying Single Whole Fuel Pin Mesh Cases

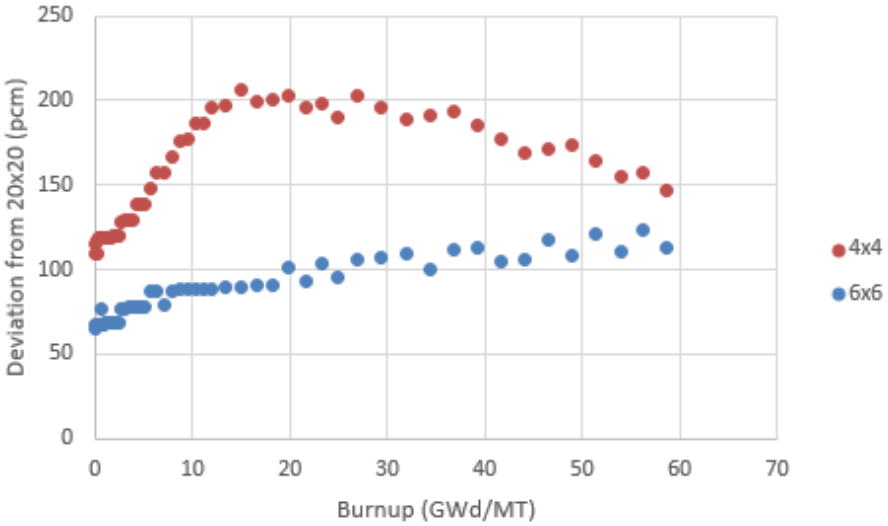

Figure 3-19. Deviation in k_{inf} among Varying Single Whole Fuel Pin Mesh Cases

Table 3-7. Computation Time for Varying Single Whole Fuel Pin Mesh Cases

Case	Time (hours)
4x4	28.29
6x6	36.92
20x20	150.72

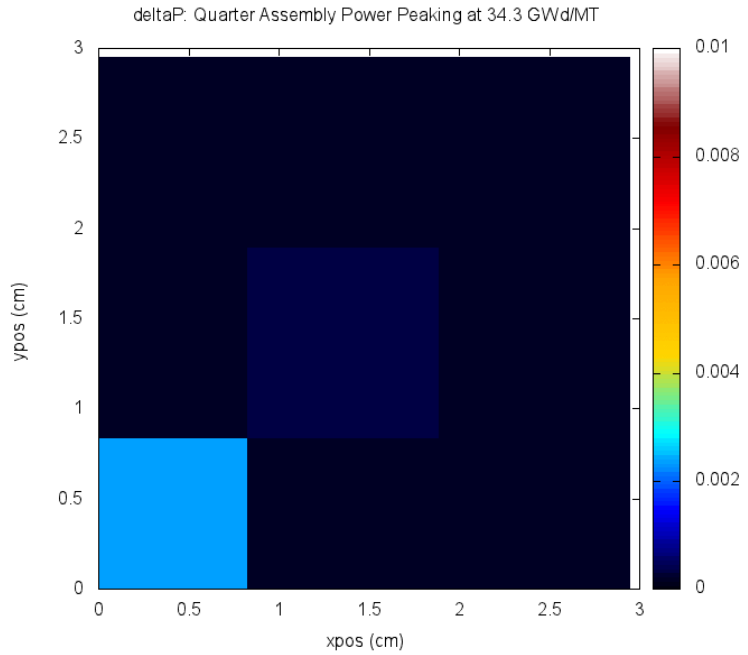

Figure 3-20. Largest Deviation in Relative Pin Power between 6x6 and 20x20 Single Whole Fuel Pin Mesh Cases

3.3.2.3. Poisoned Pin Mesh

To determine how the resolution of the radial regions in the poisoned pin under different mesh structures affects depletion results, only the mesh of the poisoned pin is varied. Structures in the quarter poisoned pin are chosen as 6x6 and 8x8 for comparison against the original 10x10 case, while the mesh of the remaining pins is held constant at 4x4 for the sake of computation time. The calculation settings for these cases are summarized in Table 3-8. Visual representations of the poisoned pin are given in Figures 3-21 and 3-22 for the 6x6 and 8x8 cases respectively. The poisoned pin for the 10x10 case is identical to Figure 3-10 above.

Table 3-8. Calculation Settings for Varying Poisoned Pin Mesh Cases

Parameter	Value
Radial Regions in Poisoned Pin	5
Single Whole Fuel Pin Mesh	4x4
P_N Scattering Order	Fuel: 0 Helium: 3 Clad: 1 Water: 3
S_N Quadrature Order	12
Energy Groups	238
Nuclides Explicitly Tracked	388

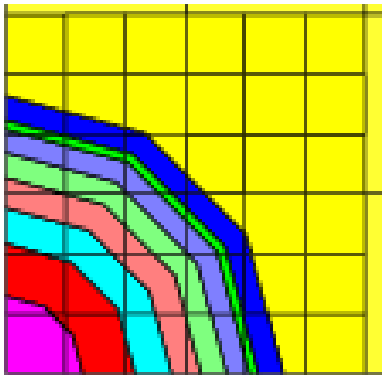

Figure 3-21. Quarter Poisoned Pin with 6x6 Mesh

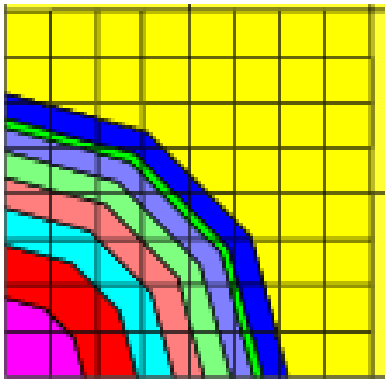

Figure 3-22. Quarter Poisoned Pin with 8x8 Mesh

Figure 3-23 below gives the k_{inf} trend for each case, and Figure 3-24 shows the deviation of k_{inf} of the 6x6 and 8x8 cases from the 10x10 case. Table 3-9 gives the computation time for each case. The deviations in k_{inf} are very small; the 6x6 case differs from the 10x10 case by no more than 12 pcm. The savings in computational effort, while certainly not insignificant, are relatively small as well. The difference in power peaking is compared between the 6x6 and

10x10 cases. The largest difference in relative pin power between these two cases is shown in Figure 3-25 below. This maximum difference is no more than 0.2 percent.

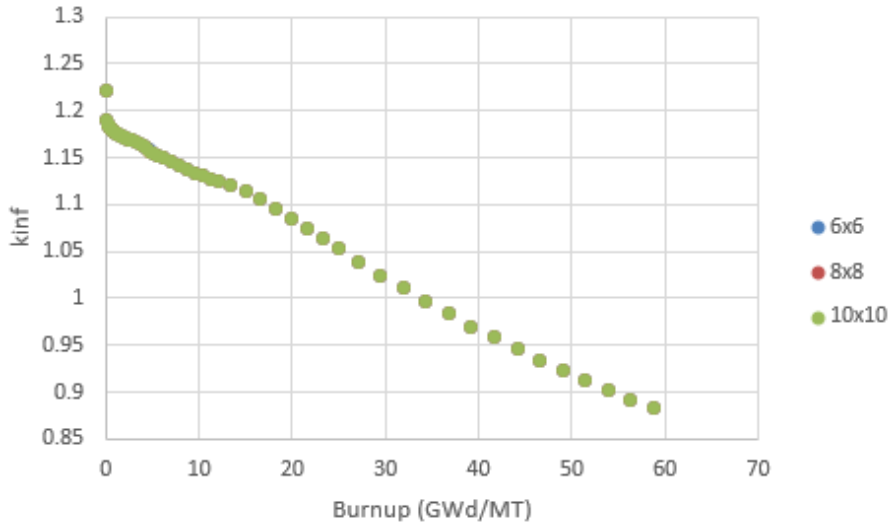

Figure 3-23. Depletion of Varying Poisoned Pin Mesh Cases

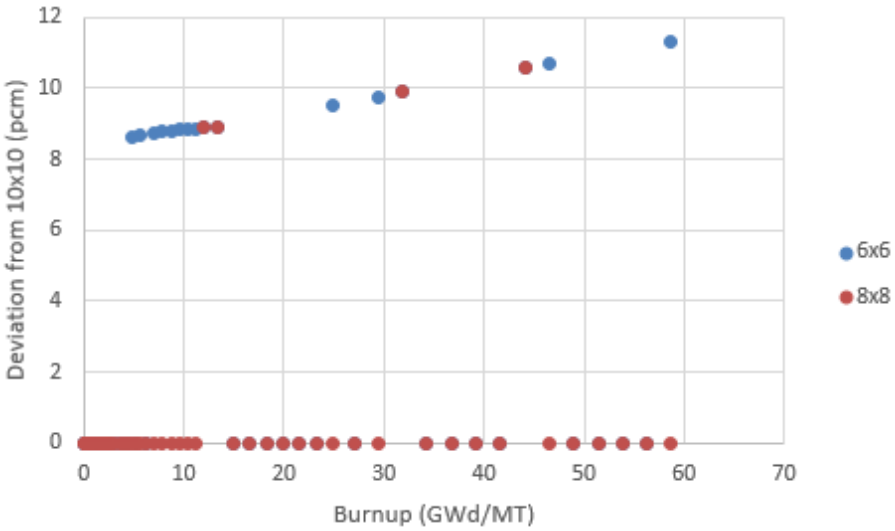

Figure 3-24. Deviation in k_{inf} among Varying Poisoned Pin Mesh Cases

Table 3-9. Computation Time for Varying Poisoned Pin Mesh Cases

Case	Time (hours)
6x6	22.89
8x8	23.38
10x10	28.29

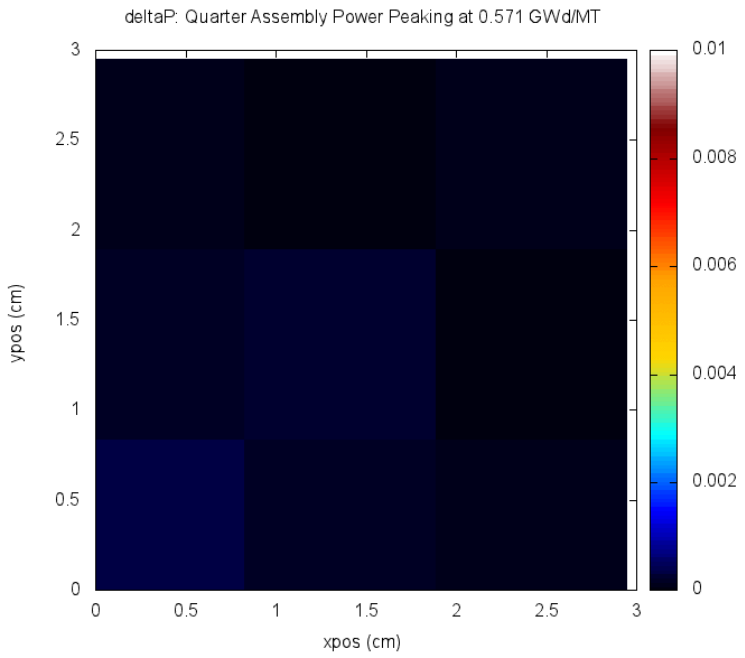

Figure 3-25. Largest Deviation in Relative Pin Power between 6x6 and 10x10 Poisoned Pin Mesh Cases

3.3.2.4. P_N Scattering Order

The scattering order of the fuel material (including the poisoned fuel) is now chosen as 0, 1, and 2, while that of the remaining materials are kept constant as discussed in Section IID. The "recommended" scattering order settings are tested as well (i.e., scattering order 1 for fuel, 0 for helium, 1 for clad, and 2 for water). The remaining calculation settings for these cases are summarized in Table 3-10 and are based on minimizing computation time while maintaining acceptable fidelity based on the results of cases studied up to this point. It should be emphasized that the data for the P_0 case is based on a model with a 10x10 mesh in the quarter poisoned pin; this data was available from previously run cases and is not expected to differ from a case with a 6x6 mesh by more than 12 pcm (based on the results presented in Section IIIC). The fuel assembly model for the P_0 case is identical to Figure 3-17 above, while the quarter poisoned pins for the remaining cases are identical to Figure 3-21.

Table 8. Calculation Settings for Varying Scattering Order Cases

Parameter	Value
Radial Regions in Poisoned Pin	5
Single Whole Fuel Pin Mesh	6x6
Quarter Poisoned Pin Mesh	6x6 (10x10 in P_0 case)
S_N Quadrature Order	12
Energy Groups	238
Nuclides Explicitly Tracked	388

Figure 3-26 below gives the k_{inf} trend for each case, and Figure 3-27 gives the deviation of k_{inf} from the P_2 case, which is expected to be the most accurate. Table 3-11 gives the computation time for each case. These results indicate that the recommended settings provide a high degree of accuracy with minimal computation time (although the reduction in time from the highest fidelity case is relatively minor). The power peaking shall therefore be compared between the P_2 and recommended cases. The largest difference in relative pin power between these two cases is given in Figure 3-28, and it is seen to be no greater than 0.2 percent.

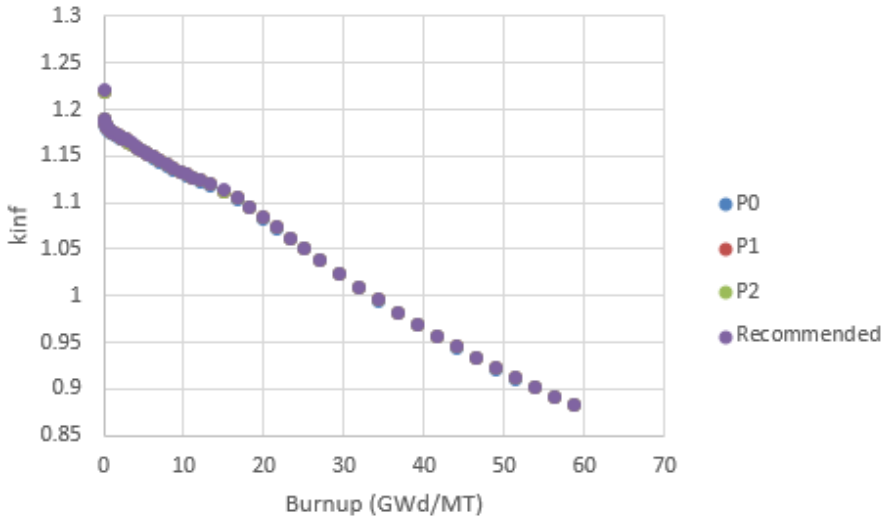

Figure 3-26. Depletion of Varying Scattering Order Cases

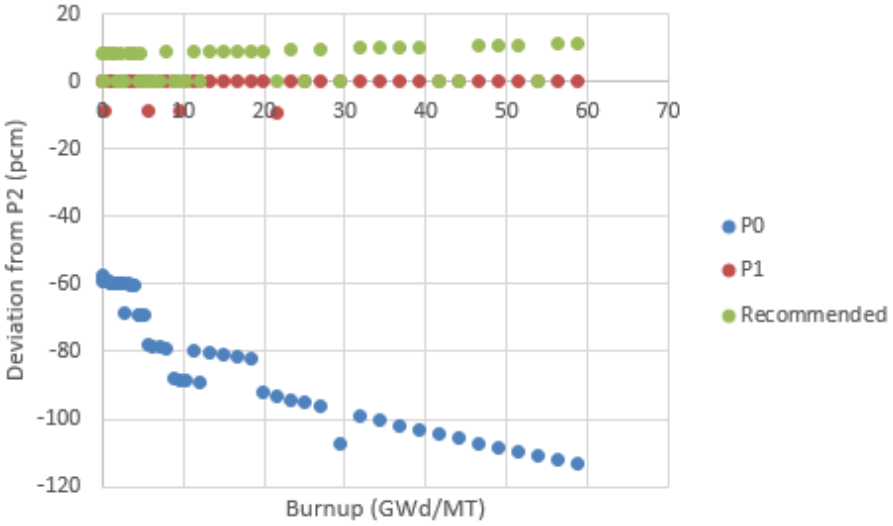

Figure 3-27. Deviation in k_{inf} among Varying Scattering Order Cases

Table 3-11. Computation Time for Varying Scattering Order Cases

Case	Time (hours)
P_0	36.92
P_1	29.2
P_2	29.63
Recommended	28.52

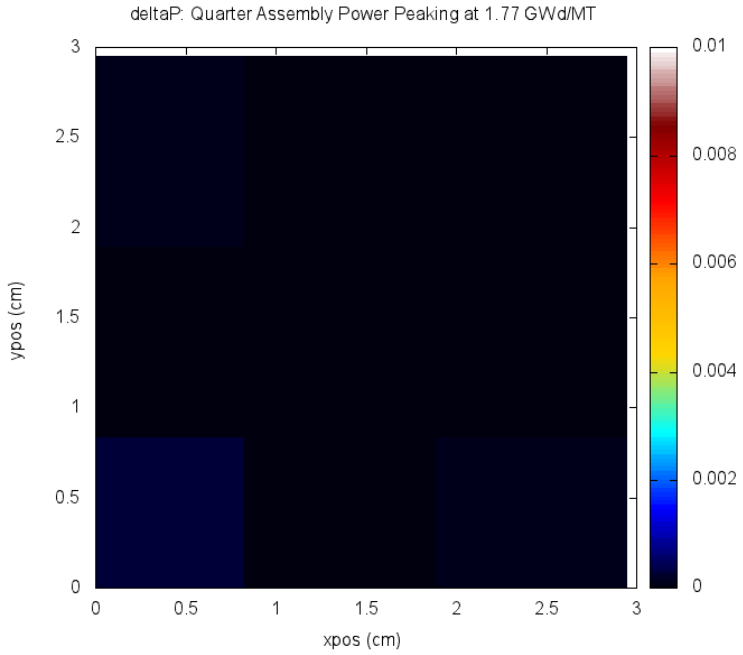

Figure 3-28. Largest Deviation in Relative Pin Power between Recommended and P_2 Scattering Order Cases

3.3.2.5. S_N Quadrature Order

Cases previously run with S_{12} transport calculations have demonstrated relatively short computation time; therefore, any loss in accuracy relative to the S_{16} setting should be quantified. The remaining calculation parameters are given in Table 3-12. The fuel assembly models used in these cases are visually identical to that given in Figure 3-9.

Table 3-12. Calculation Settings for Varying Quadrature Order Cases

Parameter	Value
Radial Regions in Poisoned Pin	5
Single Whole Fuel Pin Mesh	20x20
Quarter Poisoned Pin Mesh	10x10
P_N Scattering Order	Fuel: 0 Helium: 3 Clad: 1 Water: 3
Energy Groups	238
Nuclides Explicitly Tracked	388

Figure 3-29 below gives the depletion trend in k_{inf} for both cases, and Figure 3-30 gives the deviation in k_{inf} of the S_{12} case from the S_{16} case. Table 3-13 gives the computation time used for these cases. The difference in k_{inf} is minimal, and significant savings in computation time are realized as well. Figure 3-31 shows the largest difference in relative pin power between the two cases. This maximum difference is well under 0.3 percent.

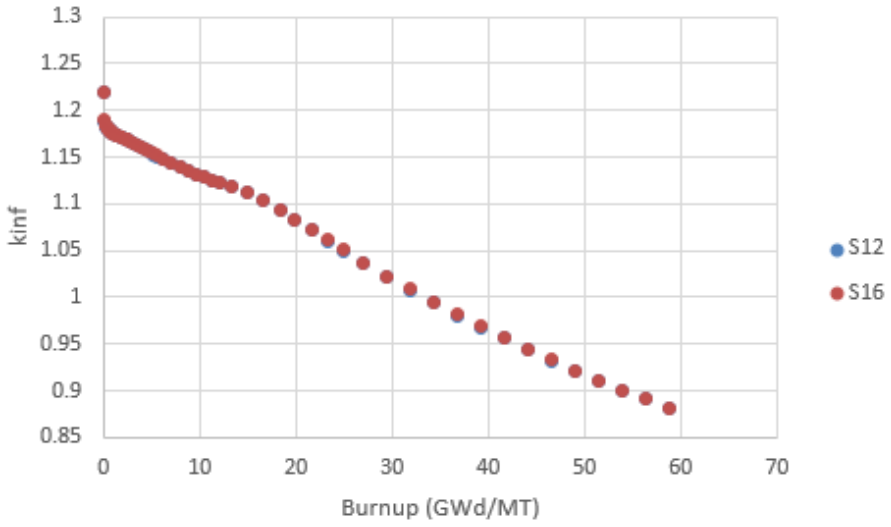

Figure 3-29. Depletion of Varying Quadrature Order Cases

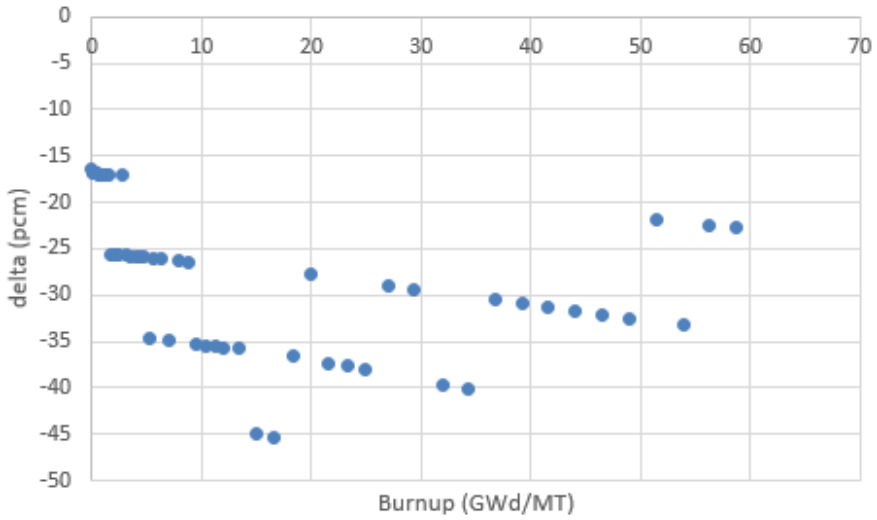

Figure 3-30. Deviation in k_{inf} of S_{12} Case from S_{16} Case

Table 3-13. Computation Time for Varying Quadrature Order Cases

Case	Time (hours)
S_{12}	150.72
S_{16}	230.66

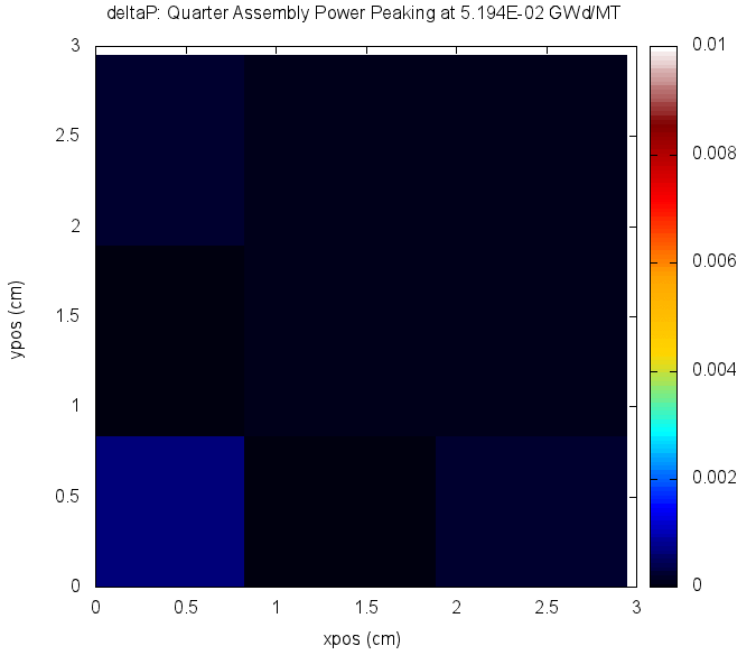

Figure 3-31. Largest Deviation in Relative Pin Power between S_{12} and S_{16} Cases

3.3.2.6. Energy Groups

The impact of the cross section library on depletion results is now explored. As discussed previously, cross section libraries of 44, 49, and 238 groups shall be considered. The remaining calculation parameters are given in Table 3-14 below. In these cases, comparison is made against a 238-group case with a 10x10 mesh in the quarter poisoned pin while the remaining cases have a 6x6 mesh; again, this data was already available from previous calculations and is not expected to deviate from a corresponding 6x6 structure by greater than 12 pcm. The fuel assembly model for the 238-group case is identical to Figure 3-17, while the remaining cases have quarter poisoned pins identical to Figure 3-21.

Table 3-14. Calculation Settings for Varying Energy Groups Cases

Parameter	Value
Radial Regions in Poisoned Pin	5
Single Whole Fuel Pin Mesh	6x6
Quarter Poisoned Pin Mesh	6x6 (10x10 in 238-group case)
P_N Scattering Order	Fuel: 0 Helium: 3 Clad: 1 Water: 3
S_N Quadrature Order	12
Nuclides Explicitly Tracked	388

Figure 3-32 gives the k_{inf} trend for each case, and Figure 3-33 gives the deviation in k_{inf} of each case relative to the 238-group case. Table 3-15 gives the computation time used for each case. A significant reduction in computation time is realized in the 49-group case with acceptable accuracy in k_{inf}. The relative pin power for this case shall therefore be compared with that of the 238-group case. The largest deviation in relative pin power between these two cases is given in Figure 3-34. This maximum discrepancy is within 2 percent, which is noticeably larger than the discrepancies found in previous cases.

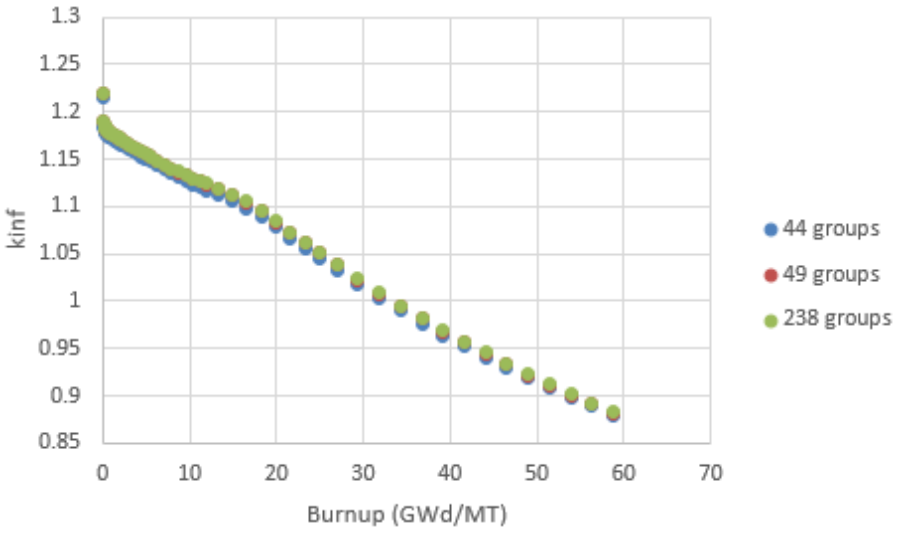

Figure 3-32. Depletion of Varying Energy Groups Cases

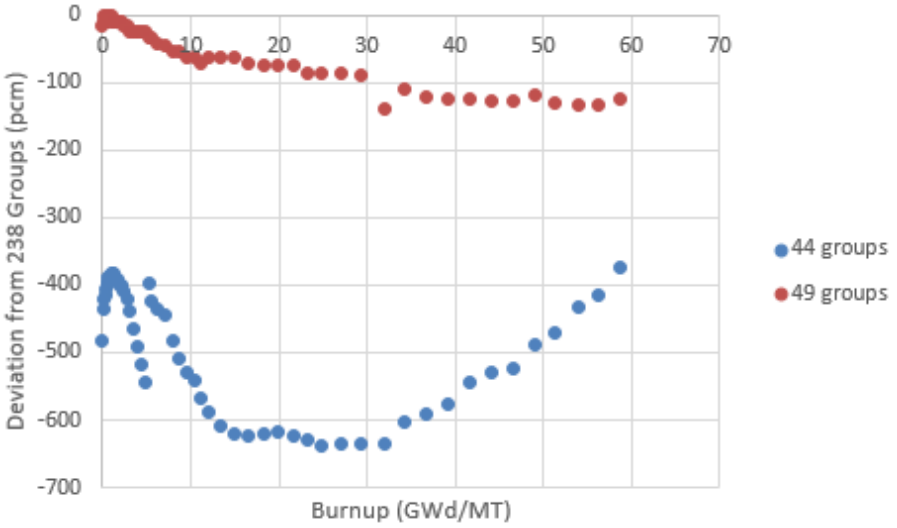

Figure 3-33. Deviation in k_{inf} among Varying Energy Groups Cases

Table 3-15. Computation Time for Varying Energy Groups Cases

Case	Time (hours)
44 groups	13.62
49 groups	6.65
238 groups	36.92

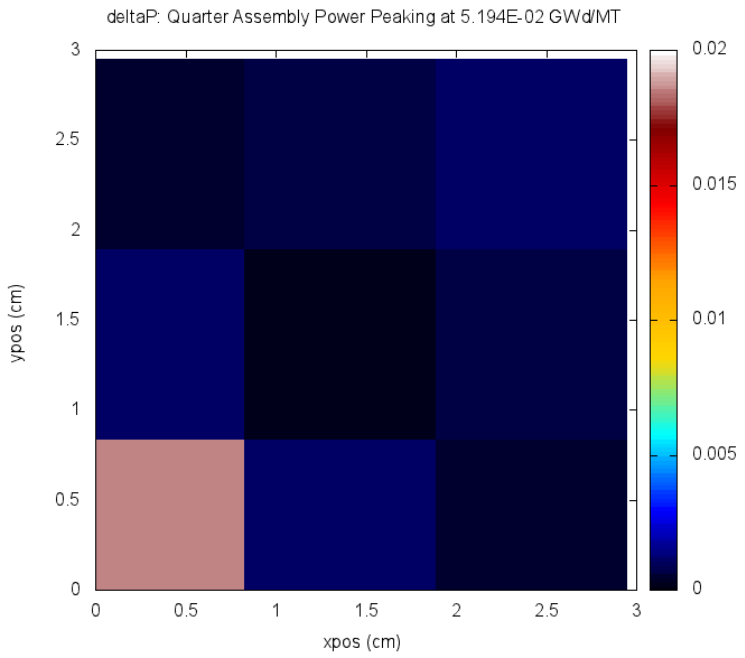

Figure 3-34. Largest Deviation in Relative Pin Power between 49- and 238-Group Cases

3.3.2.7. Explicit Nuclide Tracking

The "addnux" parameter in the SCALE input file is now varied to determine the impact of the number of nuclides explicitly tracked on depletion results. Cases will be run with 15, 94, 230, and 388 nuclides tracked. Again, the fuel assembly model for the 388-nuclide case is identical to Figure 3-17, while those of the other cases have quarter poisoned pins identical to Figure 3-21 (the results for the 388-nuclide case were again available from previous studies and should not significantly differ from cases with a 6x6 mesh in the quarter poisoned pin). The calculation settings for these cases are summarized in Table 3-16.

Table 3-16. Calculation Settings for Varying Nuclide Tracking Cases

Parameter	Value
Radial Regions in Poisoned Pin	5
Single Whole Fuel Pin Mesh	6x6
Quarter Poisoned Pin Mesh	6x6 (10x10 in 388-nuclide case)
P_N Scattering Order	Fuel: 0 Helium: 3 Clad: 1 Water: 3
S_N Quadrature Order	12
Energy Groups	238

The k_{inf} trend for these cases is given in Figure 3-35, and the deviation in k_{inf} relative to the 388-nuclide case is given in Figure 3-36. Figure 3-37 gives a clearer view of the deviation of the 94- and 230-nuclide cases. Table 3-17 gives the computation time used for each case as well. These results indicate only a minor reduction in computation time with introduction of significant error by reducing the number of nuclides tracked. Thus there is no need to examine the power peaking for these cases.

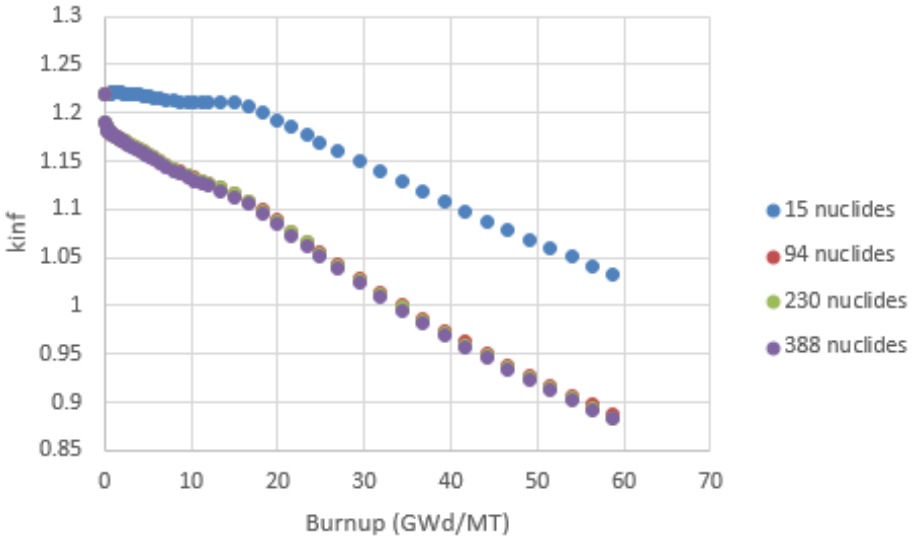

Figure 3-35. Depletion of Varying Nuclide Tracking Cases

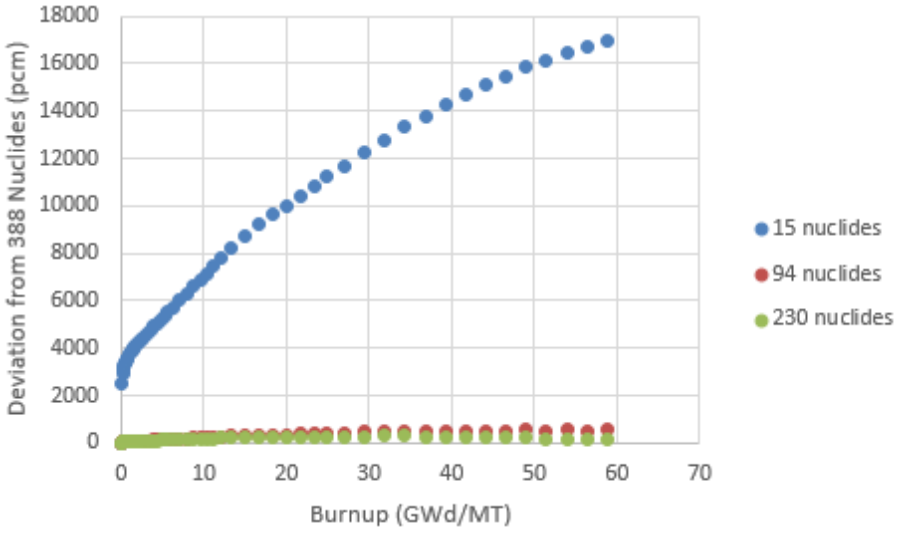

Figure 3-36. Deviation in k_{inf} among Varying Nuclide Tracking Cases

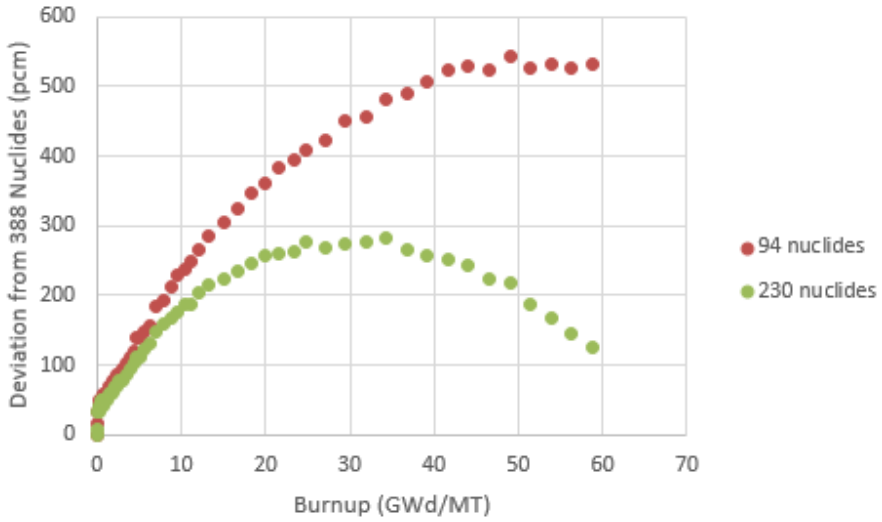

Figure 3-37. Deviation in k_{inf} of 94- and 230-Nuclide Cases from 388-Nuclide Case

Table 3-17. Computation Time for Varying Nuclide Tracking Cases

Case	Time (hours)
15 nuclides	20.43
94 nuclides	22.78
230 nuclides	25.33
388 nuclides	36.92

3.3.3. Recommendations

Based on the results presented above, the variables which have the largest impact on computation time are the single whole fuel pin mesh, the S_N quadrature order, and the cross section library. By far the greatest reduction in computation time was achieved using the 49-group problem-specific cross section library. It is therefore worthwhile to employ this setting to optimize computation time and alter the remaining variables to recover losses in accuracy in k_{inf} and relative pin power.

The results of the previous section indicate a relatively strong dependence of relative pin power on the number of radial regions in the poisoned pin. Therefore, in order to maintain reasonable accuracy, 10 radial regions shall be used in future models. Significant savings in computation time are realized by coarsening the mesh, but nontrivial error is introduced as well. This trade-off shall be reconciled by employing a 12x12 mesh in a single whole fuel pin, and a

6x6 mesh in the quarter poisoned pin (thus yielding a constant mesh size throughout the model). The P_N scattering order settings shall be chosen to match the "recommended" case, as these settings yield the best computation time with only a small loss in accuracy. The quadrature order shall be set at S_{12}, as again this setting yields significant reduction in computation time with a small loss in accuracy. Finally, the nuclide tracking should remain at 388 nuclides, as any reduction introduces large error with only a small reduction in computation time. These recommended settings are summarized in Table 3-18.

Table 3-18. Recommended Calculation Settings

Parameter	Value
Radial Regions in Poisoned Pin	10
Single Whole Fuel Pin Mesh	12x12
Quarter Poisoned Pin Mesh	6x6
P_N Scattering Order	Fuel: 1 Helium: 0 Clad: 1 Water: 2
S_N Quadrature Order	12
Energy Groups	49
Nuclides Explicitly Tracked	388

These settings are tested in a final run for comparison against the 15-region case from Section 3.3.2.1 above, which is expected to be the most accurate of the cases tested in this study. The deviation in k_{inf} from the 15-region case throughout the depletion is shown in Figure 3-38 below. This calculation ran in approximately 12 hours, and the maximum difference in k_{inf} from the 15-region case is no greater than 140 pcm. It was verified by hand that the maximum difference in pin power peaking was less than 0.6 percent. These settings shall therefore be considered appropriate for use with larger assembly models in future calculations.

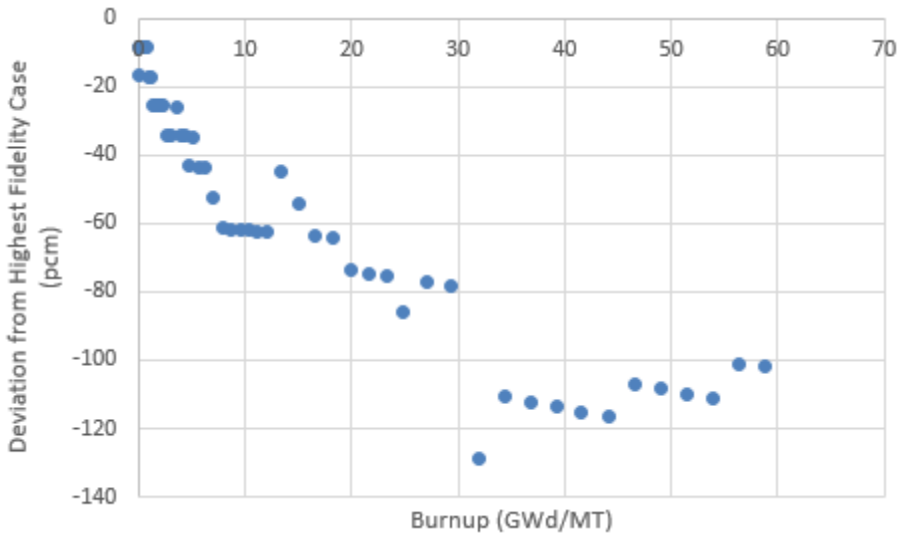

Figure 3-38. Deviation in k_{inf} of Final Settings Case from Highest Fidelity Case

4. RESULTS

In this chapter, the results of the control rod and BA design calculations are presented separately. Section 4.1 gives the control rod CBC and reactivity worth results, and Section 4.2 gives the BA optimization results.

4.1. Control Rods

As discussed in Chapter 3, the CBC for each design is first calculated to feed into subsequent control rod worth calculations. The rodded and unrodded reactivity of each case is then calculated so that worth may be determined from Equations 1 and 2.

4.1.1. CBC

It is expected that the following CBC values will be unrealistically high, as they approximately represent the combined spectral effect of soluble boron and BAs and bring the multiplication eigenvalue to unity. Figures 4-1 to 4-4 below plot the neutron multiplication eigenvalue against boron concentration for each assembly configuration considered (24, 28, and 32 guide tubes per assembly as well as the reference case) in four quarter assembly geometry only. This data is given explicitly in Tables 4-1 to 4-4. Finally, Table 4-5 gives the critical boron concentration for each case, determined from linear interpolation of the preceding data. This interpolation is appropriately accurate, as the k_{inf} vs. boron curves appear to exhibit linear behavior. Only the results for the four quarter assembly geometry are presented here, as the single quarter cases are essentially identical to the four quarter assembly cases with all control rods withdrawn and reflective boundary conditions imposed on all boundaries.

Table 4-1. Neutron Multiplication vs. Boron for 19x19 Silicide Assembly with 24 Control Rods Withdrawn

Boron (ppm)	Four Unrodded Quarter Assemblies k_{inf}
0	1.33075
2000	1.19612
3000	1.14069
4000	1.09141
5000	1.04730
6000	1.00758
7000	0.97161
8000	0.93889

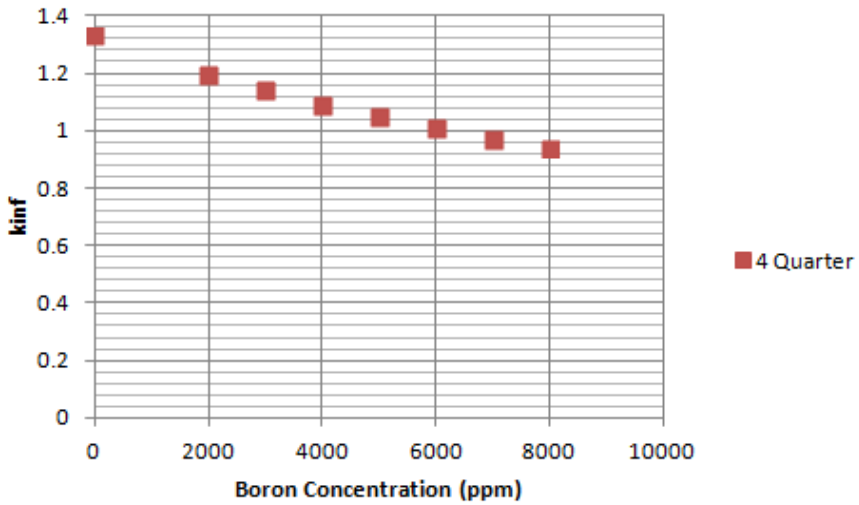

Figure 4-1. Neutron Multiplication vs. Boron for 19x19 Silicide Assembly with 24 Control Rods Withdrawn

Table 4-2. Neutron Multiplication vs. Boron for 19x19 Silicide Assembly with 28 Control Rods Withdrawn

Boron (ppm)	Four Unrodded Quarter Assemblies k_{inf}
0	1.33321
2000	1.19570
3000	1.13926
4000	1.08918
5000	1.04443
6000	1.00420
7000	0.96781
8000	0.93475

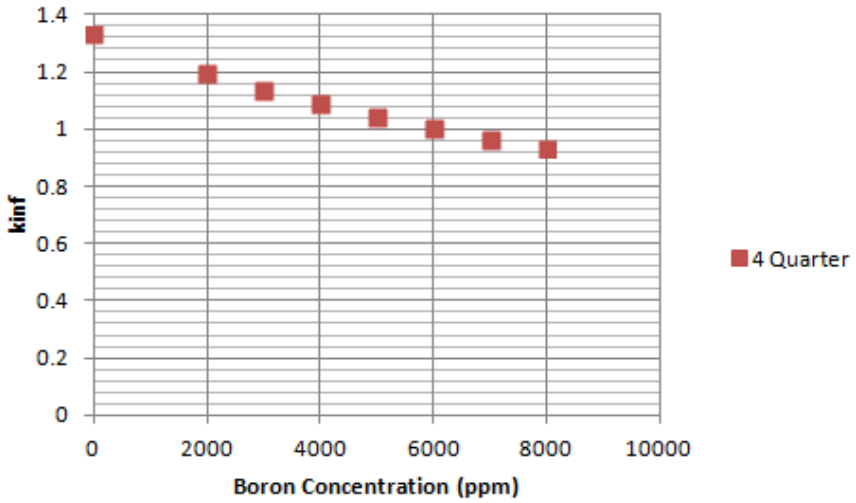

Figure 4-2. Neutron Multiplication vs. Boron for 19x19 Silicide Assembly with 28 Control Rods Withdrawn

Table 4-3. Neutron Multiplication vs. Boron for 19x19 Silicide Assembly with 32 Control Rods Withdrawn

Boron (ppm)	Four Unrodded Quarter Assemblies k_{inf}
0	1.33554
2000	1.19502
3000	1.13757
4000	1.08669
5000	1.04130
6000	1.00055
7000	0.96375
8000	0.93035

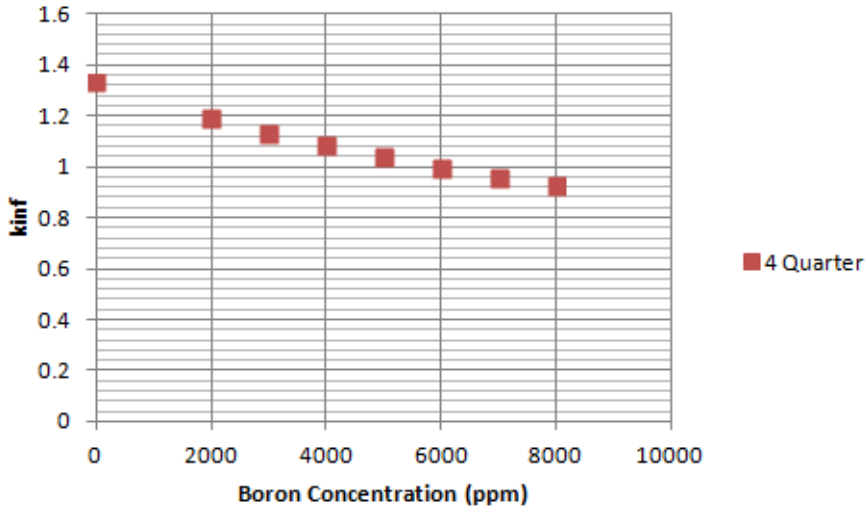

Figure 4-3. Neutron Multiplication vs. Boron for 19x19 Silicide Assembly with 32 Control Rods Withdrawn

Table 4-4. Neutron Multiplication vs. Boron for 17x17 Oxide Assembly with 24 Control Rods Withdrawn

Boron (ppm)	Four Unrodded Quarter Assemblies k_{inf}
0	1.39876
2000	1.21779
3000	1.14655
4000	1.08472
5000	1.03054
6000	0.98268
7000	0.94007
8000	0.90189

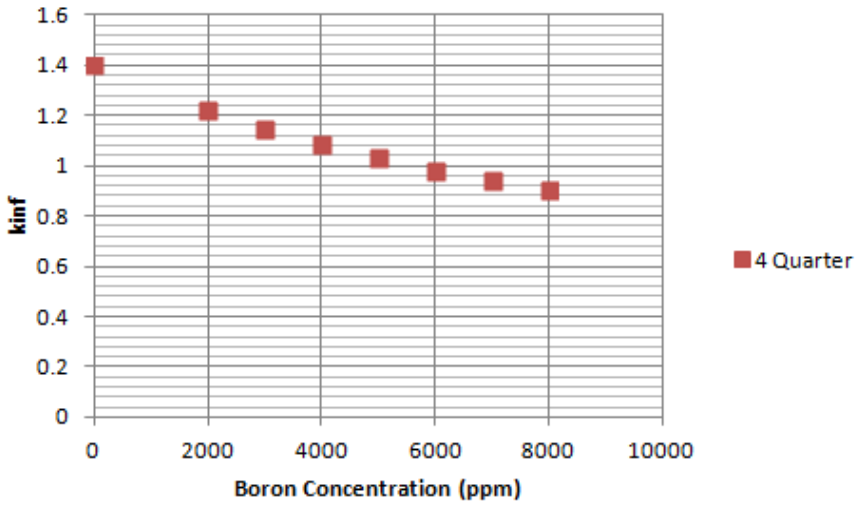

Figure 4-4. Neutron Multiplication vs. Boron for 17x17 Oxide Assembly with 24 Control Rods Withdrawn

Table 4-5. Critical Boron Concentrations

Case	Four Unrodded Quarter Assemblies CBC (ppm)
19x19 Silicide Assembly with 24 Control Rods	6211
19x19 Silicide Assembly with 28 Control Rods	6115
19x19 Silicide Assembly with 32 Control Rods	6015
17x17 Oxide Assembly with 24 Control Rods	5638

4.1.2. Reactivity Worth

Tables 4-6 to 4-11 below give the neutron multiplication eigenvalues for each control rod material and core configuration with the critical soluble boron (taken from Table 4-5) and without soluble boron.

Table 4-6. Neutron Multiplication Eigenvalues with AIC Control Rods – Single Quarter Assembly Rodded

Case	No Boron k_{out}	No Boron k_{in}	CBC k_{out}	CBC k_{in}
19x19 Silicide Assembly with 24 Control Rods	1.33073	1.07501	0.99971	0.86095
19x19 Silicide Assembly with 28 Control Rods	1.33321	1.04184	0.99981	0.84056
19x19 Silicide Assembly with 32 Control Rods	1.33553	1.01060	0.99997	0.82116
17x17 Oxide Assembly with 24 Control Rods	1.39943	1.04443	0.99934	0.81674

Table 4-7. Neutron Multiplication Eigenvalues with AIC Control Rods – 2 of 4 Quarter Assemblies Rodded

Case	No Boron k_{out}	No Boron k_{in}	CBC k_{out}	CBC k_{in}
19x19 Silicide Assembly with 24 Control Rods	1.33075	1.20712	0.99971	0.93238
19x19 Silicide Assembly with 28 Control Rods	1.33321	1.19366	0.99981	0.92312
19x19 Silicide Assembly with 32 Control Rods	1.33554	1.18110	0.99997	0.91442
17x17 Oxide Assembly with 24 Control Rods	1.39876	1.22681	0.99934	0.91046

Table 4-8. Neutron Multiplication Eigenvalues with B_4C Control Rods – Single Quarter Assembly Rodded

Case	No Boron k_{out}	No Boron k_{in}	CBC k_{out}	CBC k_{in}
19x19 Silicide Assembly with 24 Control Rods	1.33073	0.97212	0.99971	0.78437
19x19 Silicide Assembly with 28 Control Rods	1.33321	0.92935	0.99981	0.75591
19x19 Silicide Assembly with 32 Control Rods	1.33553	0.88933	0.99997	0.72905
17x17 Oxide Assembly with 24 Control Rods	1.39943	0.92495	0.99934	0.72928

Table 4-9. Neutron Multiplication Eigenvalues with B_4C Control Rods – 2 of 4 Quarter Assemblies Rodded

Case	No Boron k_{out}	No Boron k_{in}	CBC k_{out}	CBC k_{in}
19x19 Silicide Assembly with 24 Control Rods	1.33075	1.15833	0.99971	0.89587
19x19 Silicide Assembly with 28 Control Rods	1.33321	1.14126	0.99981	0.88337
19x19 Silicide Assembly with 32 Control Rods	1.33554	1.12536	0.99997	0.87166
17x17 Oxide Assembly with 24 Control Rods	1.39876	1.16937	0.99934	0.86834

Table 4-10. Neutron Multiplication Eigenvalues with Hf Control Rods – Single Quarter Assembly Rodded

Case	No Boron k_{out}	No Boron k_{in}	CBC k_{out}	CBC k_{in}
19x19 Silicide Assembly with 24 Control Rods	1.33073	1.07746	0.99971	0.85977
19x19 Silicide Assembly with 28 Control Rods	1.33321	1.04439	0.99981	0.83924
19x19 Silicide Assembly with 32 Control Rods	1.33553	1.01301	0.99997	0.81961
17x17 Oxide Assembly with 24 Control Rods	1.39943	1.04922	0.99934	0.81629

Table 4-11. Neutron Multiplication Eigenvalues with Hf Control Rods – 2 of 4 Quarter Assemblies Rodded

Case	No Boron k_{out}	No Boron k_{in}	CBC k_{out}	CBC k_{in}
19x19 Silicide Assembly with 24 Control Rods	1.33075	1.20842	0.99971	0.93189
19x19 Silicide Assembly with 28 Control Rods	1.33321	1.19503	0.99981	0.92260
19x19 Silicide Assembly with 32 Control Rods	1.33554	1.18243	0.99997	0.91383
17x17 Oxide Assembly with 24 Control Rods	1.39876	1.22928	0.99934	0.91035

The data presented above are then used to calculate the reactivity worth for each control rod material in each assembly configuration with and without boron. The percentage of control rod worth lost due to the presence of soluble boron is calculated as well. These results are given in Tables 4-12 to 4-17 below and are plotted for visual comparison in Figures 4-5 to 4-10. Tables 4-12 to 4-17 give the worth calculated from both Equations 1 and 2, but Figures 4-5 to 4-10 only plot the results obtained using Equation 1.

Table 4-12. AIC Control Rod Worth – Single Quarter Assembly Rodded

Case	Equation 1 Worth (pcm) – No Boron	Equation 1 Worth (pcm) – CBC	Equation 2 Worth (pcm) – No Boron	Equation 2 Worth (pcm) – CBC	% Equation 1 Worth Lost due to Boron	% Equation 2 Worth Lost due to Boron
19x19 Silicide Assembly with 24 Control Rods	19217	13880	21340	14943	27.77	29.98
19x19 Silicide Assembly with 28 Control Rods	21854	15929	24660	17350	27.12	29.64
19x19 Silicide Assembly with 32 Control Rods	24330	17881	27879	19701	26.50	29.33
17x17 Oxide Assembly with 24 Control Rods	25367	18273	29259	20178	27.97	31.04

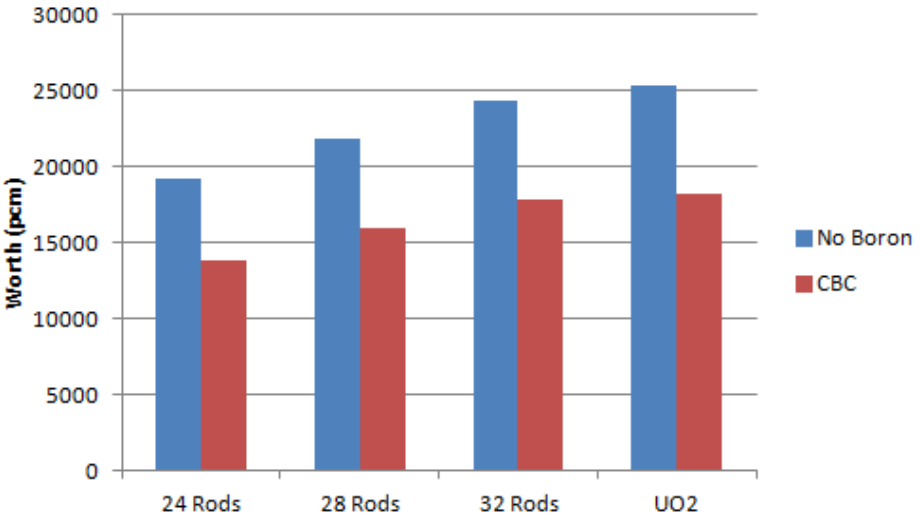

Figure 4-5. AIC Control Rod Worth – Single Quarter Assembly Rodded

Table 4-13. AIC Control Rod Worth – 2 of 4 Quarter Assemblies Rodded

Case	Equation 1 Worth (pcm) – No Boron	Equation 1 Worth (pcm) – CBC	Equation 2 Worth (pcm) – No Boron	Equation 2 Worth (pcm) – CBC	% Equation 1 Worth Lost due to Boron	% Equation 2 Worth Lost due to Boron
19x19 Silicide Assembly with 24 Control Rods	9290	6735	9750	6973	27.50	28.49
19x19 Silicide Assembly with 28 Control Rods	10467	7671	11056	7981	26.71	27.82
19x19 Silicide Assembly with 32 Control Rods	11564	8556	12289	8944	26.01	27.22
17x17 Oxide Assembly with 24 Control Rods	12293	8893	13117	9314	27.66	28.99

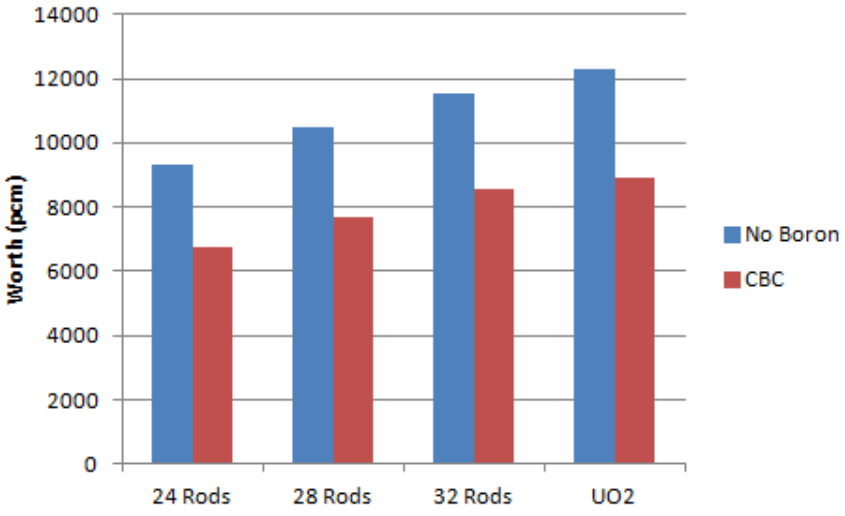

Figure 4-6. AIC Control Rod Worth – 2 of 4 Quarter Assemblies Rodded

Table 4-14. B_4C Control Rod Worth – Single Quarter Assembly Rodded

Case	Equation 1 Worth (pcm) – No Boron	Equation 1 Worth (pcm) – CBC	Equation 2 Worth (pcm) – No Boron	Equation 2 Worth (pcm) – CBC	% Equation 1 Worth Lost due to Boron	% Equation 2 Worth Lost due to Boron
19x19 Silicide Assembly with 24 Control Rods	26948	21540	31401	24258	20.07	22.75
19x19 Silicide Assembly with 28 Control Rods	30292	24395	36086	27965	19.47	22.50
19x19 Silicide Assembly with 32 Control Rods	33410	27093	40661	31598	18.91	22.29
17x17 Oxide Assembly with 24 Control Rods	33905	27024	41408	31504	20.30	23.92

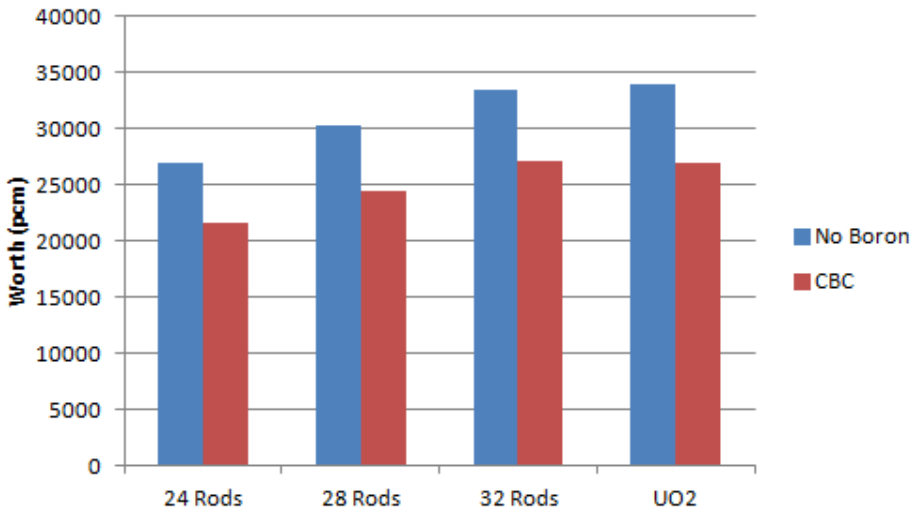

Figure 4-7. B_4C Control Rod Worth – Single Quarter Assembly Rodded

Table 4-15. B_4C Control Rod Worth – 2 of 4 Quarter Assemblies Rodded

Case	Equation 1 Worth (pcm) – No Boron	Equation 1 Worth (pcm) – CBC	Equation 2 Worth (pcm) – No Boron	Equation 2 Worth (pcm) – CBC	% Equation 1 Worth Lost due to Boron	% Equation 2 Worth Lost due to Boron
19x19 Silicide Assembly with 24 Control Rods	12957	10387	13876	10967	19.84	20.97
19x19 Silicide Assembly with 28 Control Rods	14398	11647	15546	12383	19.11	20.35
19x19 Silicide Assembly with 32 Control Rods	15737	12832	17123	13733	18.46	19.80
17x17 Oxide Assembly with 24 Control Rods	16400	13108	17912	14051	20.07	21.56

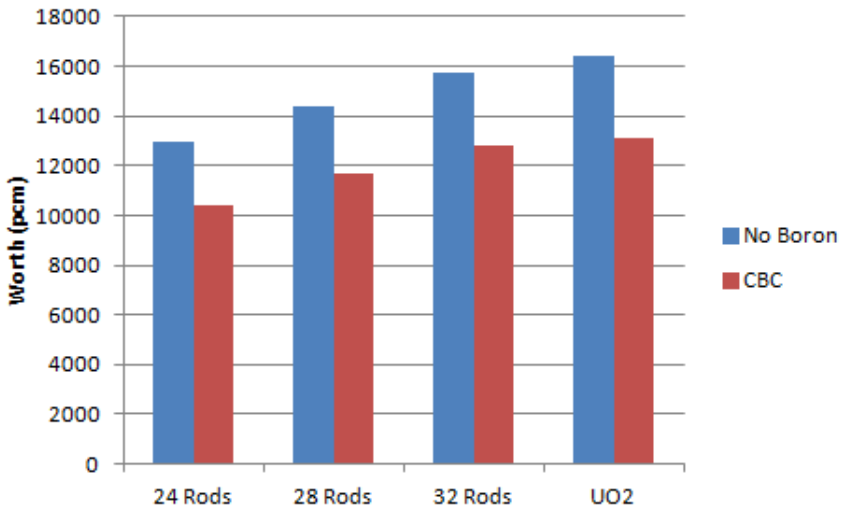

Figure 4-8. B_4C Control Rod Worth – 2 of 4 Quarter Assemblies Rodded

Table 4-17. Hf Control Rod Worth – Single Quarter Assembly Rodded

Case	Equation 1 Worth (pcm) – No Boron	Equation 1 Worth (pcm) – CBC	Equation 2 Worth (pcm) – No Boron	Equation 2 Worth (pcm) – CBC	% Equation 1 Worth Lost due to Boron	% Equation 2 Worth Lost due to Boron
19x19 Silicide Assembly with 24 Control Rods	19033	13998	21113	15079	26.46	28.58
19x19 Silicide Assembly with 28 Control Rods	21663	16061	24415	17508	25.86	28.29
19x19 Silicide Assembly with 32 Control Rods	24149	18036	27640	19889	25.31	28.04
17x17 Oxide Assembly with 24 Control Rods	25025	18317	28802	20233	26.80	29.75

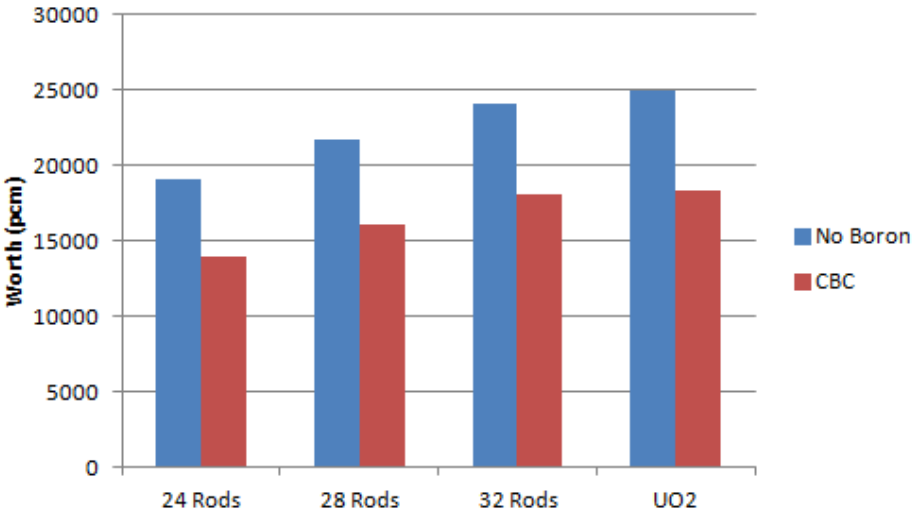

Figure 4-9. Hf Control Rod Worth – Single Quarter Assembly Rodded

Table 4-17. Hf Control Rod Worth – 2 of 4 Quarter Assemblies Rodded

Case	Equation 1 Worth (pcm) – No Boron	Equation 1 Worth (pcm) – CBC	Equation 2 Worth (pcm) – No Boron	Equation 2 Worth (pcm) – CBC	% Equation 1 Worth Lost due to Boron	% Equation 2 Worth Lost due to Boron
19x19 Silicide Assembly with 24 Control Rods	9193	6784	9643	7025	26.21	27.15
19x19 Silicide Assembly with 28 Control Rods	10365	7723	10942	8037	25.49	26.55
19x19 Silicide Assembly with 32 Control Rods	11464	8615	12176	9009	24.85	26.01
17x17 Oxide Assembly with 24 Control Rods	12116	8905	12916	9327	26.50	27.79

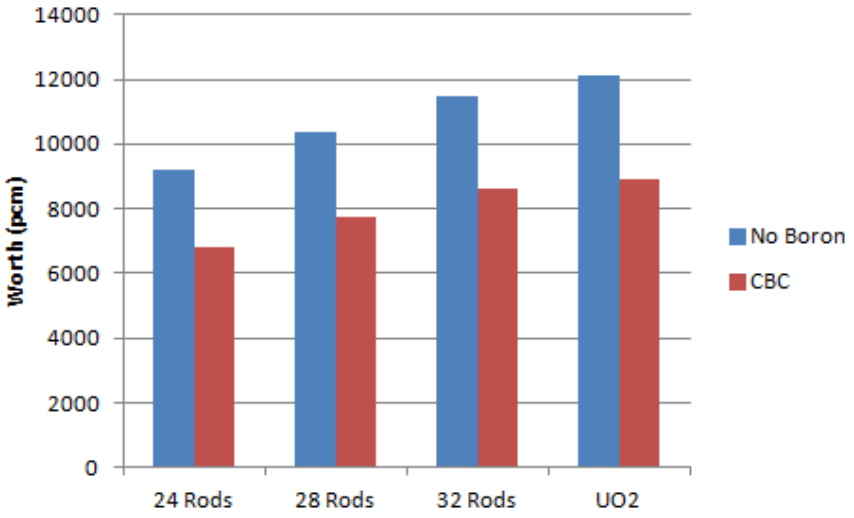

Figure 4-10. Hf Control Rod Worth – 2 of 4 Quarter Assemblies Rodded

4.2. Burnable Absorbers

Eight iterations of BA design populations have been accumulated for each case. The depletion characteristics of each case are addressed first before examining specifically the BOC reactivity characteristics.

4.2.1. Depletion Results

The key depletion performance metrics for each iteration of each case, including the uncontrolled lattice, are given in Tables 4-18 to 4-24 below. In order to provide a quantifiable measure of the BA arrangement in each case, the average poison position is reported for each iteration as well. This value gives the midpoint of all the poisoned pin positions in a single fuel

assembly quadrant, where (0,0) corresponds to the center of the lattice and (9,9) corresponds to the outer corner. Only one coordinate is reported, as the midpoint will always lie on the line y=x due to the symmetry of the assembly. The exact BA arrangements are shown for each iteration in Appendix B. The metrics given are the BOC neutron multiplication eigenvalue, BA reactivity worth relative to the uncontrolled lattice, maximum and minimum power peaking, burnup at which these maxima and minima occur, discharge burnup, and the cycle length.

Table 4-18. Depletion Performance Metrics – Uncontrolled

Iteration	Avg Poison Position	BOC k	BA Worth (pcm)	Max Power Peaking	BU of Max Peaking (GWd/MT)	Min Power Peaking	BU of Min Peaking (GWd/MT)	Discharge BU (GWd/MT)	Cycle Length (days)
NA	NA	1.3320	NA	1.0637	0.109	0.9435	0	30.70	851

Table 4-19. Depletion Performance Metrics – 8 Gd Pins, 4 w/o

Iteration	Avg Poison Position	BOC k	BA Worth (pcm)	Max Power Peaking	BU of Max Peaking (GWd/MT)	Min Power Peaking	BU of Min Peaking (GWd/MT)	Discharge BU (GWd/MT)	Cycle Length (days)
1	2.333	1.2796	-3934	1.0806	0	0.3590	0	30.35	841
2	2.500	1.2819	-3761	1.0701	0	0.3534	0	30.35	841
3	3.500	1.2801	-3896	1.0797	0	0.3585	0	30.35	841
4	4.000	1.2803	-3881	1.0999	0	0.3587	0	30.35	841
5	3.500	1.2816	-3784	1.0892	0	0.3554	0	30.35	841
6	3.000	1.2809	-3836	1.0724	0.328	0.3559	0	30.35	841
7	3.000	1.2828	-3694	1.0838	0	0.3523	0	30.35	841
8	2.500	1.2819	-3761	1.0701	0	0.3534	0	30.35	841

Table 4-20. Depletion Performance Metrics – 8 Gd Pins, 8 w/o

Iteration	Avg Poison Position	BOC k	BA Worth (pcm)	Max Power Peaking	BU of Max Peaking (GWd/MT)	Min Power Peaking	BU of Min Peaking (GWd/MT)	Discharge BU (GWd/MT)	Cycle Length (days)
1	2.333	1.2710	-4580	1.0863	0	0.2435	0	30.11	833
2	2.500	1.2737	-4377	1.0743	0	0.2398	0	30.13	834
3	3.500	1.2715	-4542	1.0854	0	0.2431	0	30.13	834
4	4.000	1.2716	-4535	1.1054	0	0.2440	0	30.13	834
5	3.500	1.2730	-4429	1.0924	0	0.2421	0	30.13	834
6	3.000	1.2725	-4467	1.0760	0	0.2417	0	30.13	834
7	3.000	1.2745	-4317	1.0860	0	0.2390	0	30.13	834
8	2.500	1.2737	-4377	1.0743	0	0.2398	0	30.13	834

Table 4-21. Depletion Performance Metrics – 16 Gd Pins, 4 w/o

Iteration	Avg Poison Position	BOC k	BA Worth (pcm)	Max Power Peaking	BU of Max Peaking (GWd/MT)	Min Power Peaking	BU of Min Peaking (GWd/MT)	Discharge BU (GWd/MT)	Cycle Length (days)
1	3.750	1.2303	-7635	1.0911	0	0.3713	0	30.02	831
2	3.750	1.2288	-7748	1.0895	0	0.3669	0	30.01	830
3	4.500	1.2283	-7785	1.1080	0	0.3707	0	30.01	830
4	4.250	1.2288	-7748	1.0986	0	0.3686	0	30.01	830
5	4.000	1.2311	-7575	1.0928	0	0.3662	0	30.02	831
6	4.000	1.2275	-7845	1.0896	0	0.3730	0	30.01	830
7	3.250	1.2283	-7785	1.1049	0	0.3703	0	30.01	830
8	3.750	1.2274	-7853	1.1107	0	0.3731	0	30.01	830

Table 4-22. Depletion Performance Metrics – 16 Gd Pins, 8 w/o

Iteration	Avg Poison Position	BOC k	BA Worth (pcm)	Max Power Peaking	BU of Max Peaking (GWd/MT)	Min Power Peaking	BU of Min Peaking (GWd/MT)	Discharge BU (GWd/MT)	Cycle Length (days)
1	3.750	1.2136	-8889	1.0998	0	0.2537	0	29.58	817
2	3.750	1.2121	-9002	1.0946	0	0.2505	0	29.57	816
3	4.500	1.2112	-9069	1.1198	0	0.2550	0	29.57	816
4	4.250	1.2119	-9017	1.1058	0	0.2519	0	29.57	816
5	4.000	1.2144	-8829	1.1020	0	0.2499	0	29.58	817
6	4.000	1.2105	-9122	1.0933	0.328	0.2559	0	29.57	816
7	3.250	1.2119	-9017	1.1155	0	0.2520	0	29.57	816
8	3.750	1.2107	-9107	1.1225	0	0.2543	0	29.55	816

Table 4-23. Depletion Performance Metrics – 80 IFBA Pins, 2.5 mg/in

Iteration	Avg Poison Position	BOC k	BA Worth (pcm)	Max Power Peaking	BU of Max Peaking (GWd/MT)	Min Power Peaking	BU of Min Peaking (GWd/MT)	Discharge BU (GWd/MT)	Cycle Length (days)
1	3.955	1.2297	-7680	1.0759	0	0.9170	0	30.73	853
2	3.739	1.2278	-7823	1.0712	0	0.9026	0	30.74	853
3	3.870	1.2277	-7830	1.0600	0	0.9212	0	30.74	853
4	4.043	1.2282	-7793	1.0673	0	0.9107	0	30.73	853
5	4.000	1.2276	-7838	1.0686	0	0.9184	0	30.74	853
6	4.000	1.2272	-7868	1.0558	0	0.9196	0	30.74	853
7	4.043	1.2282	-7793	1.0548	21.6	0.9224	0	30.73	853
8	3.870	1.2278	-7823	1.0588	0	0.9286	0	30.74	853

Table 4-24. Depletion Performance Metrics – 160 IFBA Pins, 2.5 mg/in

Iteration	Avg Poison Position	BOC k	BA Worth (pcm)	Max Power Peaking	BU of Max Peaking (GWd/MT)	Min Power Peaking	BU of Min Peaking (GWd/MT)	Discharge BU (GWd/MT)	Cycle Length (days)
1	4.044	1.1353	-14767	1.0729	0	0.9280	0	30.76	853
2	4.087	1.1387	-14512	1.0543	23.1	0.9332	0	30.76	853
3	4.196	1.1383	-14542	1.0543	23.1	0.9354	0	30.76	853
4	4.261	1.1382	-14550	1.0548	18.6	0.9407	0	30.76	853
5	4.326	1.1380	-14565	1.0549	18.6	0.9380	0	30.76	853
6	4.174	1.1384	-14535	1.0546	18.6	0.9360	0	30.76	853
7	4.239	1.1383	-14542	1.0548	18.6	0.9460	0	30.76	853
8	4.283	1.1380	-14565	1.0548	18.6	0.9457	0	30.76	853

4.2.1.1. Neutron Multiplication

The depletion trends for each iteration of each case follow extremely similar trends; the reactivity differences among iterations of BA placement are most readily apparent at BOC only. The trends in neutron multiplication with burnup are given in Figures 4-11 through 4-17 below for only the uncontrolled case as well as the first round of iterations. The remaining iterations exhibit trends essentially indistinguishable from the first iterations, except for variations near BOC. This data is tabulated in Appendix E.

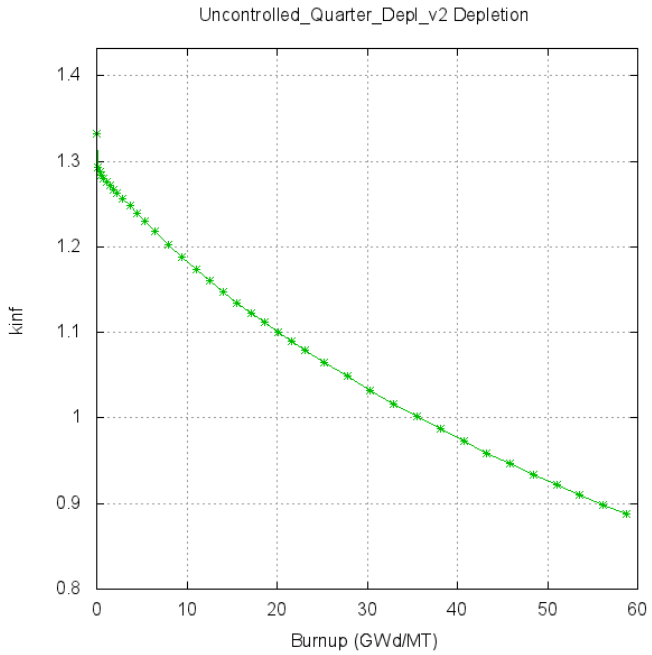

Figure 4-11. Depletion: Uncontrolled

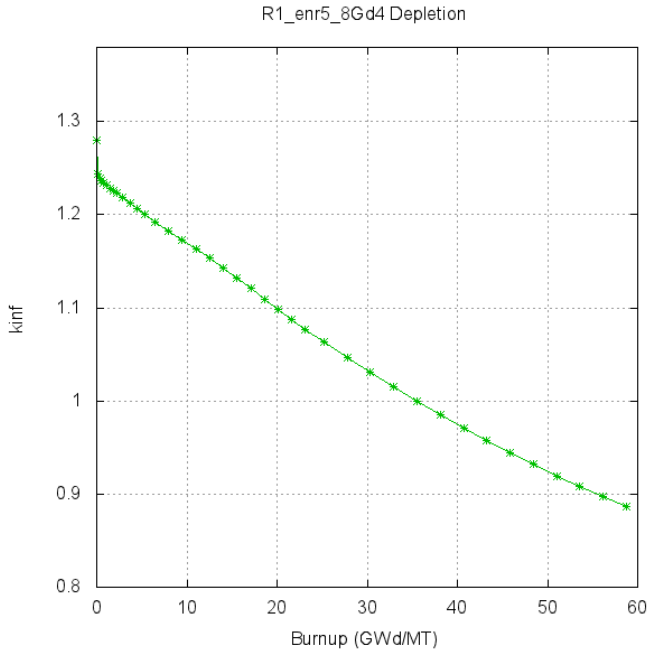

Figure 4-12. Depletion: 8 Gd Pins, 4 w/o, First Iteration

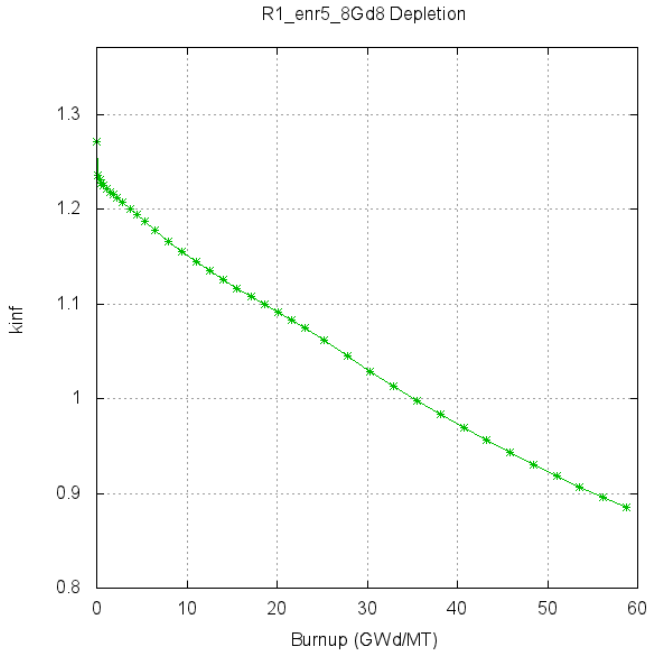

Figure 4-13. Depletion: 8 Gd Pins, 8 w/o, First Iteration

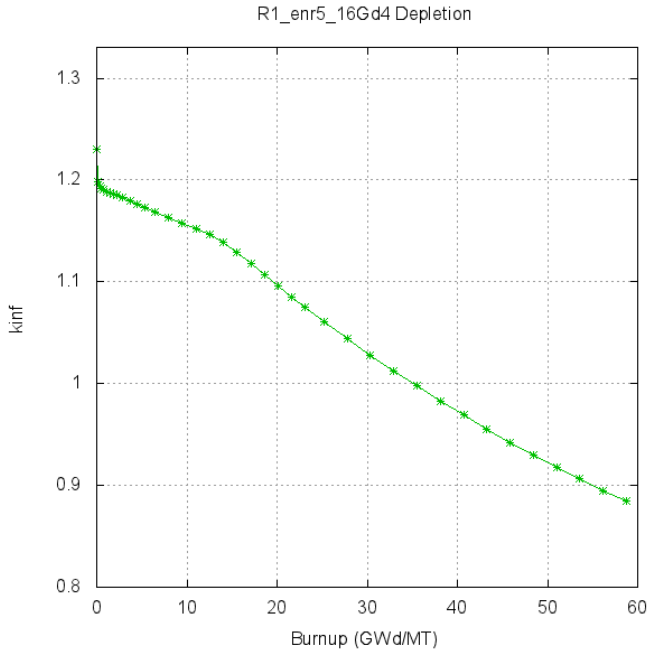

Figure 4-14. Depletion: 16 Gd Pins, 4 w/o, First Iteration

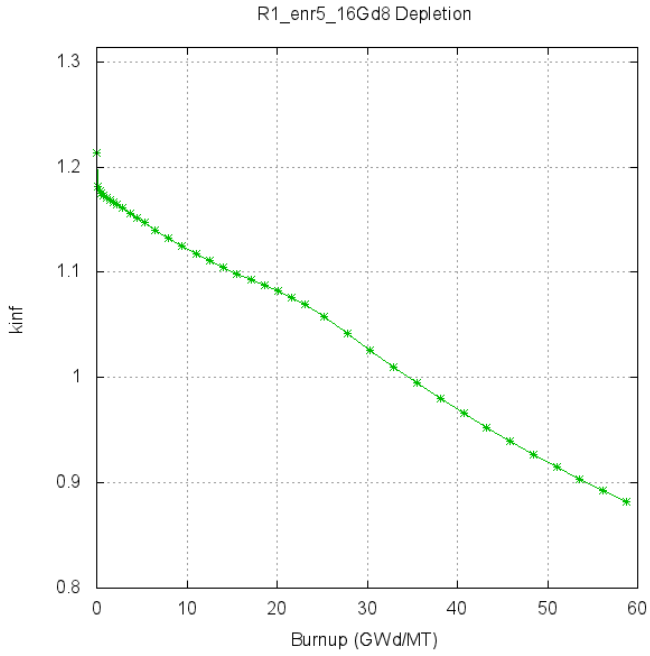

Figure 4-15. Depletion: 16 Gd Pins, 8 w/o, First Iteration

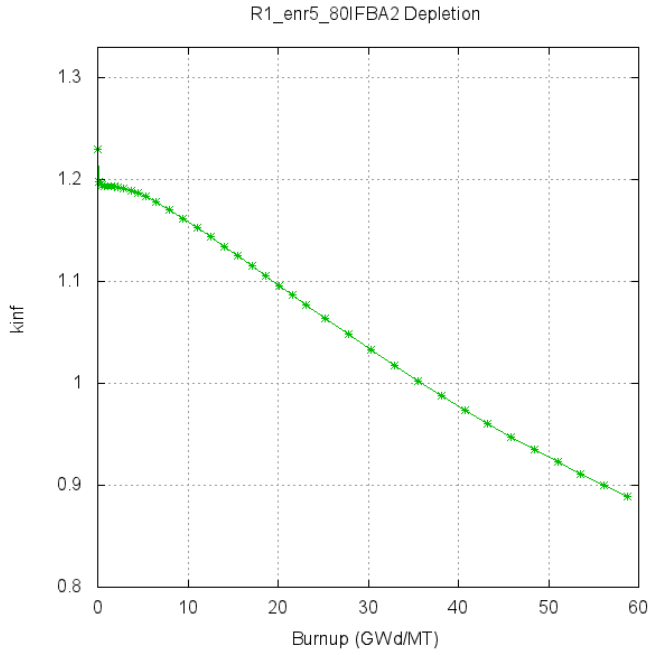

Figure 4-16. Depletion: 80 IFBA Pins, 2.5 mg/in, First Iteration

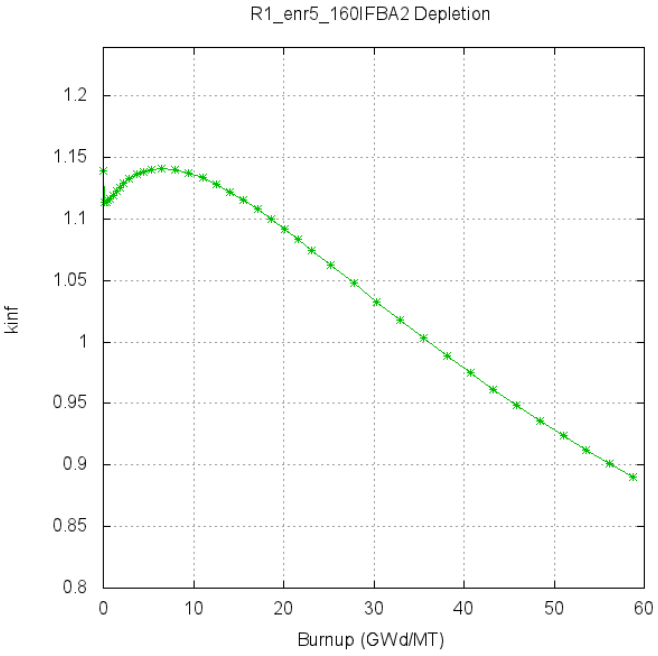

Figure 4-17. Depletion: 160 IFBA Pins, 2.5 mg/in, First Iteration

4.2.1.2. Poison Inventory

Depletion of the poison in each gadolinia case can be tracked as well, as SCALE automatically reports the concentrations of a number of default isotopes with the OPUS module.

One of these isotopes is ^{155}Gd, which will be assumed to provide a representative measure of the remaining initial poison even though other Gd isotopes are not reported. SCALE does not track ^{10}B as a default isotope either, so the poison inventory of the IFBA cases is not tracked. However, operational experience provides reasonable confidence that ^{10}B is essentially completely depleted during operation (22). It is known that the initial Gd does not generally deplete completely, and therefore its inventory these cases is of primary interest. The ^{10}B content in the IFBA cases, as well as other Gd isotopes in the Gd cases, may be requested explicitly for closer investigation in a future study. Several other neutron poisons which build up as fission products are reported by OPUS by default as well: ^{147}Sm, ^{149}Sm, ^{150}Sm, ^{151}Sm, ^{152}Sm, and ^{153}Eu. As these species play an important role in the assembly reactivity, they are also included in this section for both Gd and IFBA cases. Figures 4-18 through 4-23 give the concentrations of all of these isotopes for each case for the first iteration only (again, these trends are extremely similar across iterations). Although the IFBA cases have no initial Gd loading, they exhibit a buildup of ^{155}Gd as a fission product.

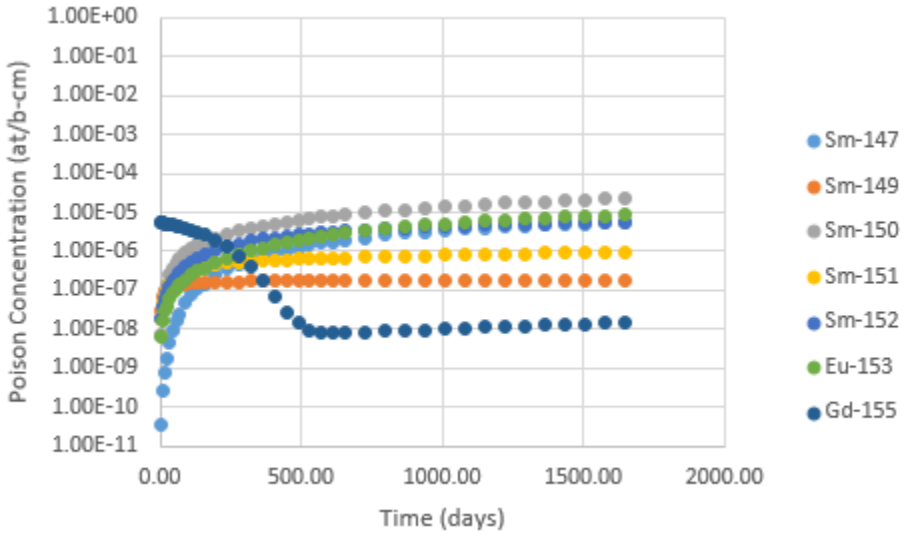

Figure 4-18. Neutron Poison Concentration: 8 Gd Pins, 4 w/o, First Iteration

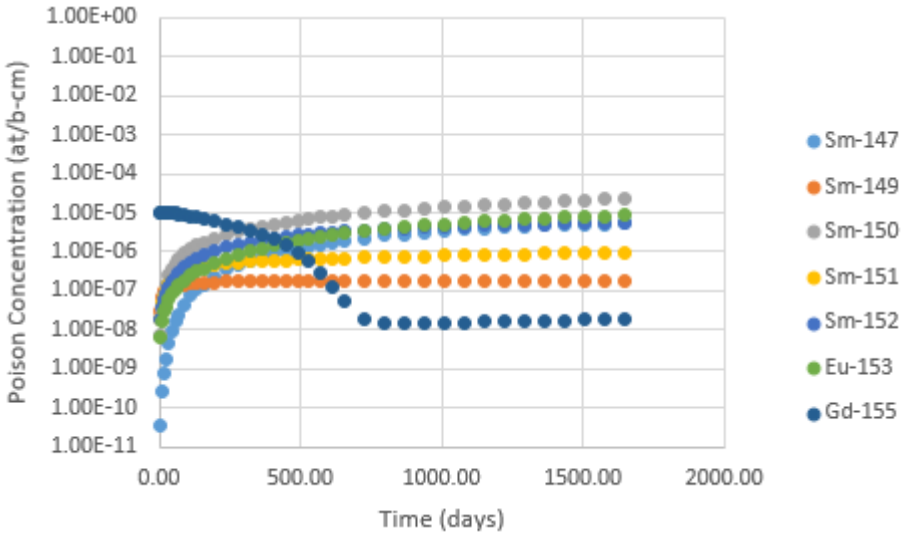

Figure 4-19. Neutron Poison Concentration: 8 Gd Pins, 8 w/o, First Iteration

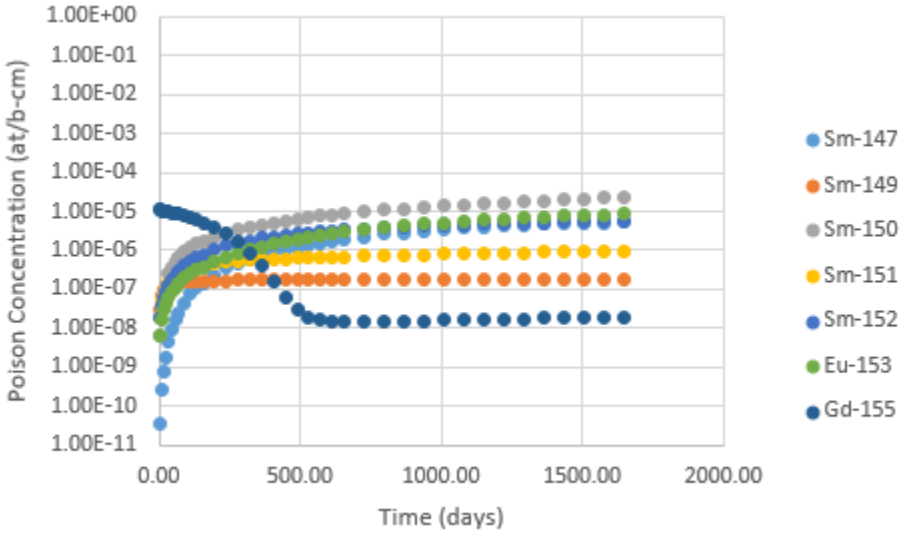

Figure 4-20. Neutron Poison Concentration: 16 Gd Pins, 4 w/o, First Iteration

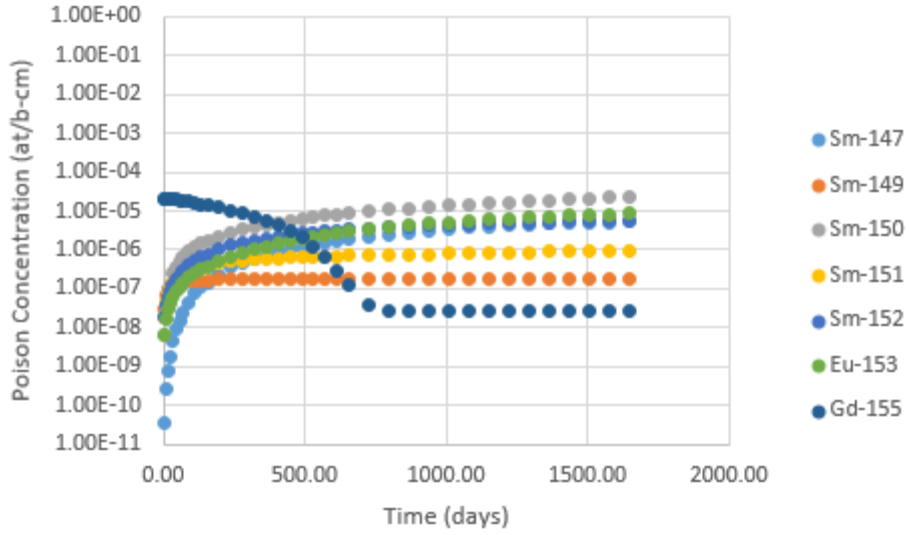

Figure 4-21. Neutron Poison Concentration: 16 Gd Pins, 8 w/o, First Iteration

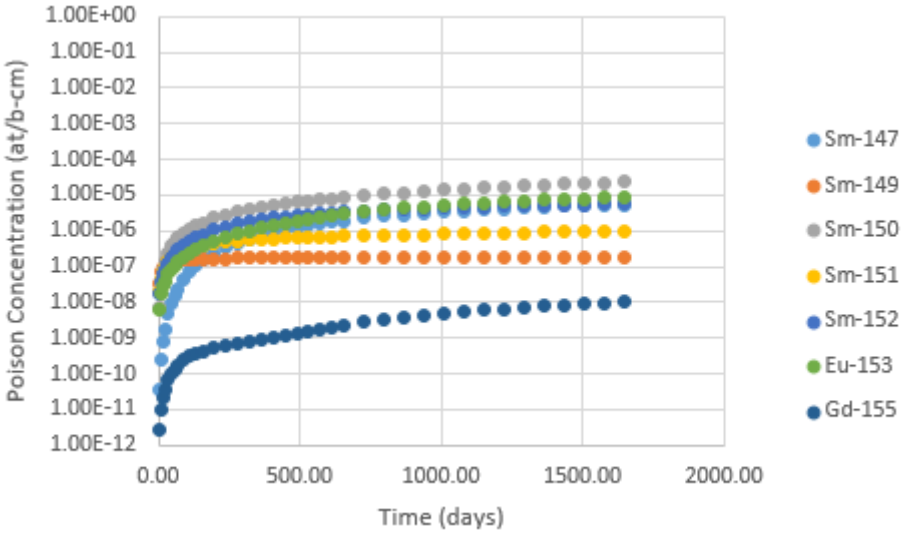

Figure 4-22. Neutron Poison Concentration: 80 IFBA Pins, 2.5 mg/in, First Iteration

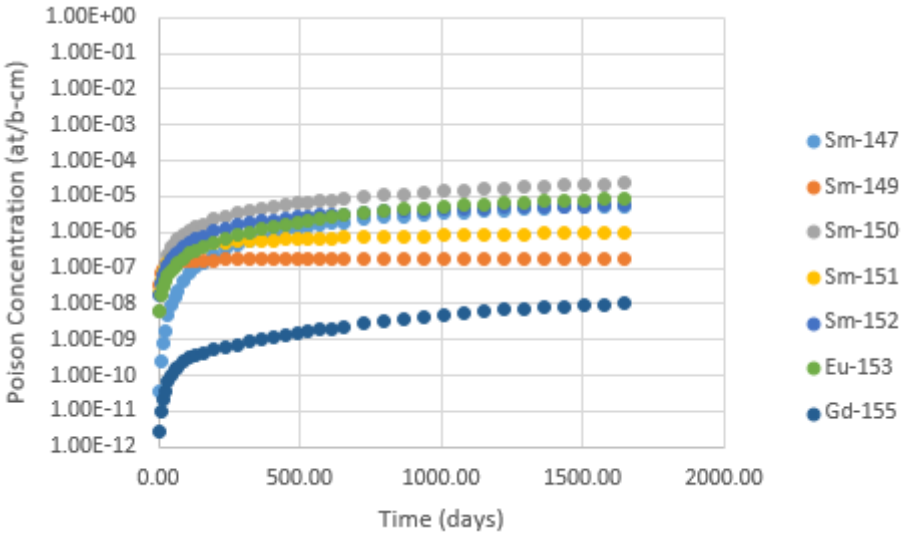

Figure 4-23. Neutron Poison Concentration: 160 IFBA Pins, 2.5 mg/in, First Iteration

4.2.1.3. Power Peaking

Figures 4-24 through 4-29 plot the maximum power peaking at each depletion step for a single iteration of each case. The iteration selected for each case is that which yielded the flattest BOC power profile. It is observed from these data that the BOC power peaking is not necessarily the greatest in the cycle – some cases exhibit an increase in power peaking after poisons have been depleted, as these initially poisoned lattice locations experience a sudden spike in thermal neutron flux which is no longer depressed by the poison.

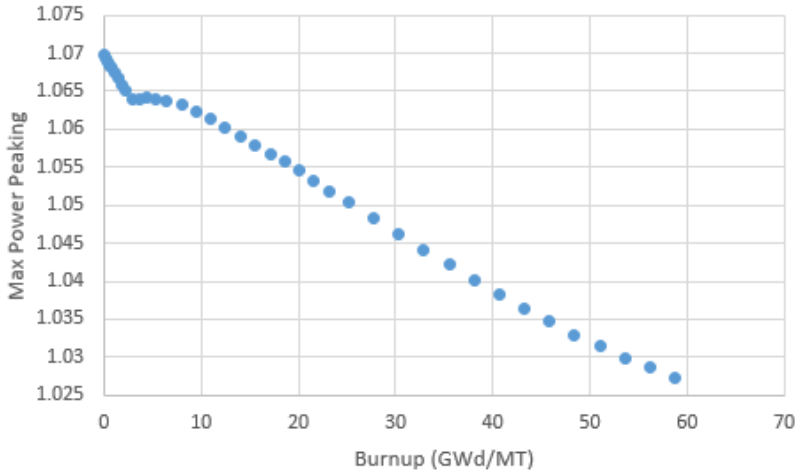

Figure 4-24. Max Power Peaking Depletion Trend for Flattest BOC Power: 8 Gd Pins, 4 w/o (Second Iteration)

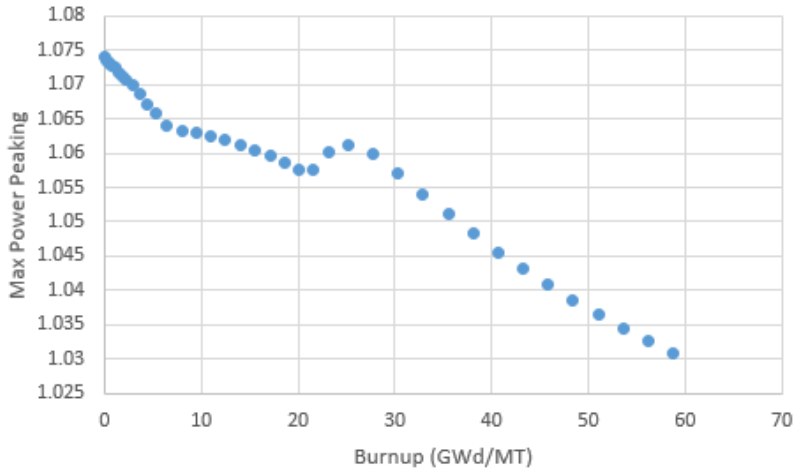

Figure 4-25. Max Power Peaking Depletion Trend for Flattest BOC Power: 8 Gd Pins, 8 w/o (Second Iteration)

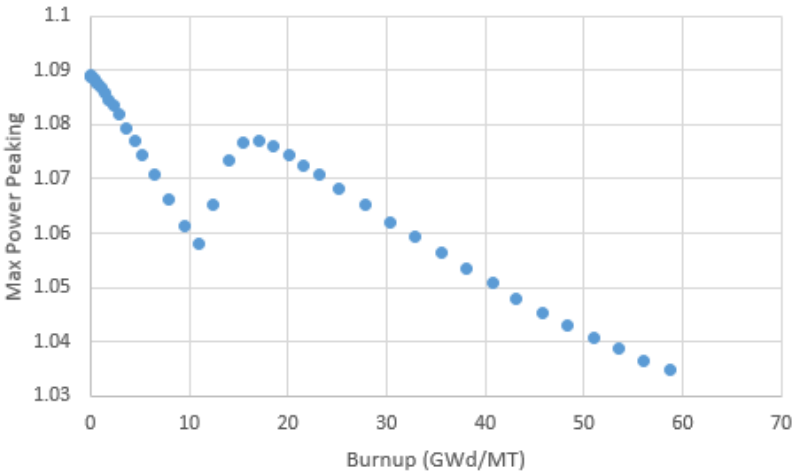

Figure 4-26. Max Power Peaking Depletion Trend for Flattest BOC Power: 16 Gd Pins, 4 w/o (Second Iteration)

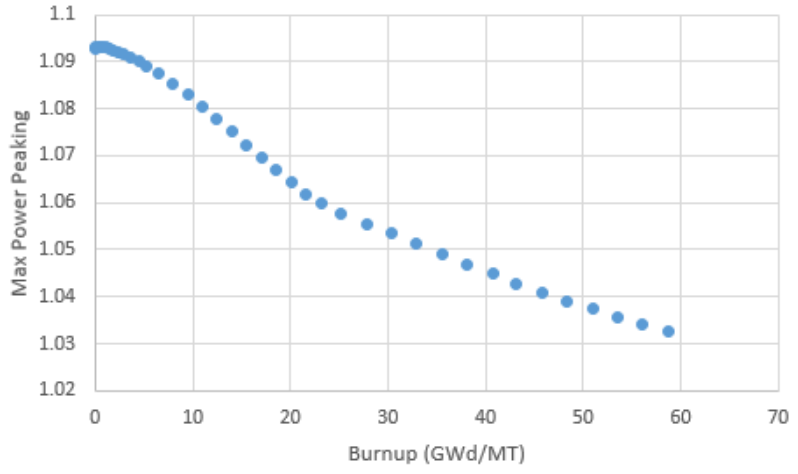

Figure 4-27. Max Power Peaking Depletion Trend for Flattest BOC Power: 16 Gd Pins, 8 w/o (Sixth Iteration)

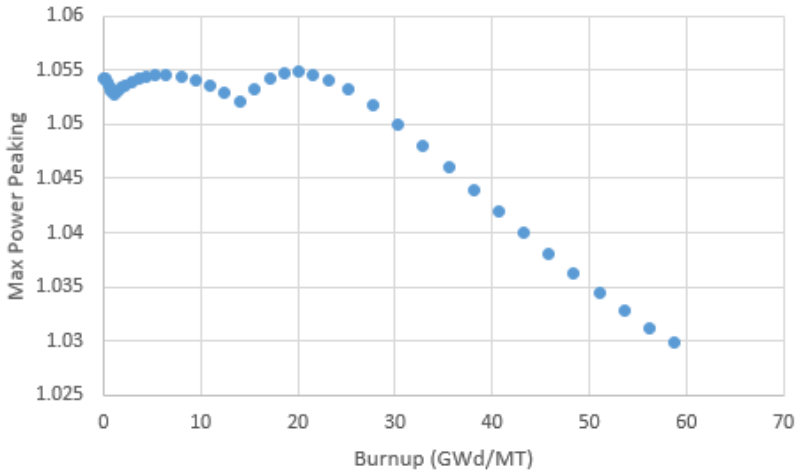

Figure 4-28. Max Power Peaking Depletion Trend for BOC Power: 80 IFBA Pins (Seventh Iteration)

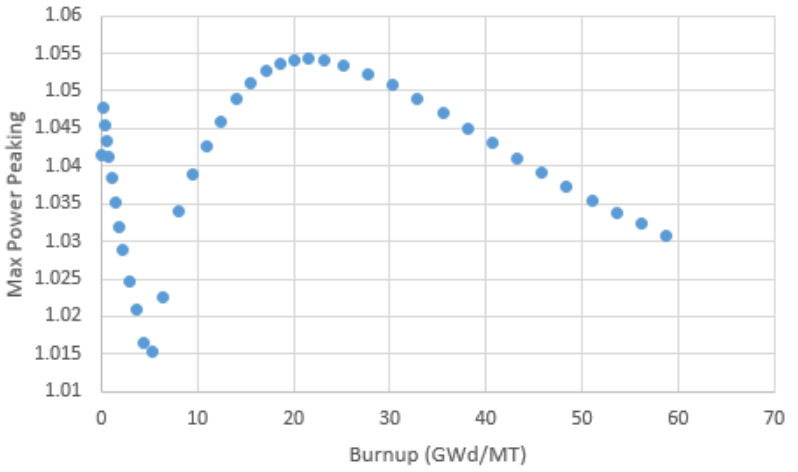

Figure 4-29. Max Power Peaking Depletion Trend for BOC Power: 160 IFBA Pins (Third Iteration)

4.2.2. BOC Reactivity Characteristics

The fuel assembly state at BOC is of particular interest because it is generally the point at which both reactivity and power peaking are greatest. However, an exception is identified in Section 4.2.1.1: cases with 160 IFBA pins are heavily poisoned and exhibit an increase in reactivity as poison is depleted early in the cycle. For the sake of consistency, all cases are analyzed at BOC; however, future studies should investigate this peak reactivity state for such heavily poisoned assemblies.

4.2.2.1. Power Peaking

Figures 4-30 through 4-35 give the BOC power peaking for each case again for only the iterations which yielded the flattest power peaking profiles, corresponding to the BOC state of the cases presented in Section 4.2.1.3 above. The corresponding BA layouts are given explicitly in Appendix B, and the BOC power peaking for the remaining iterations is given in Appendix C.

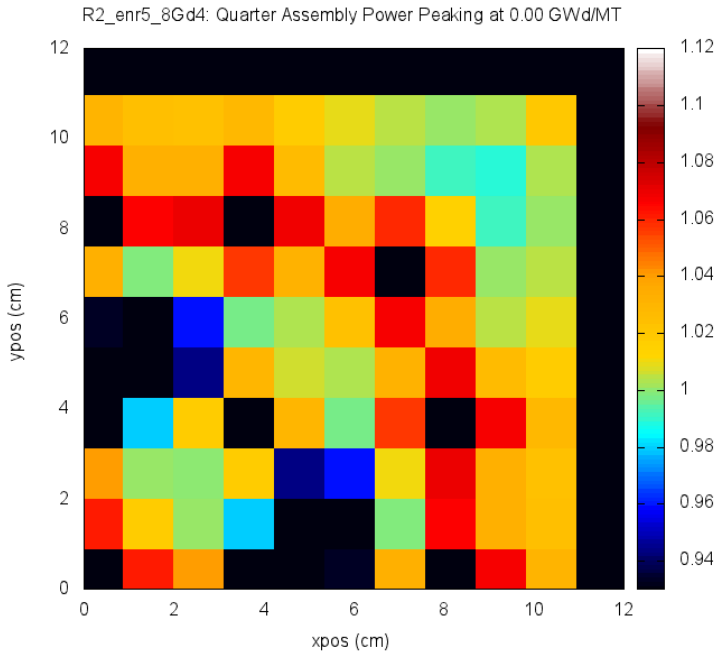

Figure 4-30. Flattest Power Peaking: 8 Gd Pins, 4 w/o (Second Iteration)

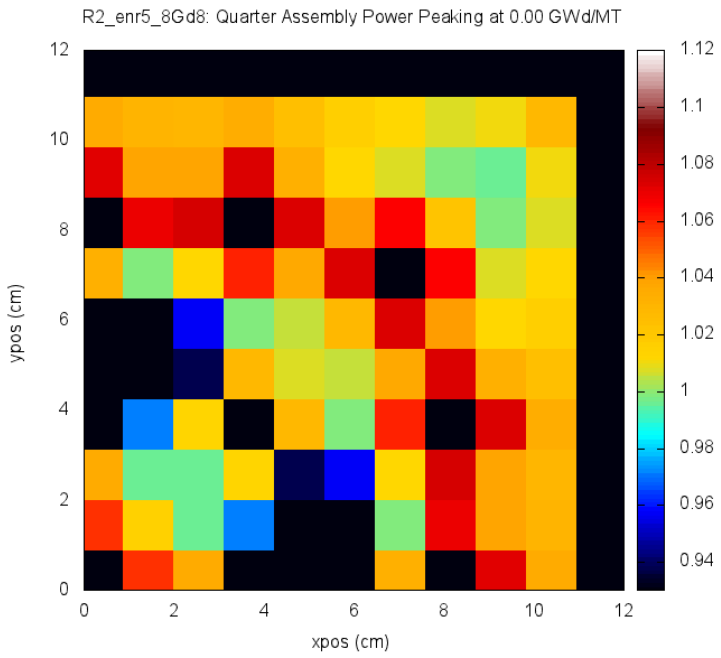

Figure 4-31. Flattest Power Peaking: 8 Gd Pins, 8 w/o (Second Iteration)

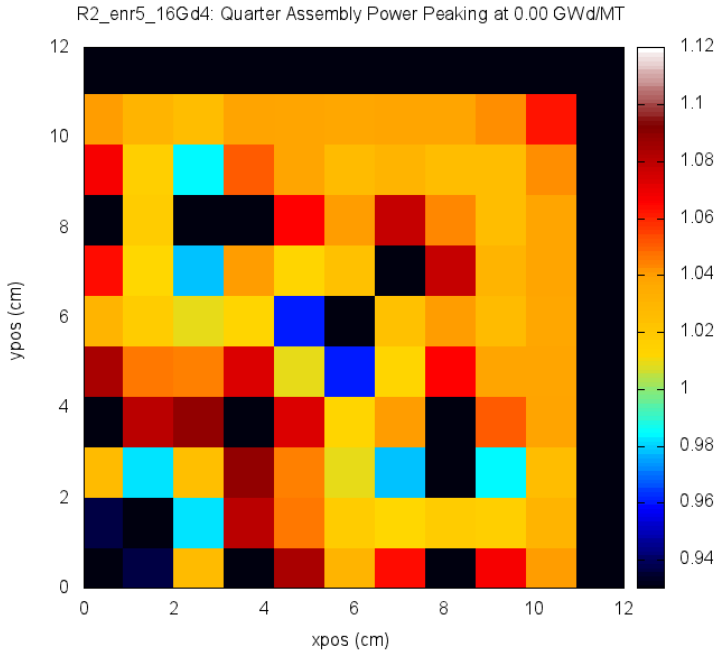

Figure 4-32. Flattest Power Peaking: 16 Gd Pins, 4 w/o (Second Iteration)

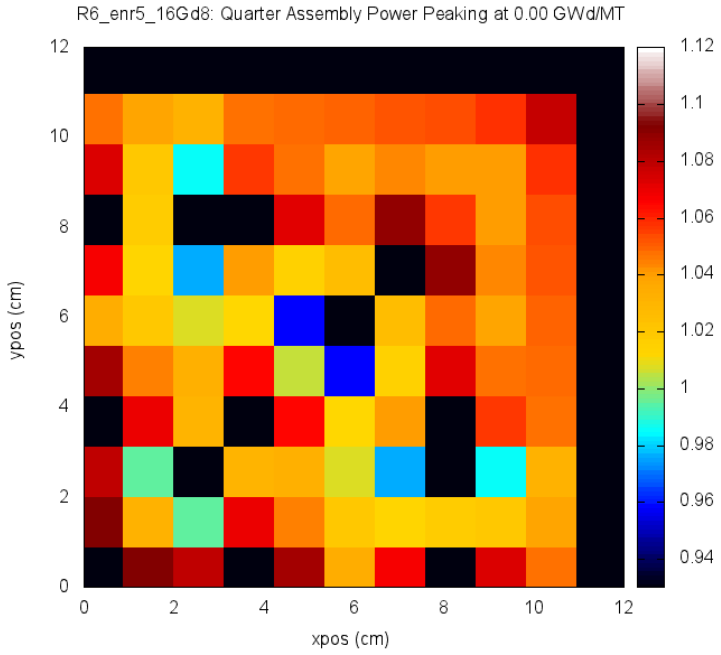

Figure 4-33. Flattest Power Peaking: 16 Gd Pins, 8 w/o (Sixth Iteration)

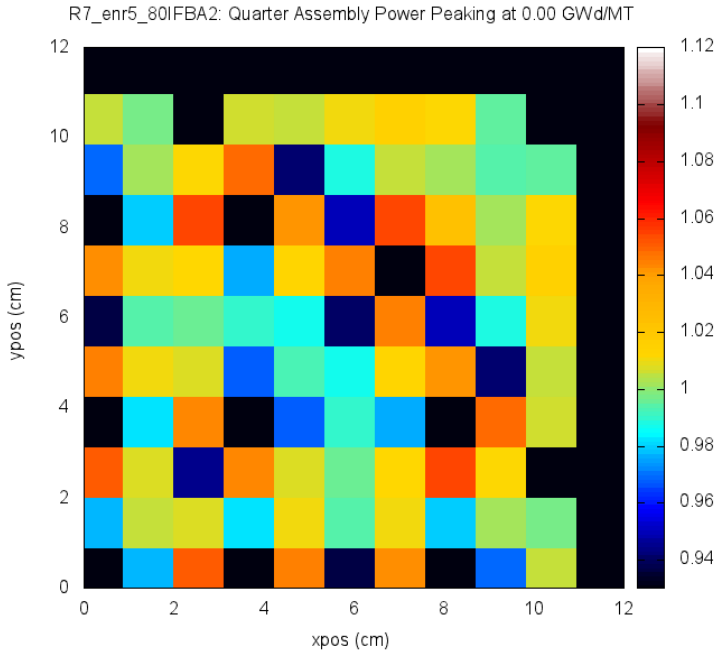

Figure 4-34. Flattest Power Peaking: 80 IFBA Pins, 2.5 mg/in (Seventh Iteration)

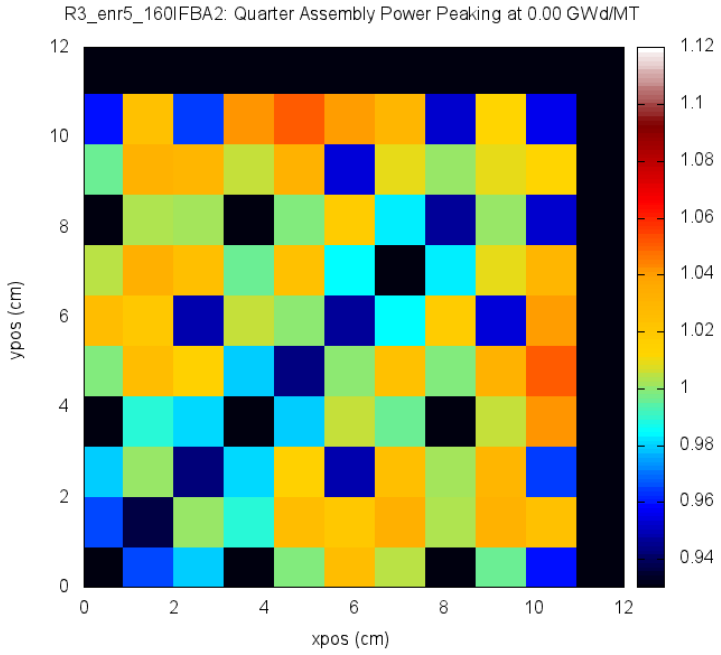

Figure 4-35. Flattest Power Peaking: 160 IFBA Pins, 2.5 mg/in (Third Iteration)

4.2.2.2. CBC and Boron Worth

Tables 4-25 through 4-30 present the BOC neutron multiplication for each soluble boron concentration considered, as well as the interpolated CBC. The boron reactivity worth is presented as well for each of three ranges of the boron concentration. For the sake of comparison, CBC data for the uncontrolled case may be taken from the RCCA calculations of Section 4.1.1; this CBC is 6211 ppm. Calculating the boron worth of the uncontrolled case may be done using Equation 5 at the 0 ppm and CBC states for a coarse estimate of -4.005 pcm/ppm. Note that all of the following boron concentrations are reported as total ppm rather that ppm ^{10}B only.

Table 4-25. Boron Calculations: 8 Gd Pins, 4 w/o

Iteration	k (0 ppm)	k (5426 ppm)	k (10852)	CBC (ppm)	Boron Worth, pcm/ppm (0-5426 ppm)	Boron Worth, pcm/ppm (5426-10852 ppm)	Boron Worth, pcm/ppm (5426-10852 ppm)
1	1.2796	1.0052	0.8472	5605	-3.952	-2.896	-3.114
2	1.2819	1.0062	0.8478	5638	-3.964	-2.902	-3.121
3	1.2801	1.0054	0.8473	5610	-3.955	-2.898	-3.115
4	1.2803	1.0055	0.8473	5610	-3.956	-2.899	-3.116
5	1.2816	1.0060	0.8476	5632	-3.964	-2.902	-3.121
6	1.2809	1.0057	0.8475	5621	-3.959	-2.900	-3.118
7	1.2828	1.0065	0.8479	5648	-3.969	-2.905	-3.124
8	1.2794	1.0051	0.8472	5600	-3.952	-2.896	-3.113

Table 4-26. Boron Calculations: 8 Gd Pins, 8 w/o

Iteration	k (0 ppm)	k (5426 ppm)	k (10852)	CBC (ppm)	Boron Worth, pcm/ppm (0-5426 ppm)	Boron Worth, pcm/ppm (5426-10852 ppm)	Boron Worth, pcm/ppm (5426-10852 ppm)
1	1.2710	0.9990	0.8423	5404	-3.944	-2.892	-3.108
2	1.2737	1.0002	0.8429	5431	-3.957	-2.898	-3.117
3	1.2715	0.9992	0.8423	5410	-3.948	-2.893	-3.111
4	1.2716	0.9992	0.8423	5410	-3.948	-2.894	-3.111
5	1.2730	0.9997	0.8426	5421	-3.956	-2.898	-3.116
6	1.2725	0.9996	0.8425	5415	-3.953	-2.896	-3.114
7	1.2745	1.0005	0.8430	5442	-3.962	-2.901	-3.120
8	1.2707	0.9988	0.8421	5404	-3.944	-2.891	-3.108

Table 4-27. Boron Calculations: 16 Gd Pins, 4 w/o

Iteration	k (0 ppm)	k (5426 ppm)	k (10852)	CBC (ppm)	Boron Worth, pcm/ppm (0-5426 ppm)	Boron Worth, pcm/ppm (5426-10852 ppm)	Boron Worth, pcm/ppm (5426-10852 ppm)
1	1.2303	0.9763	0.8274	4921	-3.806	-2.810	-3.018
2	1.2288	0.9757	0.8272	4905	-3.795	-2.805	-3.011
3	1.2283	0.9753	0.8270	4900	-3.796	-2.804	-3.011
4	1.2288	0.9757	0.8272	4905	-3.796	-2.805	-3.012
5	1.2311	0.9766	0.8276	4927	-3.810	-2.812	-3.020
6	1.2275	0.9751	0.8269	4889	-3.790	-2.801	-3.008
7	1.2283	0.9755	0.8271	4900	-3.793	-2.803	-3.010
8	1.2274	0.9751	0.8269	4889	-3.788	-2.801	-3.007

Table 4-28. Boron Calculations: 16 Gd Pins, 8 w/o

Iteration	k (0 ppm)	k (5426 ppm)	k (10852)	CBC (ppm)	Boron Worth, pcm/ppm (0-5426 ppm)	Boron Worth, pcm/ppm (5426-10852 ppm)	Boron Worth, pcm/ppm (5426-10852 ppm)
1	1.2136	0.9640	0.8175	4645	-3.790	-2.800	-3.007
2	1.2121	0.9635	0.8174	4628	-3.780	-2.795	-3.001
3	1.2112	0.9629	0.8169	4617	-3.778	-2.794	-3.000
4	1.2119	0.9634	0.8173	4628	-3.779	-2.795	-3.001
5	1.2144	0.9644	0.8178	4655	-3.794	-2.803	-3.010
6	1.2105	0.9627	0.8169	4607	-3.773	-2.791	-2.996
7	1.2119	0.9634	0.8174	4628	-3.778	-2.794	-3.000
8	1.2107	0.9629	0.8171	4612	-3.772	-2.791	-2.996

Table 4-29. Boron Calculations: 80 IFBA Pins, 2.5 mg/in

Iteration	k (0 ppm)	k (5426 ppm)	k (10852)	CBC (ppm)	Boron Worth, pcm/ppm (0-5426 ppm)	Boron Worth, pcm/ppm (5426-10852 ppm)	Boron Worth, pcm/ppm (5426-10852 ppm)
1	1.2297	0.9760	0.8283	4916	-3.802	-2.791	-3.008
2	1.2278	0.9753	0.8280	4894	-3.790	-2.784	-3.001
3	1.2277	0.9752	0.8279	4894	-3.790	-2.785	-3.001
4	1.2282	0.9753	0.8278	4894	-3.795	-2.787	-3.004
5	1.2276	0.9751	0.8278	4889	-3.791	-2.784	-3.001
6	1.2272	0.9750	0.8278	4889	-3.788	-2.783	-2.999
7	1.2282	0.9753	0.8279	4894	-3.794	-2.787	-3.004
8	1.2278	0.9753	0.8279	4894	-3.791	-2.785	-3.001

Table 4-30. Boron Calculations: 160 IFBA Pins, 2.5 mg/in

Iteration	k (0 ppm)	k (5426 ppm)	k (10852)	CBC (ppm)	Boron Worth, pcm/ppm (0-5426 ppm)	Boron Worth, pcm/ppm (5426-10852 ppm)	Boron Worth, pcm/ppm (5426-10852 ppm)
1	1.1392	0.9220	0.7918	3478	-3.514	-2.602	-2.810
2	1.1387	0.9281	0.7918	3467	-3.510	-2.600	-2.808
3	1.1383	0.9216	0.7916	3462	-3.509	-2.600	-2.807
4	1.1382	0.9215	0.7915	3462	-3.509	-2.599	-2.807
5	1.1380	0.9214	0.7915	3456	-3.508	-2.598	-2.806
6	1.1384	0.9216	0.7916	3462	-3.510	-2.600	-2.807
7	1.1383	0.9216	0.7916	3462	-3.509	-2.599	-2.807
8	1.1380	0.9214	0.7915	3456	-3.508	-2.598	-2.806

4.2.2.3. MTC

Tables 4-31 through 4-36 give the BOC neutron multiplication for each of three moderator densities as well as the MTC calculated using forward, backward, and center differences for each iteration of each case with the CBC imposed. The CBC is repeated in these results as well for the sake of easy reference. It is noteworthy that the CBC neutron multiplication results given here deviate quite significantly from unity in some cases, highlighting the limitation of the CBC calculation by linear interpolation. These results confirm that the reactivity as a function of boron concentration is highly nonlinear. It is initially concerning that the MTC estimate is positive in all cases, but the true MTC must be assessed using a full core model. Additional core design factors not accounted for in this study will likely yield a negative MTC.

Table 4-31. MTC Calculations: 8 Gd Pins, 4 w/o

Iteration	CBC (ppm)	k (T_0 – 20 °C)	k (T_0)	k (T_0 + 20 °C)	Forward MTC (pcm/K)	Backward MTC (pcm/K)	Center MTC (pcm/K)
1	1033	1.0056	1.0134	1.0214	39.55	43.11	41.23
2	1039	0.9907	0.9984	1.0064	39.94	43.38	41.56
3	1034	0.9910	0.9986	1.0065	39.66	43.11	41.28
4	1034	0.9910	0.9986	1.0065	39.72	43.17	41.34
5	1038	0.9908	0.9985	1.0064	39.89	43.34	41.51
6	1036	0.9909	0.9985	1.0065	39.79	43.23	41.40
7	1041	0.9906	0.9983	1.0063	40.12	43.56	41.74
8	1032	0.9911	0.9987	1.0066	39.56	43.01	41.18

Table 4-32. MTC Calculations: 8 Gd Pins, 8 w/o

Iteration	CBC (ppm)	k (T_0 – 20 °C)	k (T_0)	k (T_0 + 20 °C)	Forward MTC (pcm/K)	Backward MTC (pcm/K)	Center MTC (pcm/K)
1	996	0.9927	0.9997	1.0070	36.25	39.87	37.95
2	1001	0.9928	0.9999	1.0072	36.50	40.12	38.20
3	997	0.9927	0.9998	1.0070	36.26	39.89	37.97
4	997	0.9927	0.9998	1.0070	36.30	39.94	38.01
5	999	0.9928	0.9999	1.0072	36.42	40.05	38.13
6	998	0.9928	0.9999	1.0072	36.35	39.98	38.06
7	1003	0.9927	0.9999	1.0072	36.67	40.31	38.39
8	996	0.9926	0.9997	1.0069	36.18	39.82	37.89

Table 4-33. MTC Calculations: 16 Gd Pins, 4 w/o

Iteration	CBC (ppm)	k (T_0 – 20 °C)	k (T_0)	k (T_0 + 20 °C)	Forward MTC (pcm/K)	Backward MTC (pcm/K)	Center MTC (pcm/K)
1	907	0.9880	0.9942	1.0005	31.69	35.22	33.35
2	904	0.9879	0.9941	1.0004	31.60	35.13	33.26
3	903	0.9879	0.9941	1.0003	31.58	35.12	33.24
4	904	0.9879	0.9941	1.0004	31.66	35.20	33.32
5	908	0.9881	0.9943	1.0006	31.84	35.39	33.51
6	901	0.9878	0.9940	1.0003	31.42	34.95	33.08
7	903	0.9879	0.9941	1.0004	31.57	35.06	33.21
8	901	0.9878	0.9940	1.0003	31.52	35.03	33.17

Table 4-34. MTC Calculations: 16 Gd Pins, 8 w/o

Iteration	CBC (ppm)	k (T_0 – 20 °C)	k (T_0)	k (T_0 + 20 °C)	Forward MTC (pcm/K)	Backward MTC (pcm/K)	Center MTC (pcm/K)
1	856	0.9864	0.9917	0.9969	26.27	30.06	28.05
2	853	0.9864	0.9916	0.9968	26.16	29.94	27.94
3	851	0.9862	0.9915	0.9967	26.09	29.88	27.87
4	853	0.9863	0.9916	0.9968	26.20	30.00	27.99
5	858	0.9864	0.9918	0.9970	26.44	30.26	28.24
6	849	0.9862	0.9915	0.9966	25.91	29.69	27.68
7	853	0.9863	0.9916	0.9968	26.16	29.90	27.92
8	850	0.9863	0.9915	0.9967	26.06	29.82	27.83

Table 4-35. MTC Calculations: 80 IFBA Pins, 2.5 mg/in

Iteration	CBC (ppm)	k (T_0 – 20 °C)	k (T_0)	k (T_0 + 20 °C)	Forward MTC (pcm/K)	Backward MTC (pcm/K)	Center MTC (pcm/K)
1	906	0.9882	0.9941	1.0000	29.62	33.42	31.41
2	902	0.9881	0.9939	0.9998	29.43	33.22	31.21
3	902	0.9881	0.9939	0.9998	29.40	33.20	31.19
4	902	0.9980	0.9939	0.9998	29.48	33.28	31.26
5	901	0.9880	0.9939	0.9997	29.41	33.21	31.19
6	901	0.9880	0.9939	0.9997	29.36	33.16	31.15
7	902	0.9881	0.9939	0.9998	29.46	33.27	31.25
8	902	0.9881	0.9939	0.9998	29.42	33.21	31.20

Table 4-36. MTC Calculations: 160 IFBA Pins, 2.5 mg/in

Iteration	CBC (ppm)	k (T_0 – 20 °C)	k (T_0)	k (T_0 + 20 °C)	Forward MTC (pcm/K)	Backward MTC (pcm/K)	Center MTC (pcm/K)
1	641	0.9832	0.9859	0.9881	11.28	15.26	13.15
2	639	0.9832	0.9859	0.9881	11.21	15.19	13.08
3	638	0.9832	0.9859	0.9881	11.19	15.18	13.07
4	638	0.9832	0.9859	0.9881	11.18	15.16	13.05
5	637	0.9832	0.9859	0.9881	11.15	15.13	13.02
6	638	0.9832	0.9859	0.9881	11.19	15.16	13.05
7	638	0.9832	0.9859	0.9881	11.17	15.15	13.04
8	637	0.9832	0.9859	0.9881	11.14	15.12	13.01

5. ANALYSIS

The results presented in the previous chapter shall now be used to address the original problems posed. RCCA designs are assessed in Section 5.1, and BA designs are assessed in Section 5.2.

5.1. Control Rods

5.1.1. Control Rod Effectiveness

In the previous section, control rod reactivity worth calculations were presented for both single quarter assembly and four quarter assembly geometries, where control rods were inserted in half of the assemblies in the latter case. It is of interest to examine the change in control rod effectiveness in switching from all assemblies rodded (the single quarter assembly case) to half of the assemblies rodded (the four quarter assembly case); if no effectiveness is lost, the control rod worth for the four quarter assembly cases should be exactly one half of that of the corresponding single quarter assembly cases. Tables 5-1 and 5-2 below give the ratio of the four quarter assembly worth to the single quarter assembly worth for each case with no boron and at critical boron respectively.

Table 5-1. Comparison of Control Rod Worth between Geometries – No Boron

Case	Worth (pcm) – Single Quarter Assembly Rodded	Worth (pcm) – 2 of 4 Quarter Assemblies Rodded	Ratio (Four Quarters/Single Quarter)
19x19 Silicide Assembly with 24 AIC Control Rods	19217	9290	0.4834
19x19 Silicide Assembly with 28 AIC Control Rods	21854	10467	0.4790
19x19 Silicide Assembly with 32 AIC Control Rods	24330	11564	0.4753
17x17 Oxide Assembly with 24 AIC Control Rods	25367	12293	0.4846
19x19 Silicide Assembly with 24 B_4C Control Rods	26948	12957	0.4808
19x19 Silicide Assembly with 28 B_4C Control Rods	30292	14398	0.4753
19x19 Silicide Assembly with 32 B_4C Control Rods	33410	15737	0.4710
17x17 Oxide Assembly with 24 B_4C Control Rods	33905	16400	0.4837
19x19 Silicide Assembly with 24 Hf Control Rods	19033	9193	0.4830
19x19 Silicide Assembly with 28 Hf Control Rods	21663	10365	0.4785
19x19 Silicide Assembly with 32 Hf Control Rods	24149	11464	0.4747
17x17 Oxide Assembly with 24 Hf Control Rods	25025	12116	0.4842

Table 5-2. Comparison of Control Rod Worth between Geometries – CBC

Case	Worth (pcm) – Single Quarter Assembly Rodded	Worth (pcm) – 2 of 4 Quarter Assemblies Rodded	Ratio (Four Quarters/Single Quarter)
19x19 Silicide Assembly with 24 AIC Control Rods	13880	6735	0.4852
19x19 Silicide Assembly with 28 AIC Control Rods	15929	7671	0.4816
19x19 Silicide Assembly with 32 AIC Control Rods	17881	8556	0.4785
17x17 Oxide Assembly with 24 AIC Control Rods	18273	8893	0.4867
19x19 Silicide Assembly with 24 B_4C Control Rods	21540	10387	0.4822
19x19 Silicide Assembly with 28 B_4C Control Rods	24395	11647	0.4774
19x19 Silicide Assembly with 32 B_4C Control Rods	27093	12832	0.4736
17x17 Oxide Assembly with 24 B_4C Control Rods	27024	13108	0.4851
19x19 Silicide Assembly with 24 Hf Control Rods	13998	6784	0.4846
19x19 Silicide Assembly with 28 Hf Control Rods	16061	7723	0.4809
19x19 Silicide Assembly with 32 Hf Control Rods	18036	8615	0.4777
17x17 Oxide Assembly with 24 Hf Control Rods	18317	8905	0.4862

The loss in control rod effectiveness in each case is slightly lower when the assembly is critical than it is when no boron or other absorbers are used. Additionally, the worth ratio is very close to exactly one half in each case, indicating only a slight loss in control rod effectiveness when accounting for assemblies which will not be in RCCA locations in the final core.

5.1.2. Reactivity Worth Comparisons

In order to properly assess the feasibility of the control rod configurations considered, the results given in Chapter 4 should be compared with the reference fuel assembly – the 17x17 oxide assembly with 24 AIC control rods. It is desired to achieve control rod worth comparable to or better than that of this case. Therefore, the results presented in Chapter 4 are reorganized for direct comparison with the reference case in Tables 5-3 to 5-8 and Figures 5-1 to 5-6 below. Only the worth data calculated using Equation 1 are presented.

Table 5-3. AIC Rod Worth Comparison with Reference Core – Single Quarter Assembly Rodded

Case	Worth (pcm) – No Boron	Worth (pcm) – CBC
Reference	25367	18273
19x19 Silicide Assembly with 24 Control Rods	19217	13880
19x19 Silicide Assembly with 28 Control Rods	21854	15929
19x19 Silicide Assembly with 32 Control Rods	24330	17881

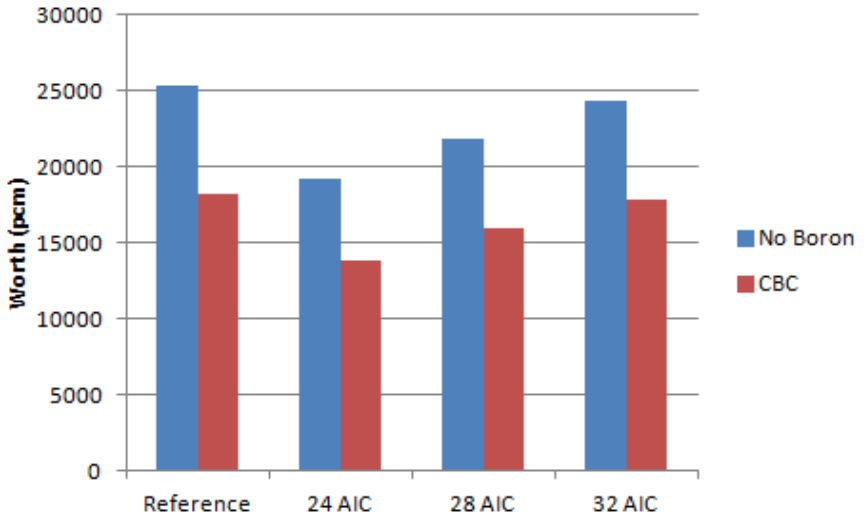

Figure 5-1. AIC Rod Worth Comparison with Reference Core – Single Quarter Assembly Rodded

Table 5-4. AIC Rod Worth Comparison with Reference Core – 2 of 4 Quarter Assemblies Rodded

Case	Worth (pcm) – No Boron	Worth (pcm) – CBC
Reference	12293	8893
19x19 Silicide Assembly with 24 Control Rods	9290	6735
19x19 Silicide Assembly with 28 Control Rods	10467	7671
19x19 Silicide Assembly with 32 Control Rods	11564	8556

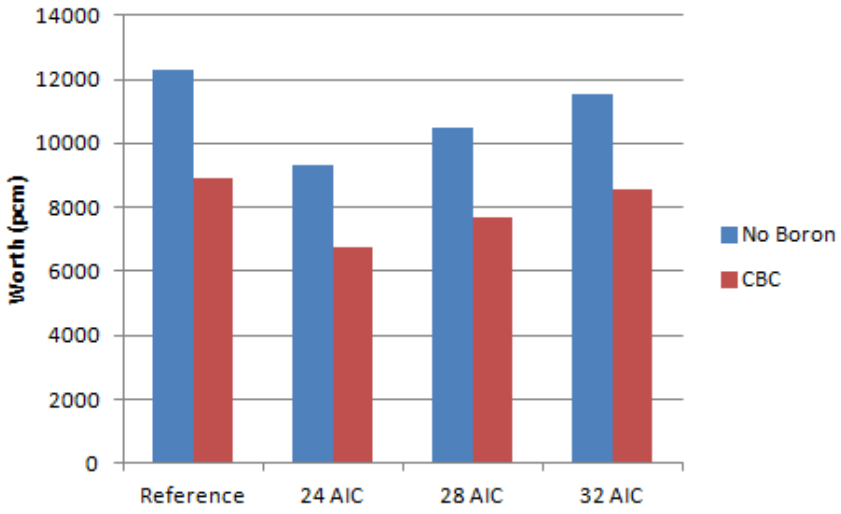

Figure 5-2. AIC Rod Worth Comparison with Reference Core – 2 of 4 Quarter Assemblies Rodded

Table 5-5. B_4C Rod Worth Comparison with Reference Core – Single Quarter Assembly Rodded

Case	Worth (pcm) – No Boron	Worth (pcm) – CBC
Reference	25367	18273
19x19 Silicide Assembly with 24 Control Rods	26948	21540
19x19 Silicide Assembly with 28 Control Rods	30292	24395
19x19 Silicide Assembly with 32 Control Rods	33409	27092

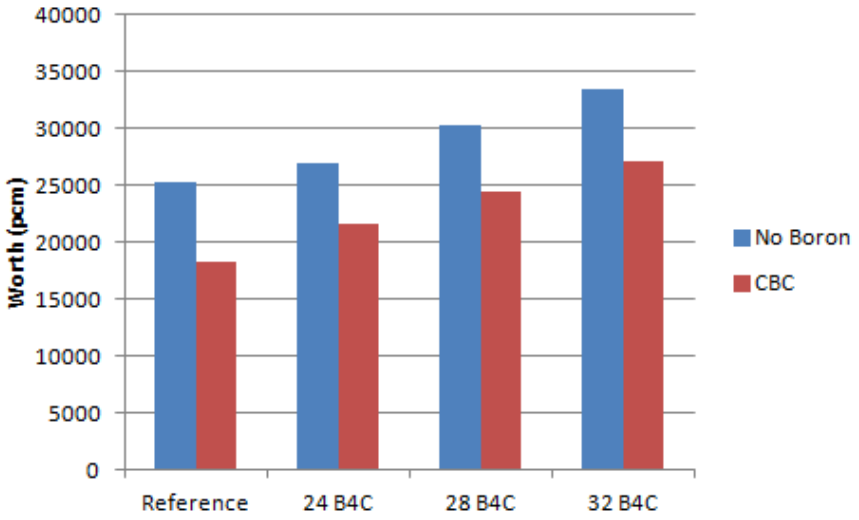

Figure 5-3. B_4C Rod Worth Comparison with Reference Core – Single Quarter Assembly Rodded

Table 5-6. B_4C Rod Worth Comparison with Reference Core – 2 of 4 Quarter Assemblies Rodded

Case	Worth (pcm) – No Boron	Worth (pcm) – CBC
Reference	12293	8893
19x19 Silicide Assembly with 24 Control Rods	12957	10387
19x19 Silicide Assembly with 28 Control Rods	14398	11647
19x19 Silicide Assembly with 32 Control Rods	15737	12832

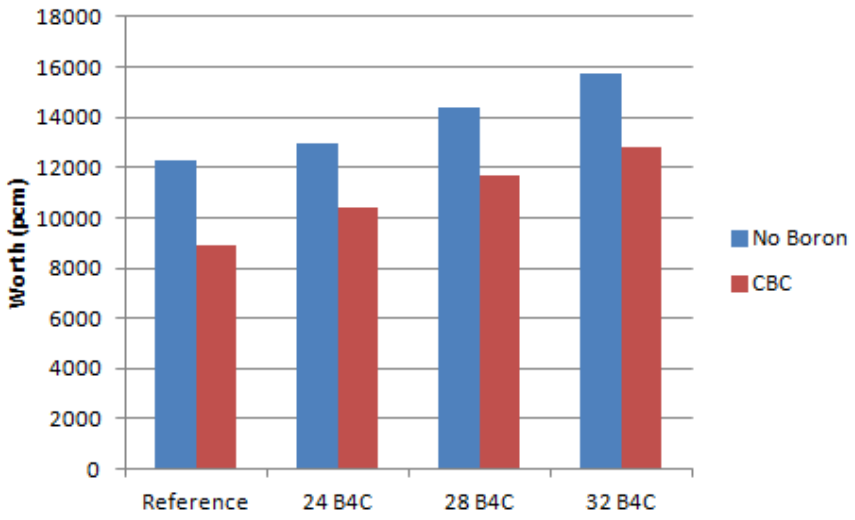

Figure 5-4. B_4C Rod Worth Comparison with Reference Core – 2 of 4 Quarter Assemblies Rodded

Table 5-7. Hf Rod Worth Comparison with Reference Core – Single Quarter Assembly Rodded

Case	Worth (pcm) – No Boron	Worth (pcm) – CBC
Reference	25367	18273
19x19 Silicide Assembly with 24 Control Rods	19033	13998
19x19 Silicide Assembly with 28 Control Rods	21663	16061
19x19 Silicide Assembly with 32 Control Rods	24149	18036

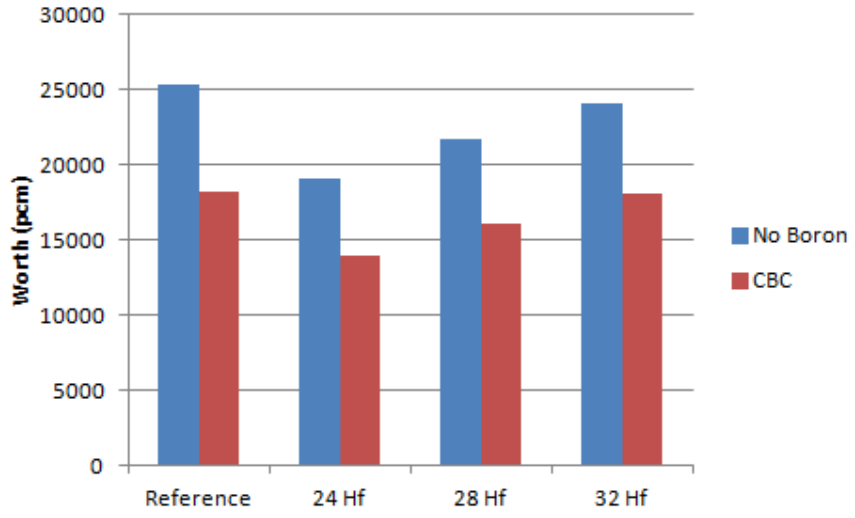

Figure 5-5. Hf Rod Worth Comparison with Reference Core – Single Quarter Assembly Rodded

Table 5-8. Hf Rod Worth Comparison with Reference Core – 2 of 4 Quarter Assemblies Rodded

Case	Worth (pcm) – No Boron	Worth (pcm) – CBC
Reference	12293	8893
19x19 Silicide Assembly with 24 Control Rods	9193	6784
19x19 Silicide Assembly with 28 Control Rods	10365	7723
19x19 Silicide Assembly with 32 Control Rods	11464	8615

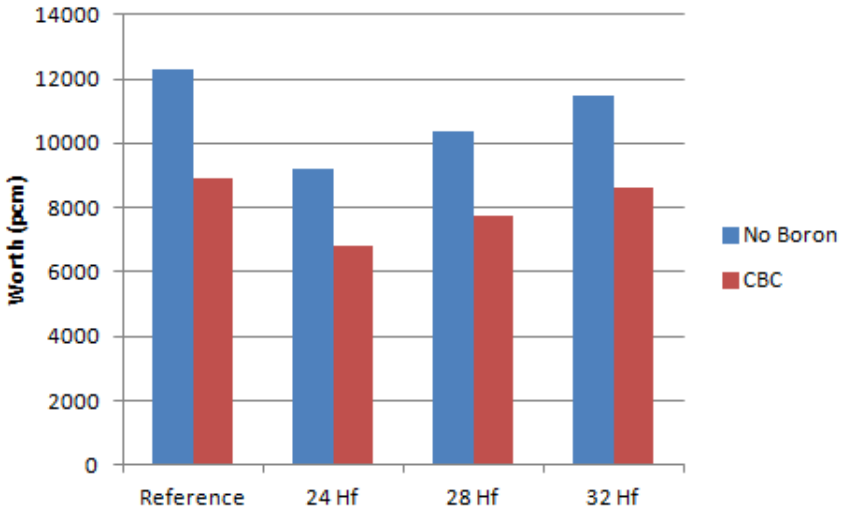

Figure 5-6. Hf Rod Worth Comparison with Reference Core – 2 of 4 Quarter Assemblies Rodded

From examination of the above comparisons, it is apparent that the control rod worth of the reference assembly can only be exceeded by employing B_4C control rods; indeed, even the minimum of 24 B_4C rods will exceed the reactivity worth of the reference case, making this material a promising option. While the maximum of 32 AIC or Hf rods cannot match the reactivity worth of the reference case, these cases do come relatively close to achieving the reference reactivity worth. As there is an appreciable basis of PWR operating experience with AIC control rods, it may be acceptable to sacrifice some margin in control rod worth to employ 32 AIC control rods.

Because of this possibility, it is worthwhile to explore the impact of choosing a larger number of control rods on the assembly cycle length. Replacing fuel pins with extra control rod

guide tubes removes reactivity from the core, but this loss in cycle length may be offset somewhat by the additional neutron moderation allowed for by the extra water-filled guide tubes. To evaluate this effect, SCALE inputs were built for a 19x19 silicide assembly with 24, 28, and 32 control rods in single quarter assembly geometry with all rods withdrawn for a depletion calculation. The depletion is carried out to a burnup of 60 GWd/MT. The results are presented as the neutron multiplication eigenvalue plotted against burnup for each case in Figure 5-7 below. Additionally, Figure 5-8 plots the difference in the neutron multiplication eigenvalue in pcm for the 28- and 32-rod cases relative to the 24-rod case as a function of the assembly burnup.

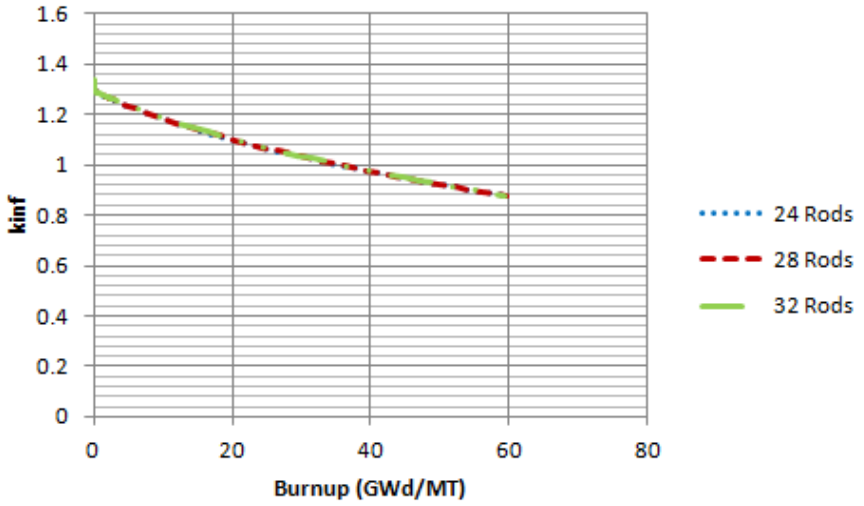

Figure 5-7. Depletion of 19x19 Silicide Assembly with 24, 28, and 32 Control Rods

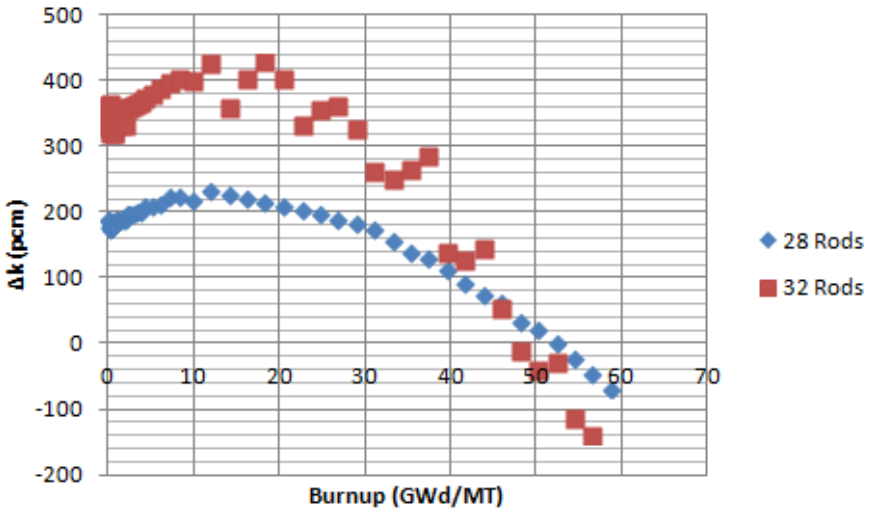

Figure 5-8. Difference in Neutron Multiplication Relative to 24 Control Rod Case

The trend in Figure 5-8 is best explained by considering the neutron energy spectrum in each fuel assembly case. The cases with 28 and 32 control rods have a larger amount of moderator and therefore a softer spectrum than the 24-rod case. Thus the reactivity of the 28- and 32-rod assemblies is initially higher than that of the 24-rod assembly; however, the 24-rod assembly experiences a greater rate of plutonium breeding due to its harder spectrum. For this reason, the reactivity of the 24-rod case will exceed that of the 28- and 32-rod cases towards the end of the cycle.

Cycle length assessment is done in a manner similar to that of the BA design evaluations. The core discharge burnup is again selected as that for which the neutron multiplication eigenvalue is equal to 1.03. The discharge burnup for each case is determined from linear interpolation, and the core initial heavy metal loading is obtained from the SCALE output. This information is then used to determine the cycle length of each case, given in Table 5-9.

Table 5-9. Cycle Length of 19x19 Silicide Assembly with 24, 28, and 32 Control Rods

	24 Rods	28 Rods	32 Rods
Initial heavy metal loading (kg)	81177	80210	79245
Discharge burnup (GWd/MT)	30.326	30.611	30.802
Cycle length (days)	818.96	816.81	812.02

Approximately one week is lost from the cycle length by increasing the number of control rods per assembly from 24 to 32. Thus only a minimal penalty in cycle length would be incurred if it is found desirable to recover control rod reactivity worth by increasing the number of control rods per assembly.

Although the rigor of the fuel assembly models used for the preceding analysis is admittedly limited, the exercise highlights some key reactor physics details of the I^2S-LWR core. It is challenging for the control rods of the 19x19 silicide assembly to achieve the reactivity worth of the 17x17 oxide assembly due to under-moderation to the 19x19 assembly. The 19x19 assembly design was constructed by reducing the fuel rod dimensions relative to a traditional 17x17 assembly to allow for packing of a larger number of fuel rods into limited space. Thus the fuel-to-moderator ratio is noticeably increased, yielding a harder neutron energy spectrum and therefore reduced control rod effectiveness. However, the control rod reactivity worth calculated in the preceding manner cannot be considered the decisive factor in determining the appropriate control rod design for the I^2S-LWR. Full-core three-dimensional analyses are necessary to sufficiently capture the control rod absorption physics and appropriately evaluate shutdown margin; such analyses are left to separate endeavors.

5.1.3. Comparison with Industry Data

Control rod worth data for the I^2S-LWR core has also been calculated by Westinghouse in (21). It is worthwhile to compare these results to those presented in this work so as to consider

the validity of the methodology employed in this study. Figure 5-9 below is reproduced from (21); it gives the reactivity worth in pcm of each control rod bank in the I^2S-LWR core. A consistent comparison of these results may be made on the basis of reactivity worth per fraction of assemblies rodded. This figure essentially provides a rough estimate of the reactivity worth with all assemblies rodded based on the results of a case in which only some assemblies are rodded; that is, it "converts" a partially rodded case to a fully rodded case for consistent comparison. Reactivity worth is estimated from Figure 5-9 for comparison with the 24 AIC results of this study; this information is used to calculate the reactivity worth per fraction of assemblies rodded for each case in Table 5-10. As reactivity worth was calculated for an equilibrium cycle in (21), the AIC worth data at CBC shall be used in an attempt to match spectra across cases.

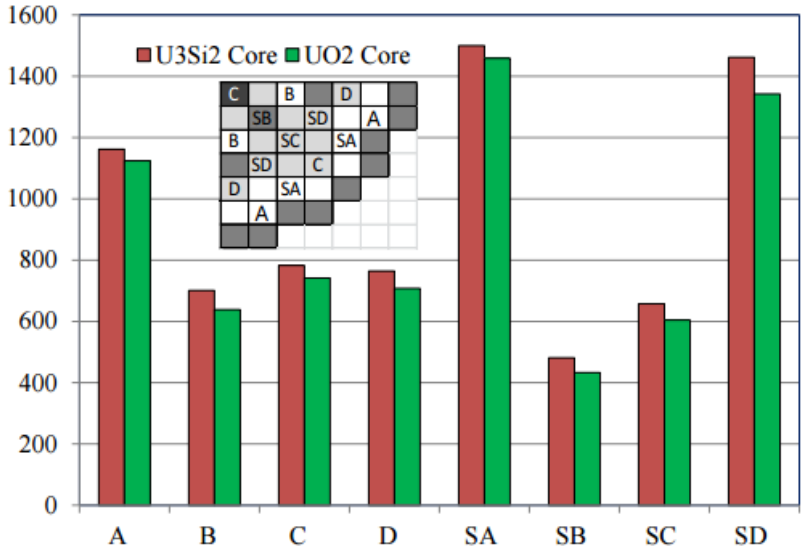

Figure 5-9. I^2S-LWR Control Rod Bank Reactivity Worth (21)

Table 5-10. Reactivity Worth per Fraction of Assemblies Rodded

Case	Reactivity Worth Estimate (pcm)	Fraction of Assemblies Rodded	Worth per Fraction of Assemblies Rodded (pcm)
Bank A	1150	8/121	17394
Bank B	700	4/121	21175
Bank C	790	5/121	19118
Bank D	790	4/121	23898
Bank SA	1450	8/121	21931
Bank SB	450	4/121	13613
Bank SC	650	4/121	19663
Bank SD	1450	8/121	21931
Single Quarter 24 AIC	13880	1	13880
Four Quarter 24 AIC	6735	1/2	13470

The normalized worth of the cases calculated in this study appears to indicate that the 2D infinite fuel assembly models yield an underestimate of reactivity worth. The discrepancy likely arises due to RCCA self-shielding in the 2D models, wherein a significantly larger fraction of the assemblies are rodded than in the Westinghouse cases, which model the true RCCA placement in the core. Even with these discrepancies in estimated control rod worth, the results produced in this study are at least of a magnitude comparable to those of the equilibrium cycle analysis, thereby justifying some confidence in the methodology employed here. The differences are likely due primarily to the modeling simplifications.

5.2. Burnable Absorbers

First, some remarks on the distinguishing characteristics of Gd-poisoned assemblies and IFBA-poisoned assemblies are in order. Naturally, greater poison loading yields a greater reactivity hold-down; cases with 8 Gd pins of 4 w/o provided the lowest magnitude of reactivity offset with a case average BA worth of -3818 pcm, while the 160 IFBA pin cases provided the greatest with a case average BA worth of -14572 pcm. Cases with 80 IFBA pins provided a similar reactivity offset to cases with 16 Gd pins of 4 w/o, with case average BA worth of 7806 and 7747 pcm respectively; however, other metrics differ significantly. Power peaking was

addressed far more easily with IFBA than with Gd, due to the very large absorption cross sections of several Gd isotopes yielding significant depressions in flux and power which must be compensated for elsewhere in the assembly. The case average maximum and minimum power peaking is calculated for all cases and summarized in Table 5-11 below.

Table 5-11. Case Average Maximum and Minimum Power Peaking

Case	Average Maximum Power Peaking	Average Minimum Power Peaking
8 Gd 4 w/o	1.0807	0.3558
8 Gd 8 w/o	1.0850	0.2416
16 Gd 4 w/o	1.0982	0.3281
16 Gd 8 w/o	1.1065	0.2242
80 IFBA	1.0641	0.9176
160 IFBA	1.0569	0.9379

As was anticipated, cycle length is more desirable in IFBA cases than in Gd cases as well. The neutron poison inventory analysis confirms the presence of residual Gd in Gd cases in quantities greater than would be built up by fission events only; the ^{155}Gd concentration in Gd cases is on the order of 10^{-8} at/b-cm when the discharge burnup is reached as opposed to 10^{-9} at/b-cm in IFBA cases. The Gd cases with the lowest poison loading (8 Gd pins of 4 w/o) had a cycle length estimate 10 days less than that of the uncontrolled case. The IFBA cases actually achieve a cycle length greater than that of the uncontrolled assembly due to greater ^{239}Pu breeding resulting from a harder neutron energy spectrum. This gain in ^{239}Pu inventory can be observed in the OPUS module output as well, as ^{239}Pu is a default tracked nuclide. This information is extracted for the uncontrolled case and the first round of each of the IFBA cases and used to generate Figure 5-10 below, which plots the ratio of the ^{239}Pu concentration in the IFBA cases to that of the uncontrolled case at each depletion step. It is a relatively small gain sufficient to extend the cycle length estimate by two days.

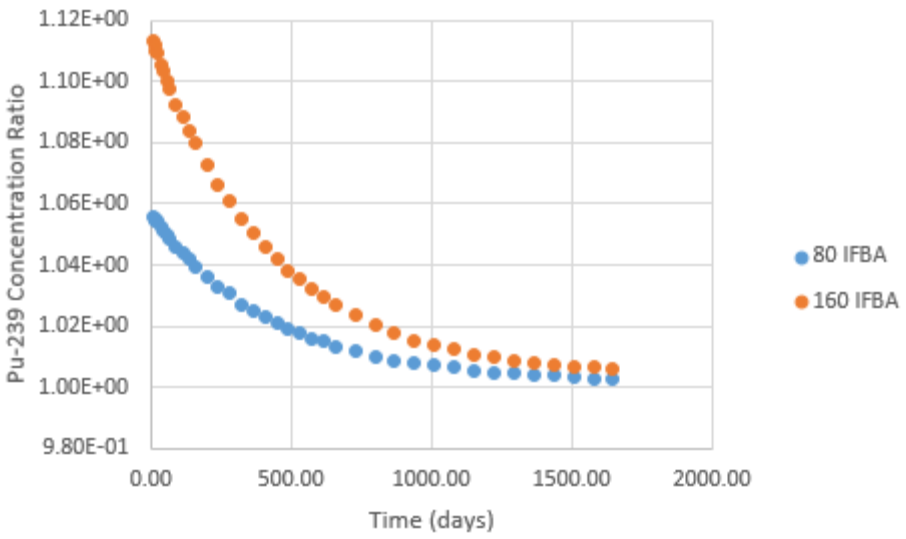

Figure 5-10. Ratio of 80 IFBA Case Pu to Uncontrolled Case Pu

While the estimated MTC was found to be positive for all cases, these values are not necessarily indicative of the true core MTC. The MTC is naturally greatest for cases with the lowest magnitude of the BA reactivity worth; these require a greater CBC to achieve criticality and therefore exhibit the greatest reduction in parasitic neutron absorption when an increase in moderator temperature yields a decrease in density and effective boron concentration. It is noteworthy that although the reactivity hold-down and CBC of the cases with 16 Gd pins of 4 w/o and cases with 80 IFBA pins are similar, the IFBA cases yield a slightly less positive MTC: 33.27 pcm/K case average center MTC for Gd versus 31.23 pcm/K case average center MTC for IFBA. This arises from the fact that all absorbers in the IFBA cases are the same species. The ^{10}B in IFBA absorbs neutrons at the same energies that the ^{10}B in the moderator absorbs, thereby altering the neutron energy spectrum in the moderator in such a way as to reduce the population of neutrons with energies that are conducive to absorption. The soluble boron is therefore not as effective in the IFBA cases as it is in the Gd cases, and thus a decrease in the effective boron concentration due to an increase in moderator temperature does not impact parasitic absorption in IFBA cases as heavily as it does in Gd cases. This observation is corroborated by the boron

worth results as well, which are slightly lower in magnitude on average in the IFBA cases than in the Gd cases. All of the cases observed exhibited boron worth smaller in magnitude than that of the uncontrolled case, which is indicative of improvements to MTC as a result of competing absorbers.

Within cases, the BA arrangement changes between iterations do not yield appreciable changes in cycle length, boron worth, or MTC; these metrics are driven primarily by the type and concentration of poison rather than the detailed BA layout. Consideration of these metrics points to IFBA as the most promising absorber candidate, as the increase in cycle length is not achieved with Gd as a poison with equivalent reactivity worth. The spectral impact of IFBA is friendly to MTC as well. The BA layout itself has the largest impact on power peaking, with a secondary impact on the BA worth (which is also driven primarily by the poison type and concentration, but finer tuning can be accomplished by adjusting the layout). With respect to power peaking, IFBA is once again found to be superior to Gd, whose large absorption cross section yields regions of highly localized parasitic absorption in the fuel assembly.

In an attempt to characterize the impact of the BA layout on the BA worth, the BA worth for each iteration of each case is plotted against the average poison pin position reported in Section 4.2.1 in Figures 5-11 through 5-16 below. The same is done for the maximum power peaking in Figures 5-17 through 5-22. It was hoped that some trends might be visually identified through this exercise, but this is not the case. The only case that could reasonably be argued to exhibit a trend is the 160 IFBA case, which seems to indicate an increase in the magnitude of the BA worth as the average poison pin position moves farther from the center of the assembly. It is therefore concluded that the average poison pin position is not a reliable predictor of the

assembly reactivity or power peaking, but some other position-based variables may be tested in future endeavors.

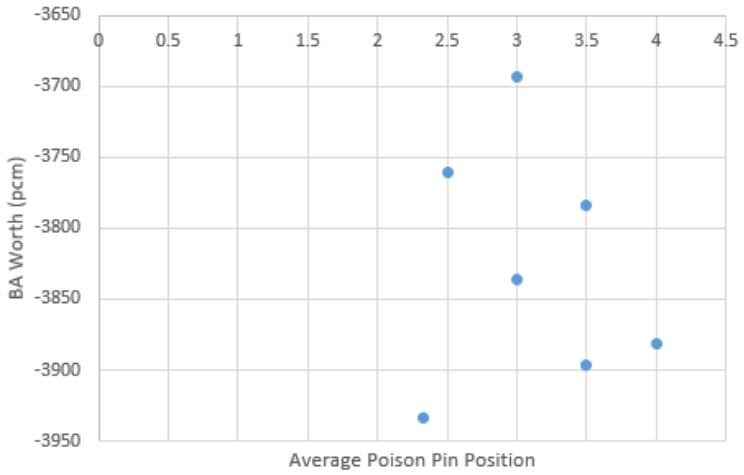

Figure 5-11. Impact of Average Poison Pin Position on BA worth: 8 Gd Pins, 4 w/o

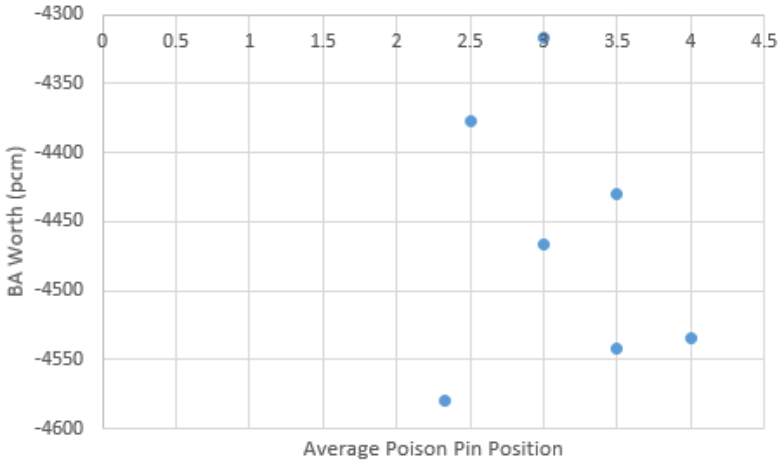

Figure 5-12. Impact of Average Poison Pin Position on BA Worth: 8 Gd Pins, 8 w/o

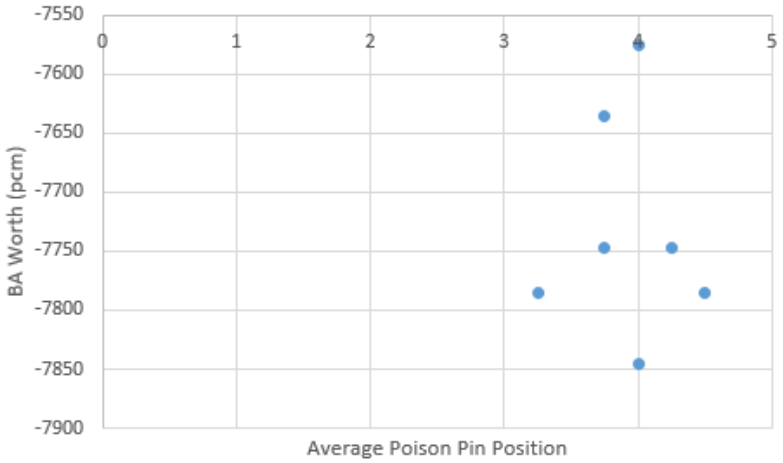

Figure 5-13. Impact of Average Poison Pin Position on BA Worth: 16 Gd Pins, 4 w/o

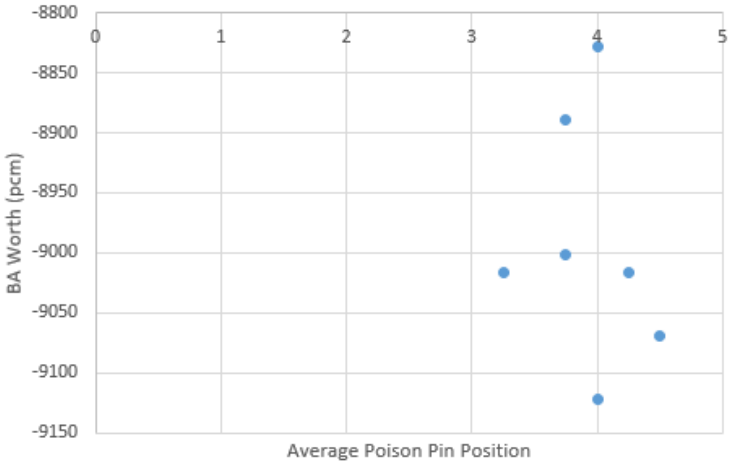

Figure 5-14. Impact of Average Poison Pin Position on BA Worth: 16 Gd Pins, 8 w/o

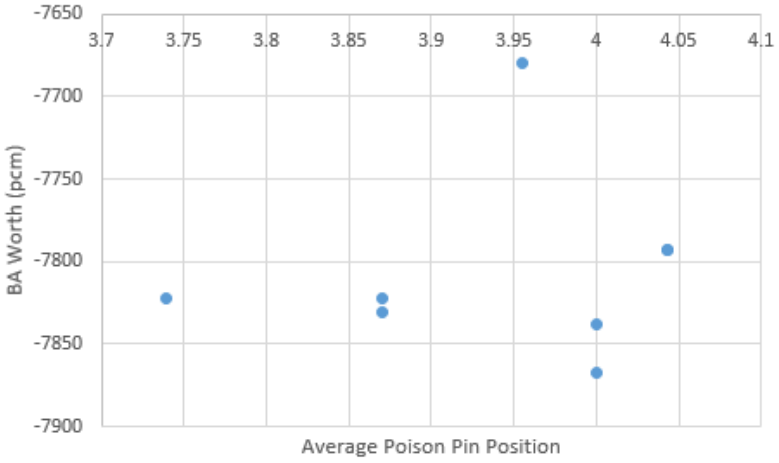

Figure 5-15. Impact of Average Poison Pin Position on BA Worth: 80 IFBA Pins, 2.5 mg/in

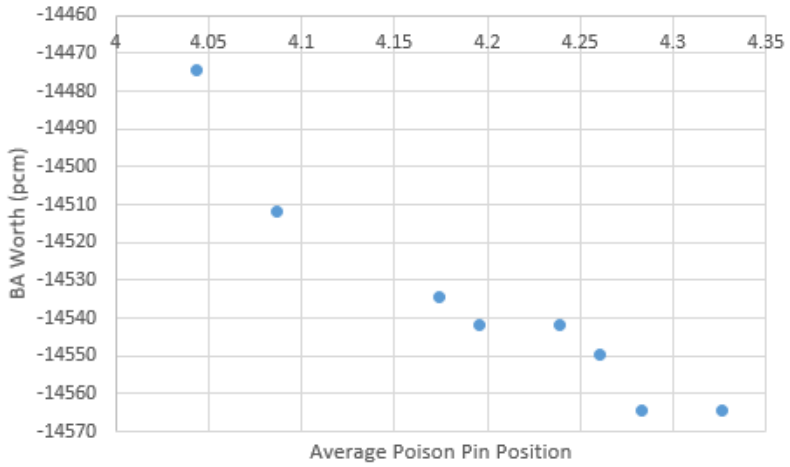

Figure 5-16. Impact of Average Poison Pin Position on BA Worth: 160 IFBA Pins, 2.5 mg/in

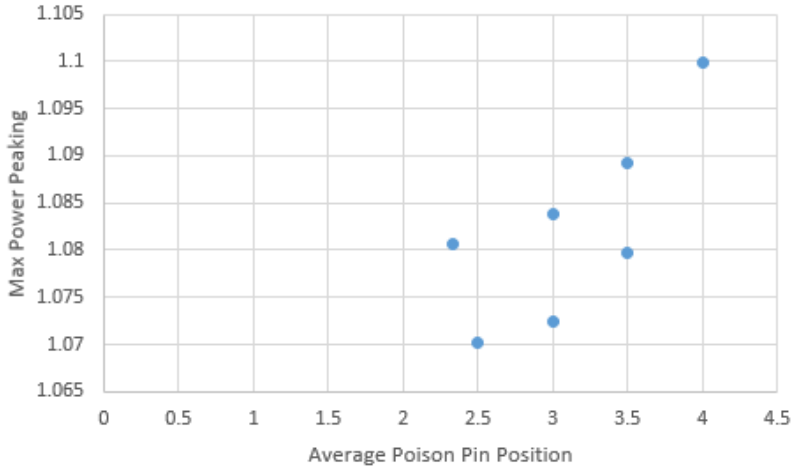

Figure 5-17. Impact of Average Poison Pin Position on Power Peaking: 8 Gd Pins, 4 w/o

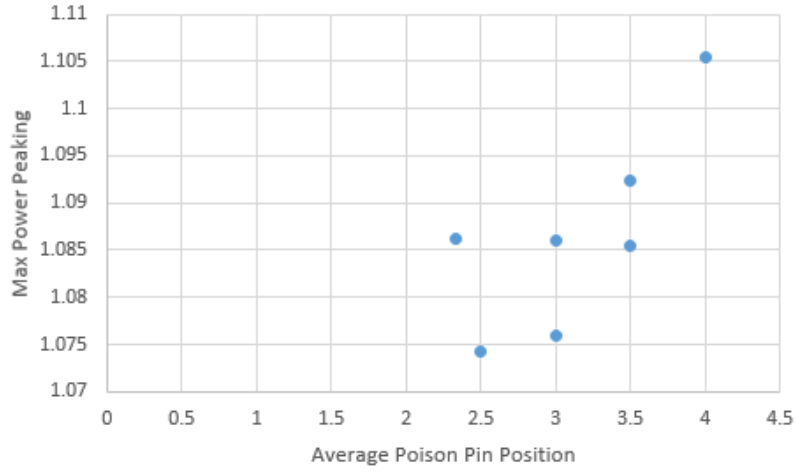

Figure 5-18. Impact of Average Poison Pin Position on Power Peaking: 8 Gd Pins, 8 w/o

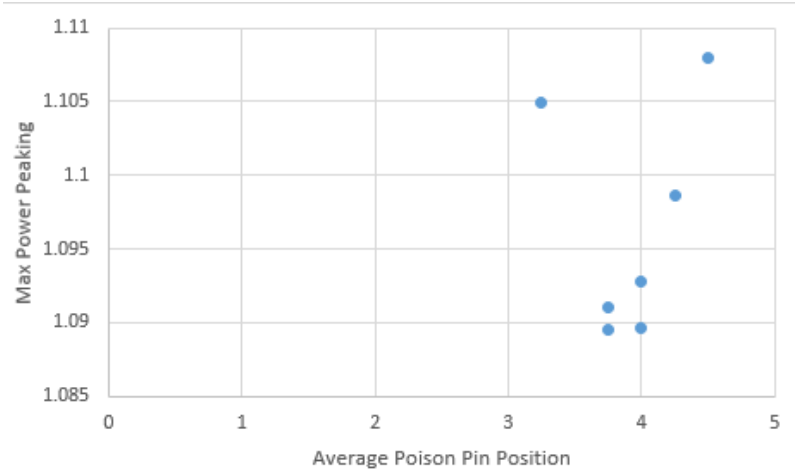

Figure 5-19. Impact of Average Poison Pin Position on Power Peaking: 16 Gd Pins, 4 w/o

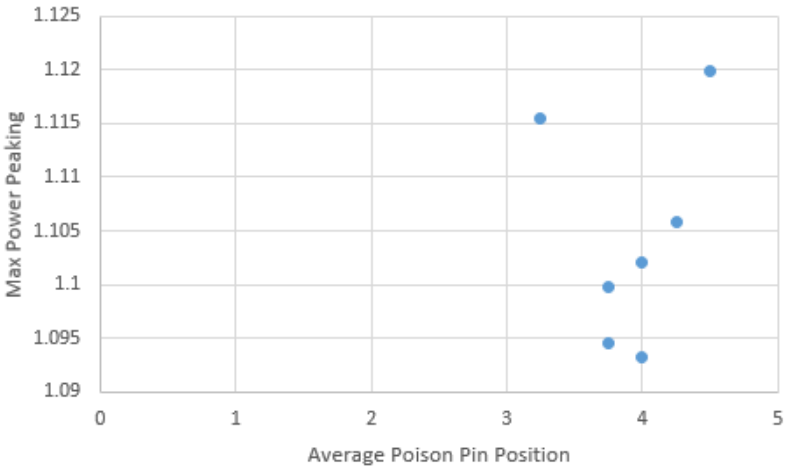

Figure 5-20. Impact of Average Poison Pin Position on Power Peaking: 16 Gd Pins, 8 w/o

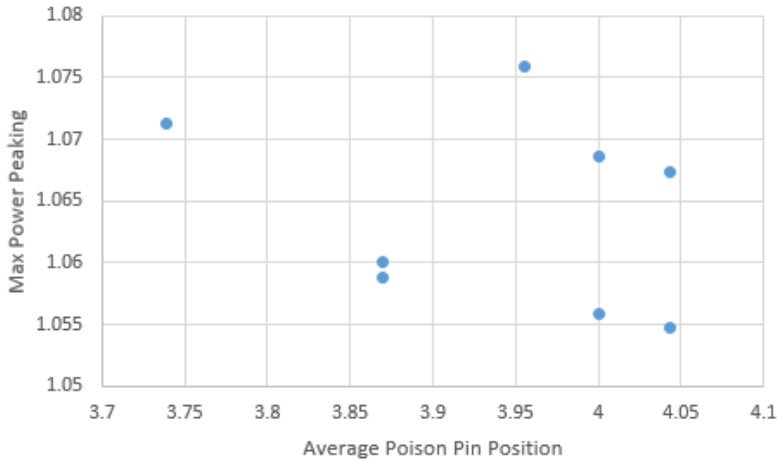

Figure 5-21. Impact of Average Poison Pin Position on Power Peaking: 80 IFBA Pins, 2.5 mg/in

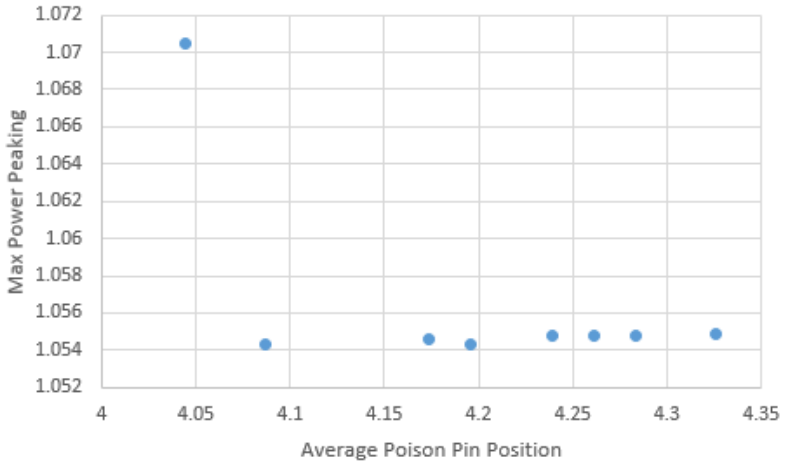

Figure 5-22. Impact of Average Poison Pin Position on Power Peaking: 160 IFBA Pins, 2.5 mg/in

6. CONCLUSION

The analyses presented in this work have provided insight into the reactor physics phenomena of the I^2S-LWR U_3Si_2 fuel assembly and their implications with respect to reactivity control. Simple two-dimensional transport models of the fuel assembly are investigated with the SCALE code system to predict the neutronic behavior associated with the various reactivity control schemes explored. Although these models are limited in rigor, key relationships between the fuel assembly design parameters and the neutronic performance indicators have been identified so as to provide a basis upon which more detailed studies may be constructed. Some engineering judgment has been developed as well that may provide some initial guidelines in making high-level design decisions.

6.1. RCCA Design Recommendations

Previous analyses indicate confidence that an RCCA design with 24 AIC control rods per assembly provides sufficient reactivity control for the I^2S-LWR U_3Si_2 core in terms of the essential control rod performance metrics such as shutdown margin (8). However, the exploration of other RCCA design options reveals some important reactor physics traits of the unique I^2S-LWR fuel assembly design. The static reactivity worth of the 24-rod AIC RCCA in the 19x19 silicide assembly is less than that in a traditional 17x17 oxide assembly due to the increase in the fuel-to-moderator ratio realized when switching from a 17x17 lattice to the 19x19 design. The RCCA worth may be improved by employing more rods per assembly or by using a stronger absorber, but such a design change necessitates additional studies to investigate other reactor physics characteristics including impact on cycle length, control rod absorber depletion, and shim. Furthermore, these analyses must be carried out using full-core models to appropriately capture all the relevant physics.

Considering the other RCCA designs explored, those with B_4C as the absorbing material proved most effective in improving RCCA reactivity worth due to the neutron absorption properties of ^{10}B. Even using just 24 B_4C rods per assembly provides a significant gain in reactivity worth over the AIC design that could not be realized by increasing the number of AIC or Hf rods. However, the reactivity worth alone is not a sufficient acceptance criterion in selecting the RCCA design; as such, separate studies have provided justification for retaining the 24-rod AIC RCCA for use in the I^2S-LWR silicide core (8). This is a desirable course of action due to the significant basis of industrial operating experience with AIC control rods in PWRs.

6.2. BA Design Recommendations

Several different performance metrics have been reported for the BA cases; while generally full-core analyses are necessary for accurate predictions of these metrics, the estimations made in this study provide high-level insight into how BA design impacts the I^2S-LWR core physics. Additionally, these estimations confirm confidence in using IFBA, as has been decided based on prior work (8). When employed in sufficient quantities, Gd is a highly effective neutron absorber which can provide a great deal of negative reactivity worth. However, the preceding analyses have highlighted several issues associated with use of Gd as a BA. Incomplete Gd depletion yields a reactivity penalty late in the depletion cycle which reduces the cycle length. Power peaking in the assembly is a challenge with Gd as well; due to its large absorption cross section, significant local flux depressions are observed in Gd-poisoned lattice locations, which yield significant peaking and non-uniform assembly burnup. Thus Gd-poisoned assemblies are useful in core designs which need particular suppression of flux and power, but there are considerable penalties to the fuel economics with respect to the cycle length and uniformity of burnup on a rod-to-rod basis.

The IFBA-poisoned assembly presents several advantages over the use of Gd. Fuel economics are improved by an increase in the cycle length relative to an uncontrolled assembly, as well as a more uniform assembly burnup afforded by improved power peaking. Core safety is benefited, as the use of the ^{10}B-based absorber as an integral absorber has a desirable impact on MTC estimates. IFBA must be employed heavily to achieve reactivity control on par with Gd, but the reactor physics benefits are considerable.

6.3. Future Work

While the fuel assembly calculations performed in this work provide valuable insight into the neutronics of the I^{2}S-LWR silicide fuel assembly, full-core analyses are necessary to determine if the reactivity control schemes explored are acceptable. In addition to investigating axial and radial phenomena not captured by the 2D infinite models used here, such analyses are necessary for accurate calculation of safety parameters such as MTC and shutdown margin. A particular set of additional studies that can be performed using the 2D infinite models might involve an attempt to parameterize the performance indicators of the BA designs. The attempt was made in this study to use the average poison rod location as the independent variable for such parameterization, but no meaningful relationships were observed. Other candidates for independent variables might be tested to determine if any correlations can be identified and captured. Such information may be useful even later for the development of an optimization algorithm based on those discussed in Chapter 2. These algorithms are relevant to the goals of this work, but their application was not considered here. The scope of this study was identified so that the analysis considers fuel assembly neutronics phenomena at a high level, and gives a foundation which can feed into more detailed core analyses and design decisions.

APPENDICES

APPENDIX A. MATERIAL DATA

The input required for the models developed in this study demands careful attention to definition of material compositions. The applied material data are summarized here on a case-by-case basis. In cases where elemental isotopics are not given, the SCALE default is used.

Material Data for RCCA Cases

Material	Purpose	Density (g/cm^3)	Density Multiplier	Temperature (K)	Isotopics (w/o)
U_3Si_2	Fuel	12.2	0.955	891.5	Si: SCALE default U: 0.54% ^{234}U 4.95% ^{235}U 95.04% ^{238}U
He	Gap	1	1	700.05	SCALE default
AMPT	Clad	7.25	1	612.45	3% Mo 21% Cr 5% Al 71% Fe
Water	Moderator	0.7	1	582.75	SCALE default
Boron	Chemical shim	0.7	(depends on desired concentration)	582.75	SCALE default
AIC	Control rod	10.2	1	582.75	80% Ag 15% In 5% Cd
B_4C	Control rod	2.52	1	582.75	SCALE default
Hf	Control rod	13.31	1	582.75	SCALE default
SS304	Guide tube	7.94	1	582.75	SCALE default

Material Data for 4 w/o Gd BA Cases

Material	Purpose	Density (g/cm^3)	Density Multiplier	Temperature (K)	Isotopics (w/o)
U_3Si_2	Fuel	12.2	0.96	900	Si: SCALE default U: 0.54% ^{234}U 4.95% ^{235}U 95.04% ^{238}U
He	Gap	0.00194	1	700	SCALE default
AMPT	Clad	7.25	1	612	3% Mo 21% Cr 5% Al 71% Fe
Water	Moderator	0.7	1	582	SCALE default
Boron	Chemical shim	0.7	(depends on desired concentration)	582	SCALE default
Gd_2O_3	Poison	11.515	0.04	900	SCALE default
U_3Si_2	Poisoned fuel	11.515	0.96	900	Si: SCALE default U: 0.04% ^{234}U 3.95% ^{235}U 96.01% ^{238}U

Material Data for 8 w/o Gd BA Cases

Material	Purpose	Density (g/cm^3)	Density Multiplier	Temperature (K)	Isotopics (w/o)
U_3Si_2	Fuel	12.2	0.96	900	Si: SCALE default U: 0.54% ^{234}U 4.95% ^{235}U 95.04% ^{238}U
He	Gap	0.00194	1	700	SCALE default
AMPT	Clad	7.25	1	612	3% Mo 21% Cr 5% Al 71% Fe
Water	Moderator	0.7	1	582	SCALE default
Boron	Chemical shim	0.7	(depends on desired concentration)	582	SCALE default
Gd_2O_3	Poison	11.318	0.08	900	SCALE default
U_3Si_2	Poisoned fuel	11.318	0.92	900	Si: SCALE default U: 0.04% ^{234}U 2.95% ^{235}U 97.01% ^{238}U

Material Data for IFBA Cases

Material	Purpose	Density (g/cm^3)	Density Multiplier	Temperature (K)	Isotopics (w/o)
U_3Si_2	Fuel	12.2	0.96	900	Si: SCALE default U: 0.54% ^{234}U 4.95% ^{235}U 95.04% ^{238}U
He	Gap	0.00194	1	700	SCALE default
AMPT	Clad	7.25	1	612	3% Mo 21% Cr 5% Al 71% Fe
Water	Moderator	0.7	1	582	SCALE default
Boron	Chemical shim	0.7	(depends on desired concentration)	582	SCALE default
^{10}B	Poison	0.21573	1	800	100% ^{10}B
U_3Si_2	Poisoned fuel	12.2	0.96	900	Si: SCALE default U: 0.04% ^{234}U 4.95% ^{235}U 95.01% ^{238}U

APPENDIX B. BA ARRANGEMENTS

Presented here are depictions of the fuel assembly models to show explicitly the BA placement for every case. Shaded cells indicate poison positions, and an "X" indicates a guid tube position.

Iteration 1: 8 Gd Pins

O	O	O	O	O	O	O	O	O	O
O	O	O	O	O	O	O	O	O	O
X	O	O	X	O	O	O	O	O	O
O	O	O	O	O	O	X	O	O	O
O	O	O	O	O	O	O	O	O	O
O	O	O	O	O	O	O	O	O	O
X	O	O	X	O	O	O	X	O	O
O	O	O	O	O	O	O	O	O	O
O	O	O	O	O	O	O	O	O	O
X	O	O	X	O	O	O	X	O	O

Iteration 1: 16 Gd Pins

O	O	O	O	O	O	O	O	O	O
O	O	O	O	O	O	O	O	O	O
X	O	O	X	O	O	O	O	O	O
O	O	O	O	O	O	X	O	O	O
O	O	O	O	O	O	O	O	O	O
O	O	O	O	O	O	O	O	O	O
X	O	O	X	O	O	O	X	O	O
O	O	O	O	O	O	O	O	O	O
O	O	O	O	O	O	O	O	O	O
X	O	O	X	O	O	O	X	O	O

Iteration 1: 80 IFBA Pins

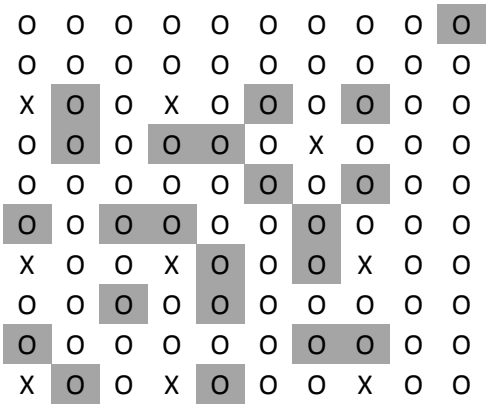

Iteration 1: 160 IFBA Pins

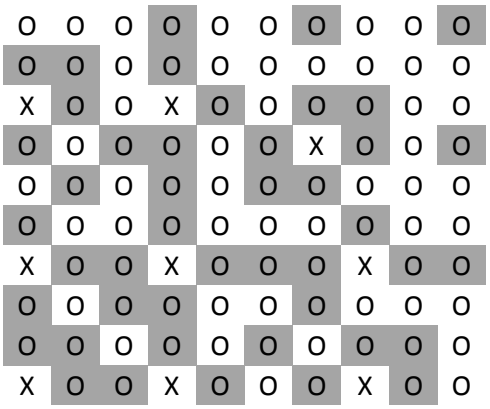

Iteration 2: 8 Gd Pins

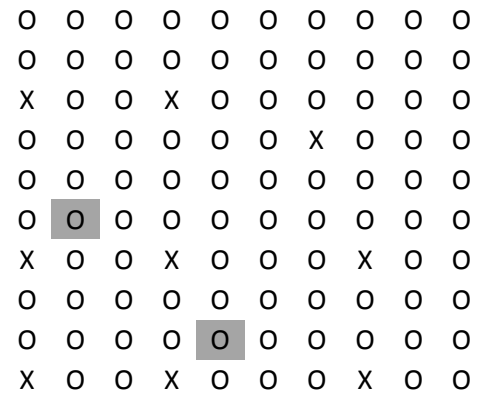

Iteration 2: 16 Gd Pins

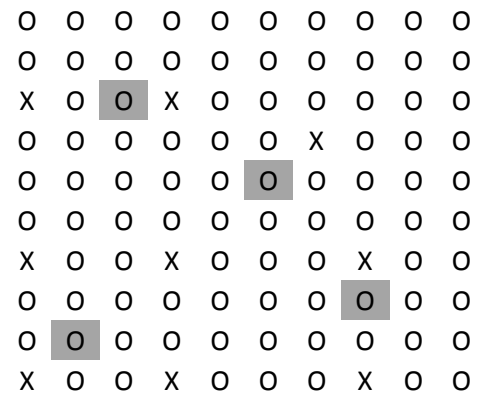

Iteration 2: 80 IFBA Pins

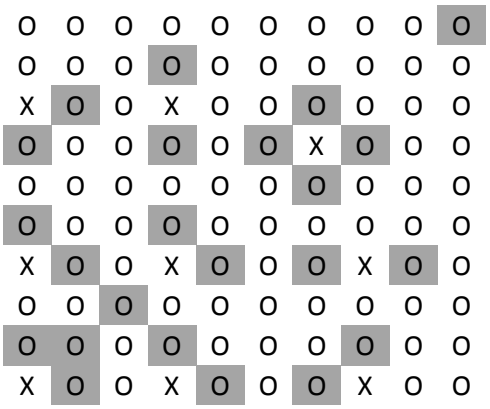

Iteration 2: 160 IFBA Pins

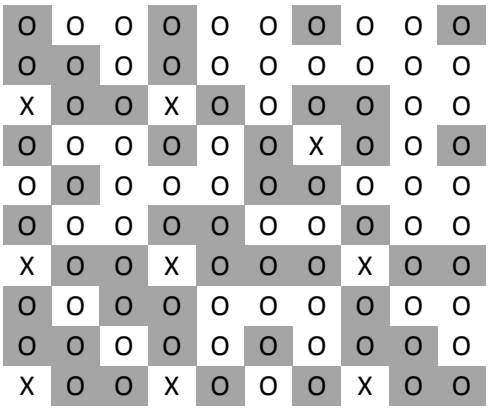

Iteration 3: 8 Gd Pins

O O O O O O O O O O
O O O O O O O O O O
X O O X O O O O O O
O O O O O O X O O O
O O O O O O O O O O
O O O O O O O O O O
X O O X O O O X O O
O O O O O O O O O O
O O O O O O O O O O
X O O X O O O X O O

Iteration 3: 16 Gd Pins

O O O O O O O O O O
O O O O O O O O O O
X O O X O O O O O O
O O O O O O X O O O
O O O O O O O O O O
O O O O O O O O O O
X O O X O O O X O O
O O O O O O O O O O
O O O O O O O O O O
X O O X O O O X O O

Iteration 3: 80 IFBA Pins

O O O O O O O O O O
O O O O O O O O O O
X O O X O O O O O O
O O O O O O X O O O
O O O O O O O O O O
O O O O O O O O O O
X O O X O O O X O O
O O O O O O O O O O
O O O O O O O O O O
X O O X O O O X O O

Iteration 3: 160 IFBA Pins

O	O	O	O	O	O	O	O	O	O
O	O	O	O	O	O	O	O	O	O
X	O	O	X	O	O	O	O	O	O
O	O	O	O	O	O	X	O	O	O
O	O	O	O	O	O	O	O	O	O
O	O	O	O	O	O	O	O	O	O
X	O	O	X	O	O	O	X	O	O
O	O	O	O	O	O	O	O	O	O
O	O	O	O	O	O	O	O	O	O
X	O	O	X	O	O	O	X	O	O

Iteration 4: 8 Gd Pins

O	O	O	O	O	O	O	O	O	O
O	O	O	O	O	O	O	O	O	O
X	O	O	X	O	O	O	O	O	O
O	O	O	O	O	O	X	O	O	O
O	O	O	O	O	O	O	O	O	O
O	O	O	O	O	O	O	O	O	O
X	O	O	X	O	O	O	X	O	O
O	O	O	O	O	O	O	O	O	O
O	O	O	O	O	O	O	O	O	O
X	O	O	X	O	O	O	X	O	O

Iteration 4: 16 Gd Pins

O	O	O	O	O	O	O	O	O	O
O	O	O	O	O	O	O	O	O	O
X	O	O	X	O	O	O	O	O	O
O	O	O	O	O	O	X	O	O	O
O	O	O	O	O	O	O	O	O	O
O	O	O	O	O	O	O	O	O	O
X	O	O	X	O	O	O	X	O	O
O	O	O	O	O	O	O	O	O	O
O	O	O	O	O	O	O	O	O	O
X	O	O	X	O	O	O	X	O	O

Iteration 4: 80 IFBA Pins

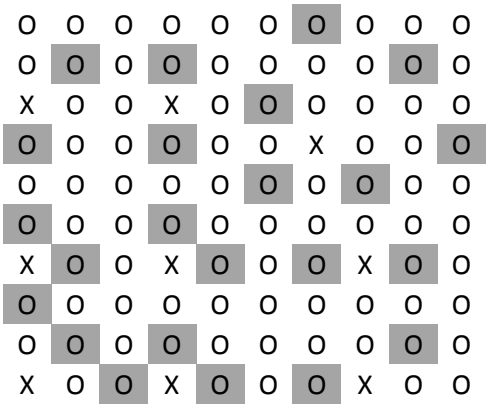

Iteration 4: 160 IFBA Pins

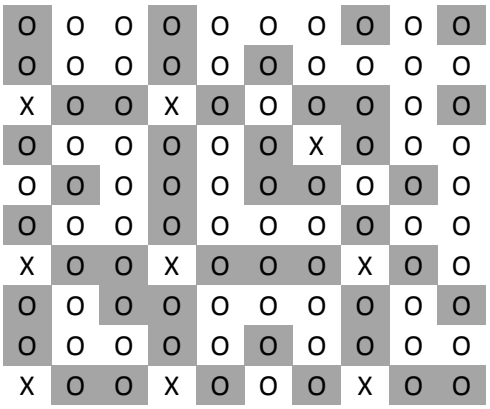

Iteration 5: 8 Gd Pins

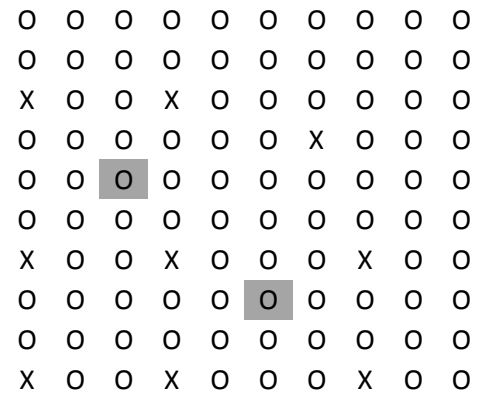

Iteration 5: 16 Gd Pins

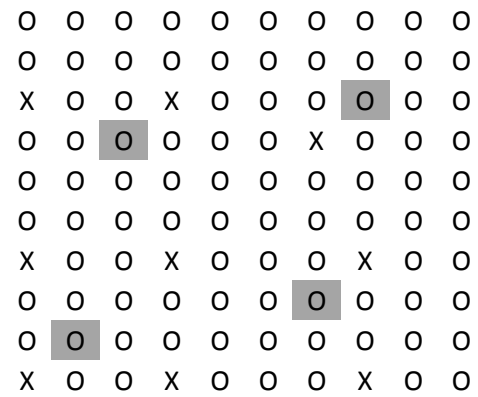

Iteration 5: 80 IFBA Pins

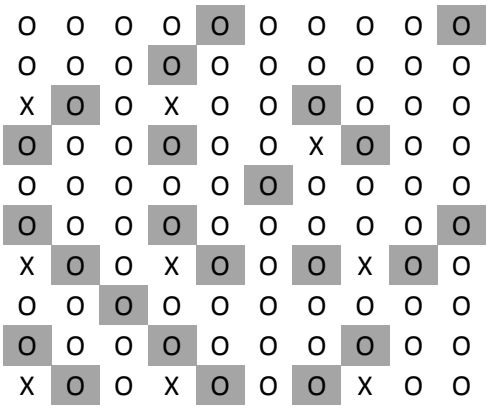

Iteration 5: 160 IFBA Pins

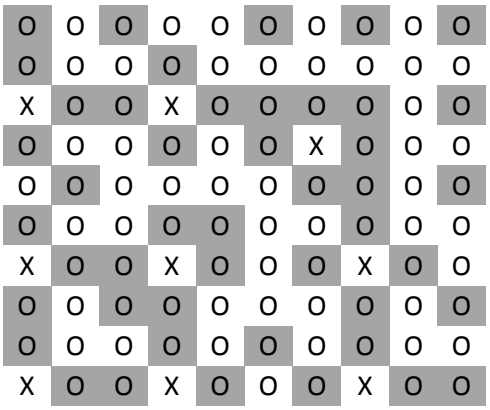

Iteration 6: 8 Gd Pins

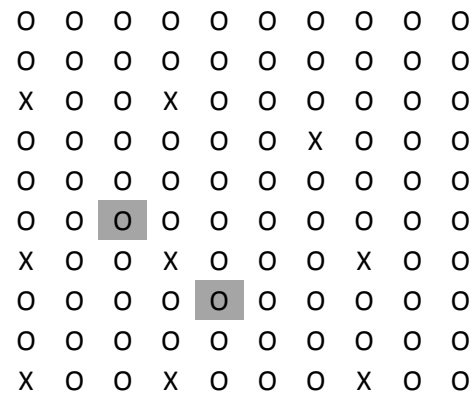

Iteration 6: 16 Gd Pins

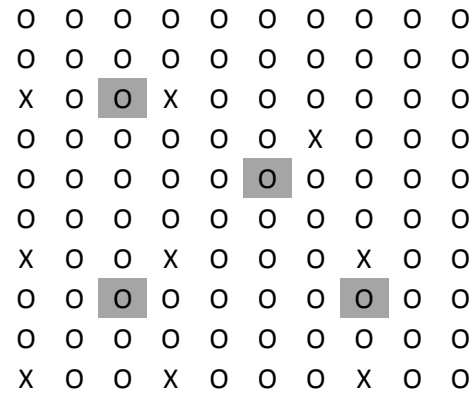

Iteration 6: 80 IFBA Pins

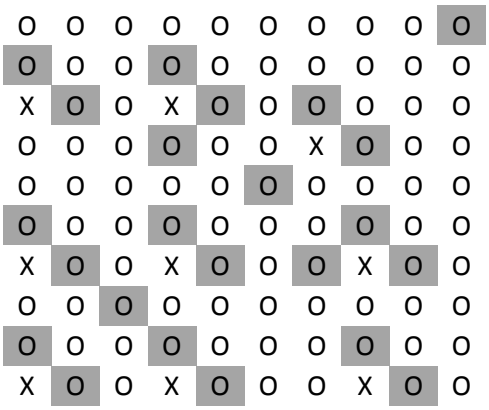

Iteration 6: 160 IFBA Pins

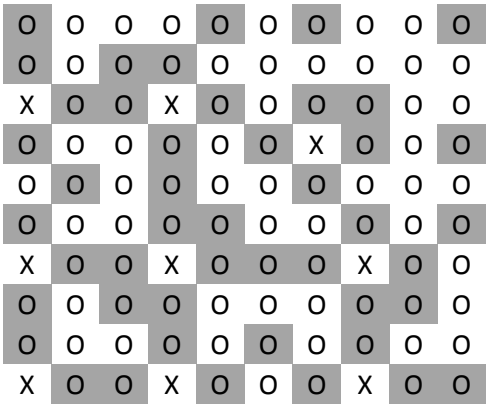

Iteration 7: 8 Gd Pins

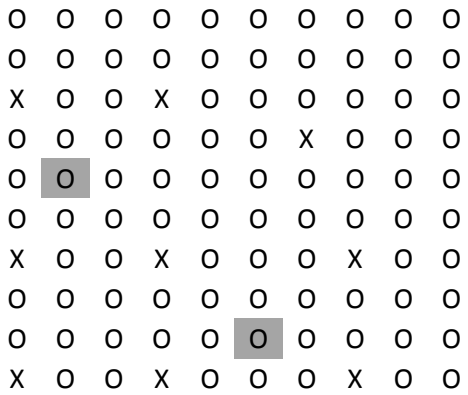

Iteration 7: 16 Gd Pins

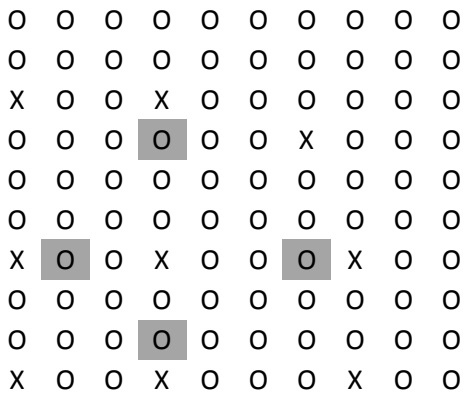

Iteration 7: 80 IFBA Pins

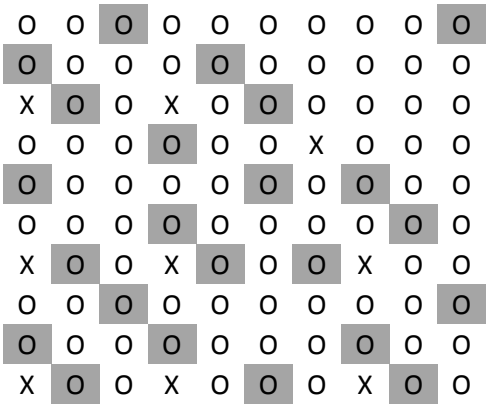

Iteration 7: 160 IFBA Pins

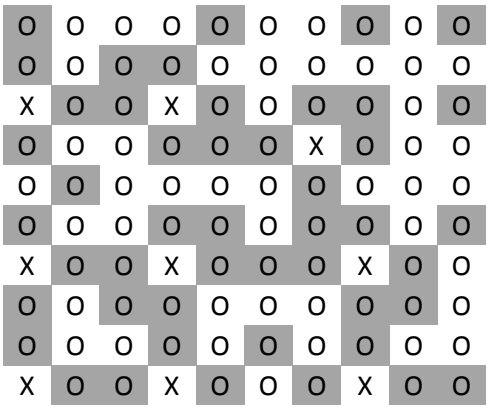

Iteration 8: 8 Gd Pins

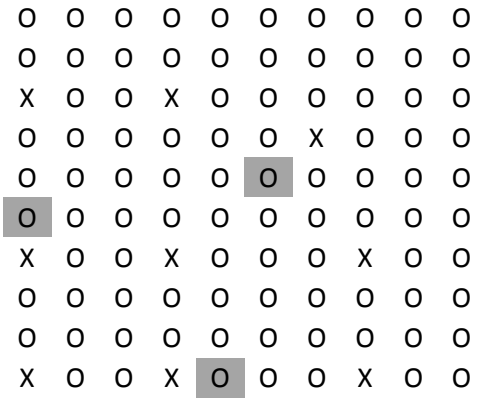

Iteration 8: 16 Gd Pins

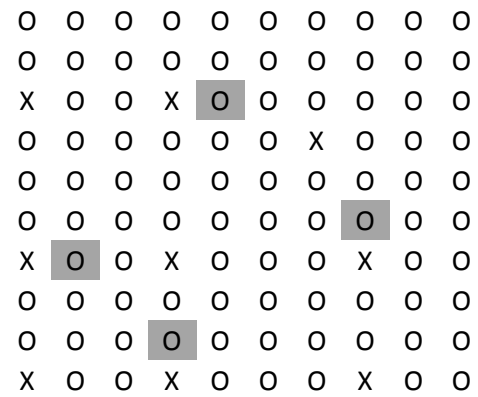

Iteration 8: 80 IFBA Pins

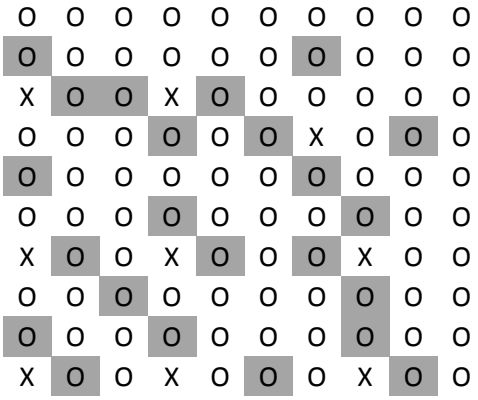

Iteration 8: 160 IFBA Pins

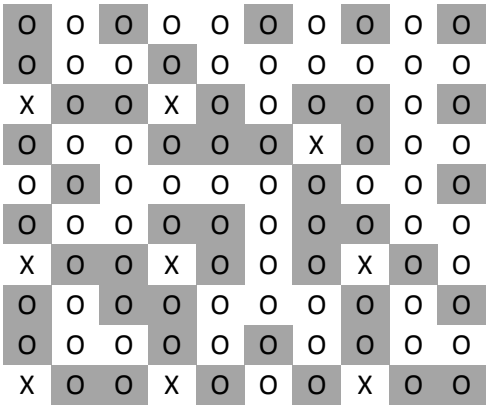

APPENDIX C. COMPLETE POWER PEAKING DATA

The BOC power peaking profiles for all iterations of all cases are given here.

Iteration 1: 8 Gd Pins, 4 w/o

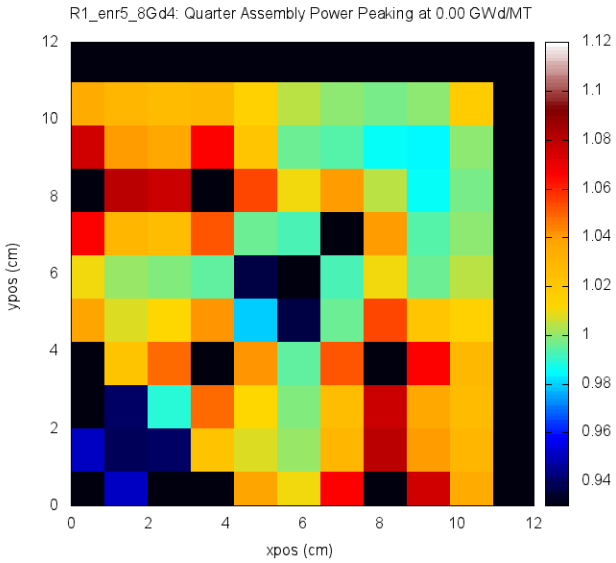

Iteration 1: 8 Gd Pins, 8 w/o

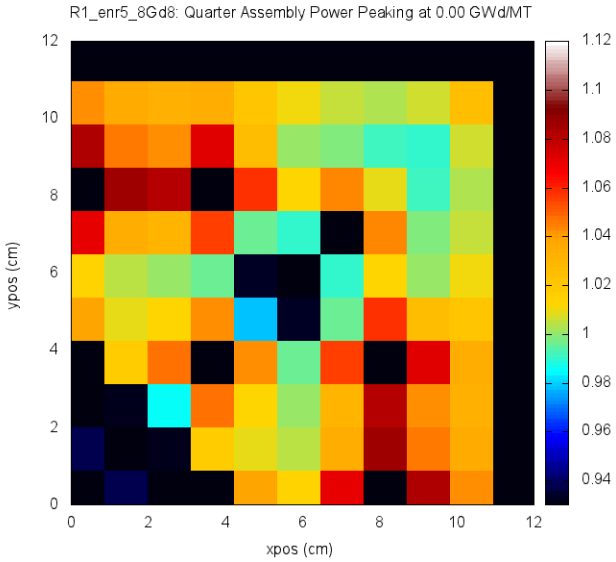

Iteration 1: 16 Gd Pins, 4 w/o

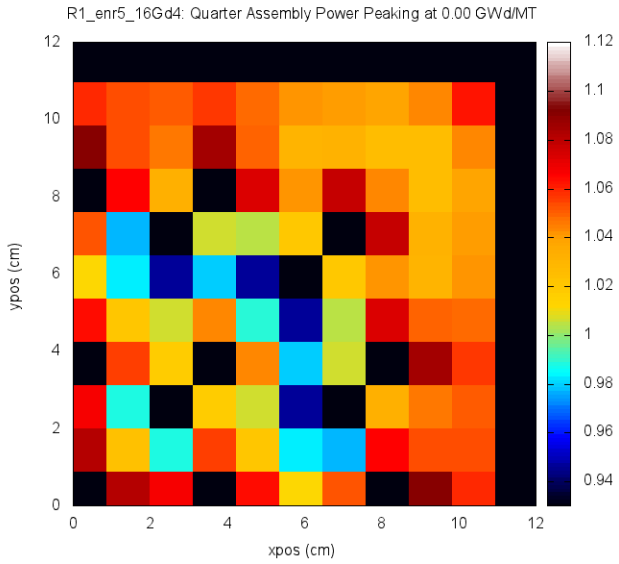

Iteration 1: 16 Gd Pins, 8 w/o

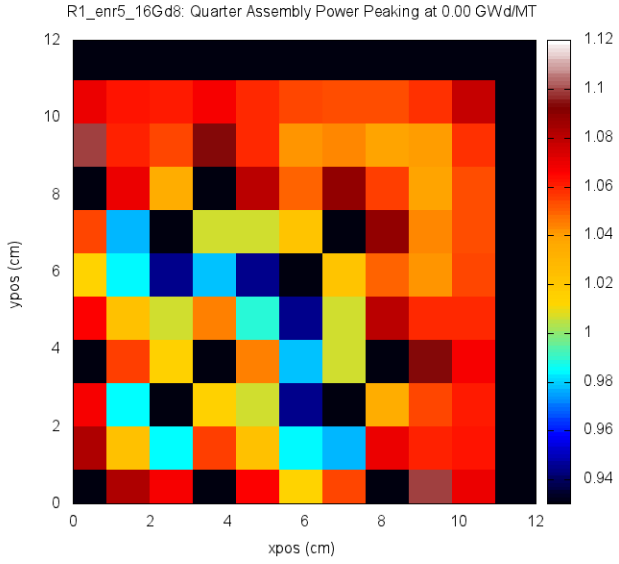

Iteration 1: 80 IFBA Pins

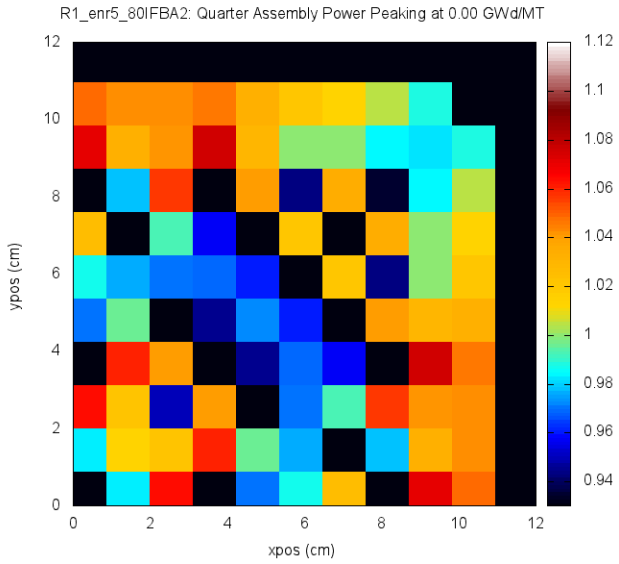

Iteration 1: 160 IFBA Pins

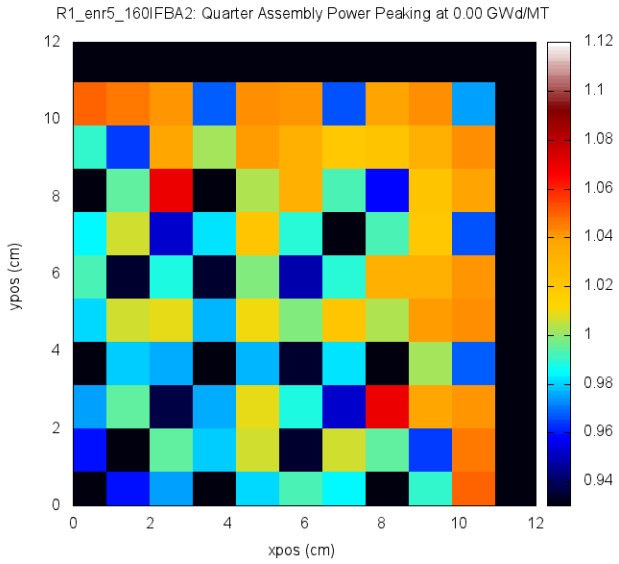

Iteration 2: 8 Gd Pins, 4 w/o

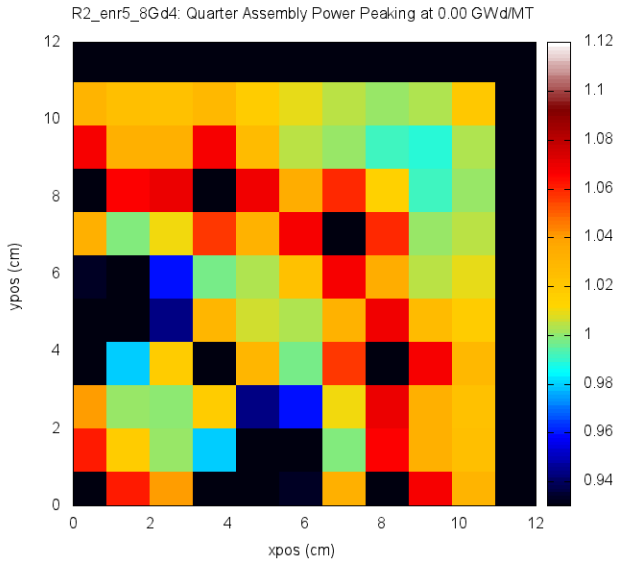

Iteration 2: 8 Gd Pins, 8 w/o

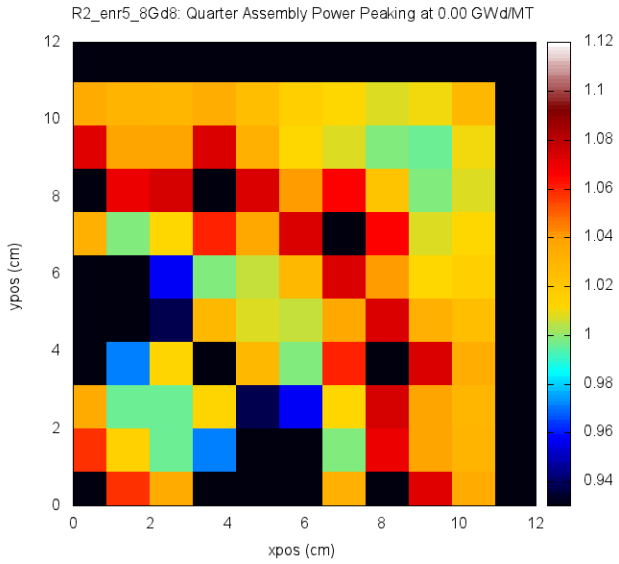

Iteration 2: 16 Gd Pins, 4 w/o

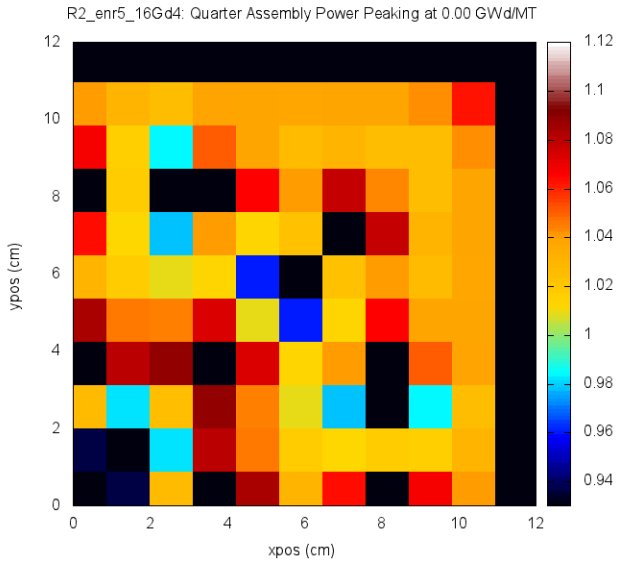

Iteration 2: 16 Gd Pins, 8 w/o

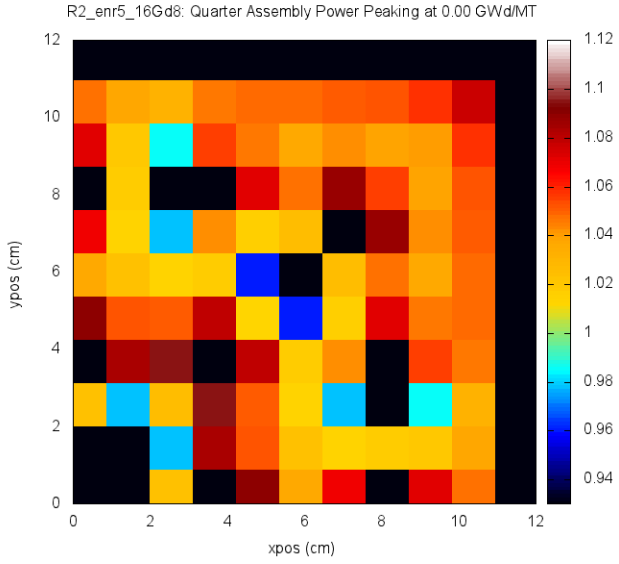

Iteration 2: 80 IFBA Pins

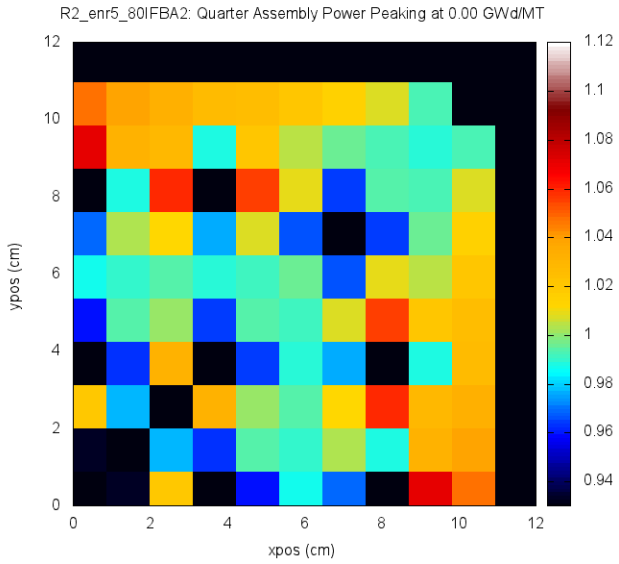

Iteration 2: 160 IFBA Pins

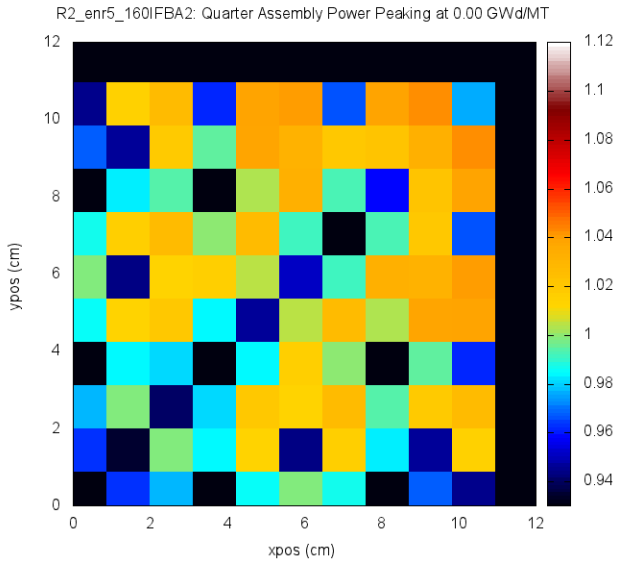

Iteration 3: 8 Gd Pins, 4 w/o

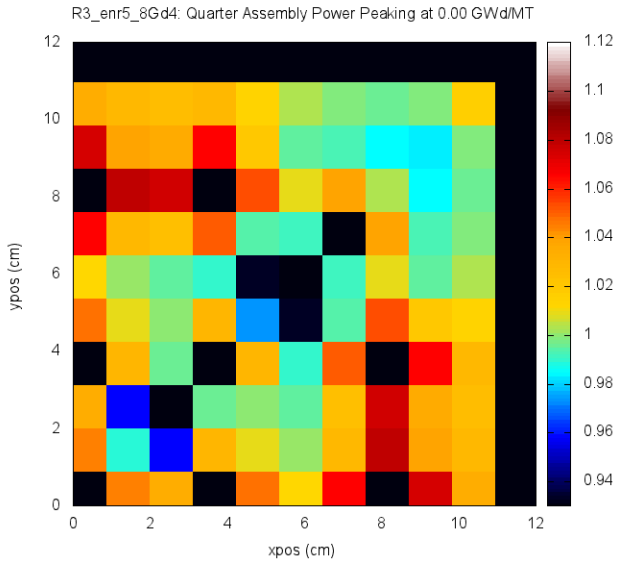

Iteration 3: 8 Gd Pins, 8 w/o

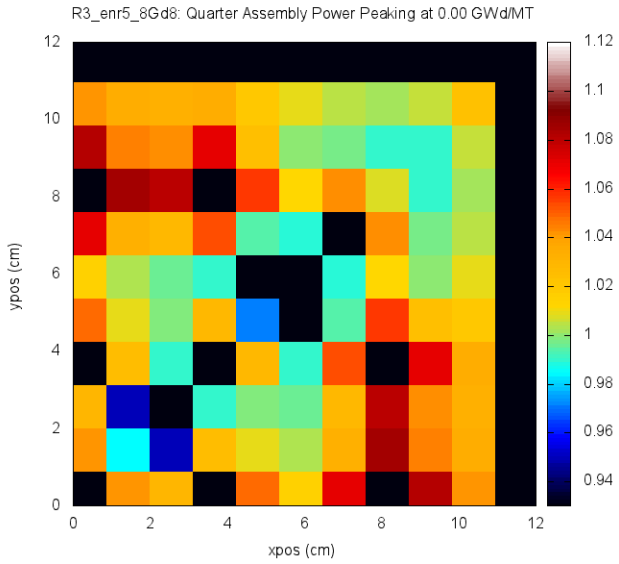

Iteration 3: 16 Gd Pins, 4 w/o

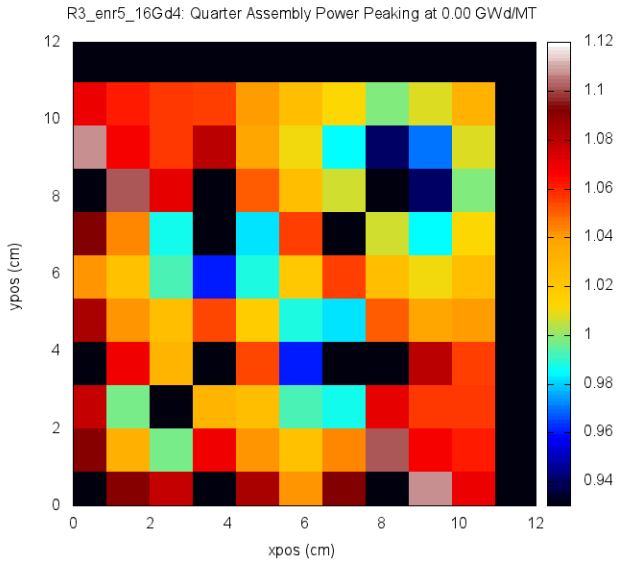

Iteration 3: 16 Gd Pins, 8 w/o

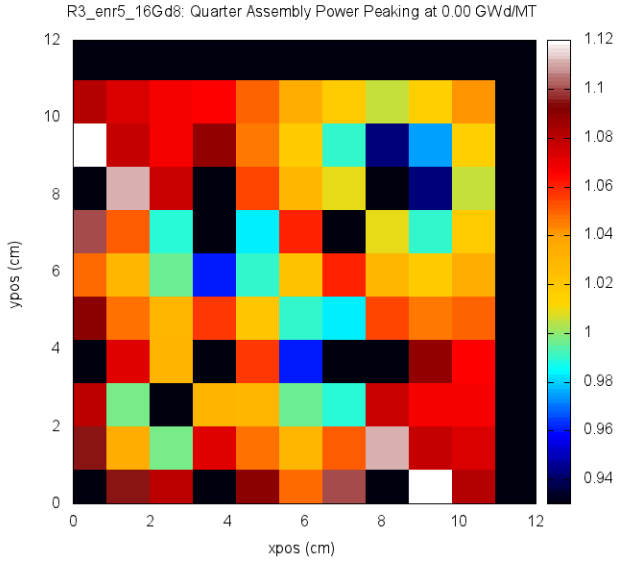

Iteration 3: 80 IFBA Pins

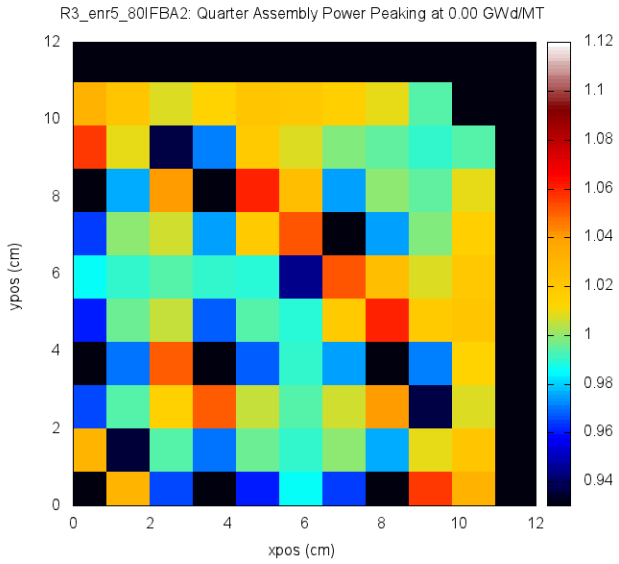

Iteration 3: 160 IFBA Pins

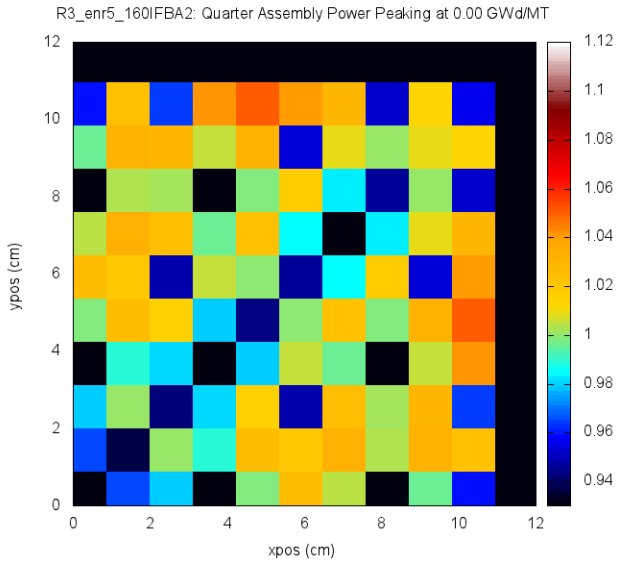

Iteration 4: 8 Gd Pins, 4 w/o

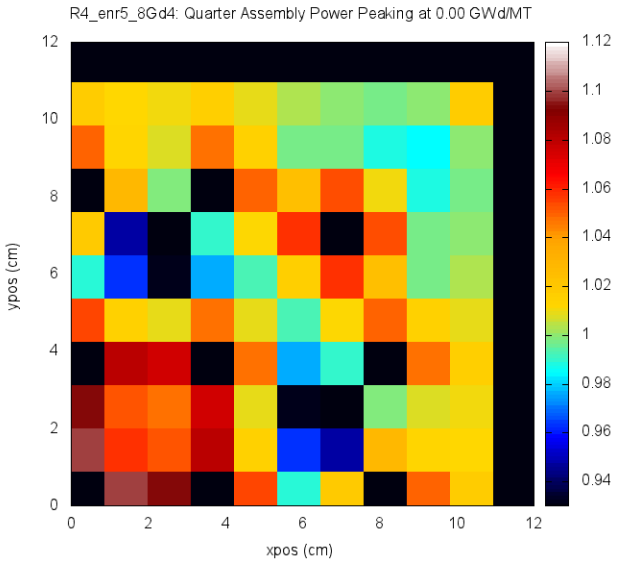

Iteration 4: 8 Gd Pins, 8 w/o

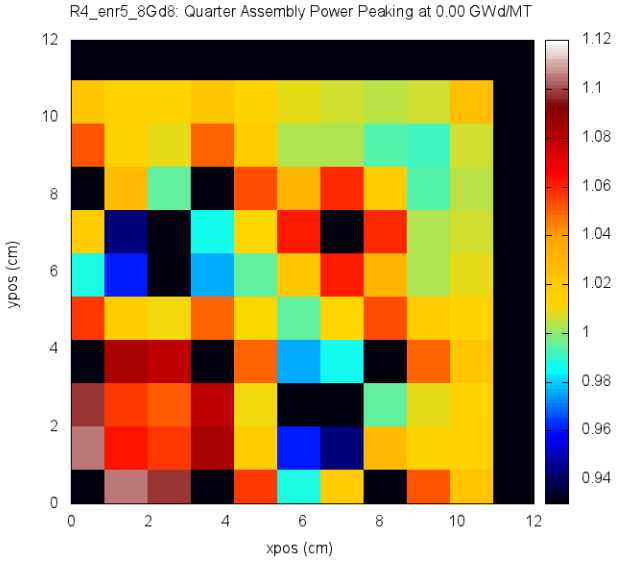

Iteration 4: 16 Gd Pins, 4 w/o

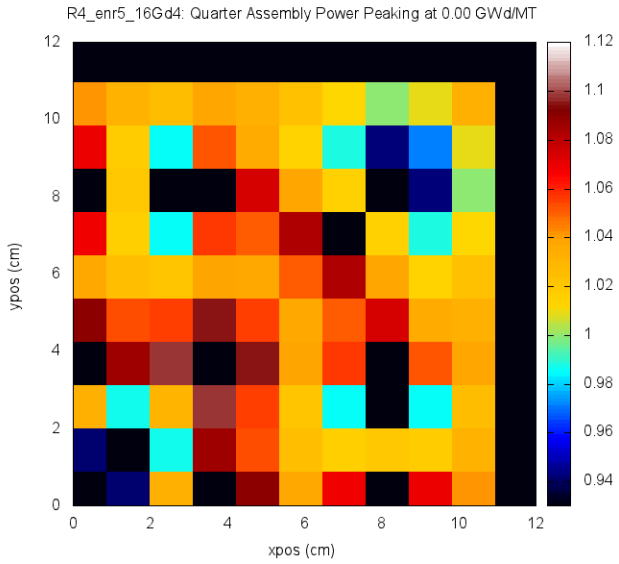

Iteration 4: 16 Gd Pins, 8 w/o

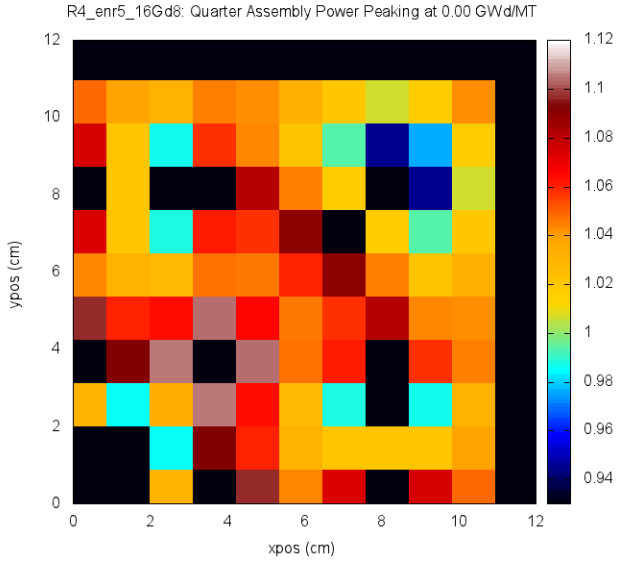

Iteration 4: 80 IFBA Pins

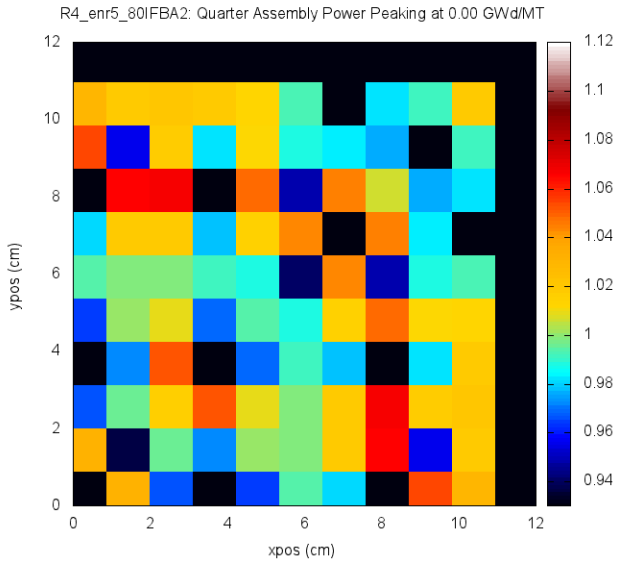

Iteration 4: 160 IFBA Pins

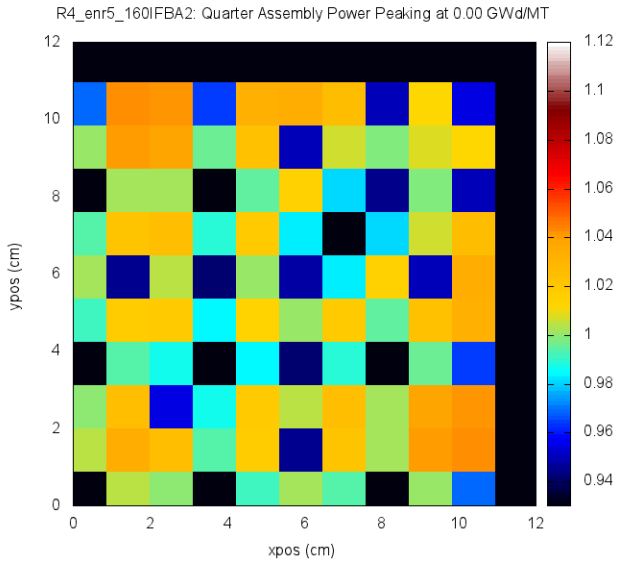

Iteration 5: 8 Gd Pins, 4 w/o

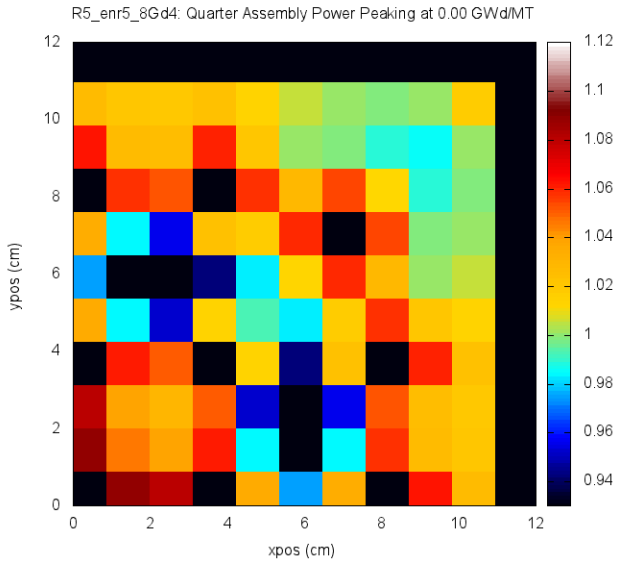

Iteration 5: 8 Gd Pins, 8 w/o

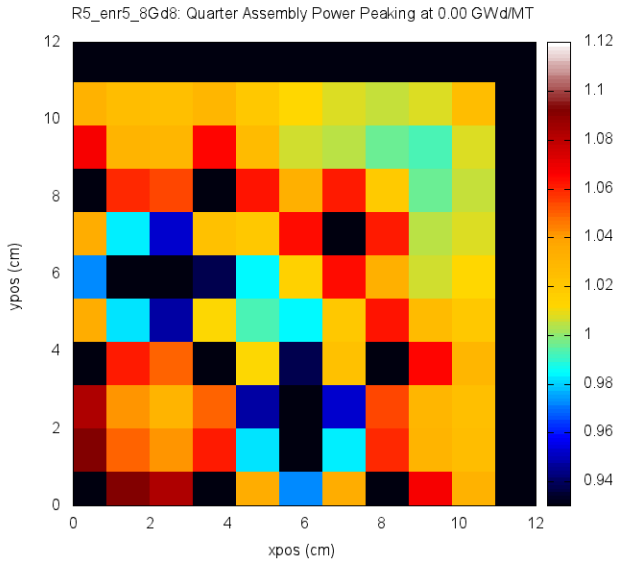

Iteration 5: 16 Gd Pins, 4 2/o

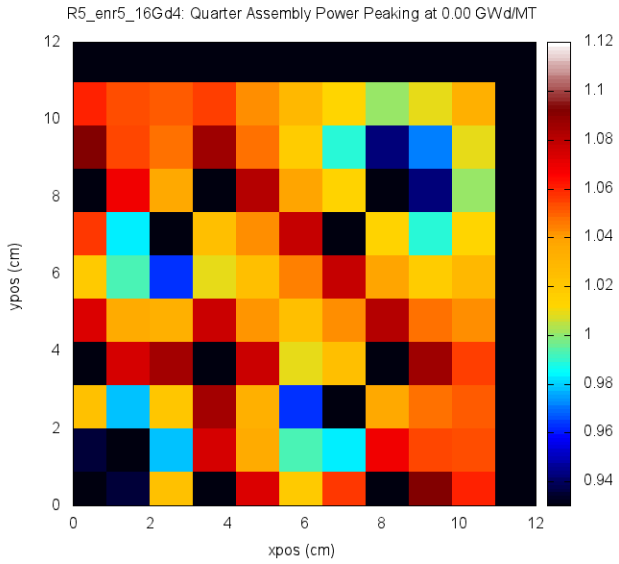

Iteration 5: 16 Gd Pins, 8 w/o

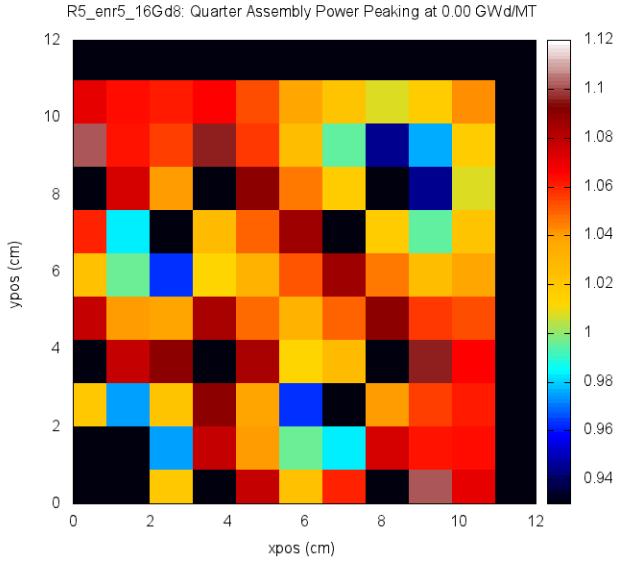

Iteration 5: 80 IFBA Pins

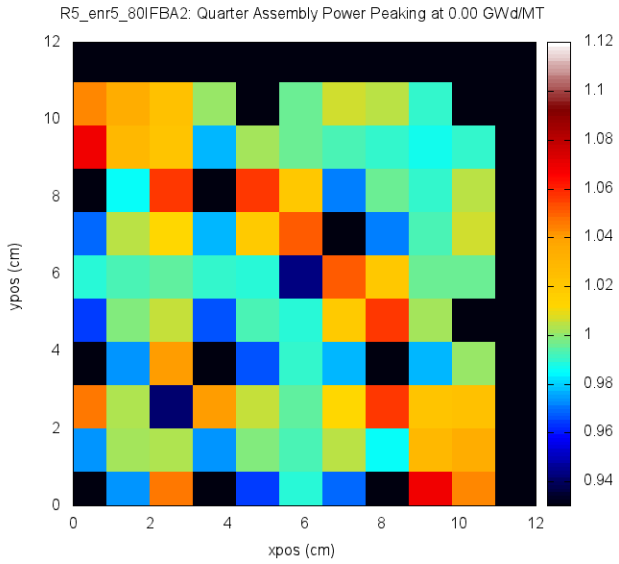

Iteration 5: 160 IFBA Pins

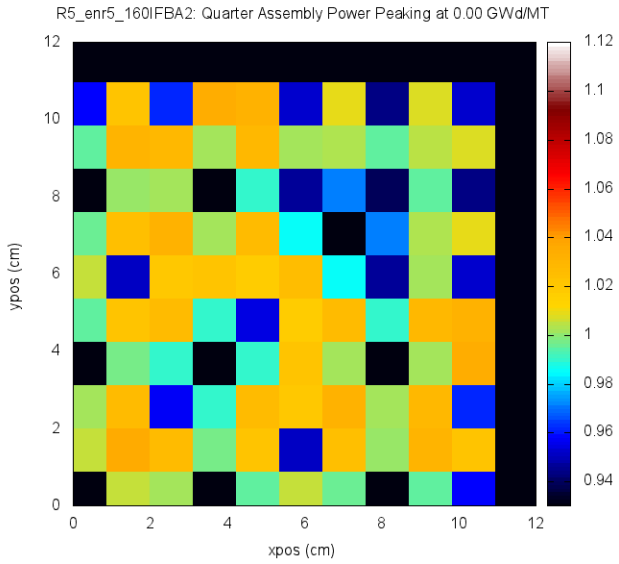

Iteration 6: 8 Gd Pins, 4 w/o

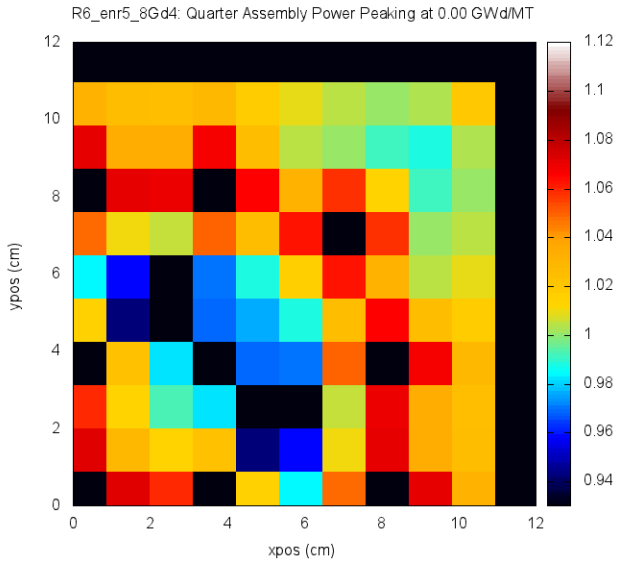

Iteration 6: 8 Gd Pins, 8 w/o

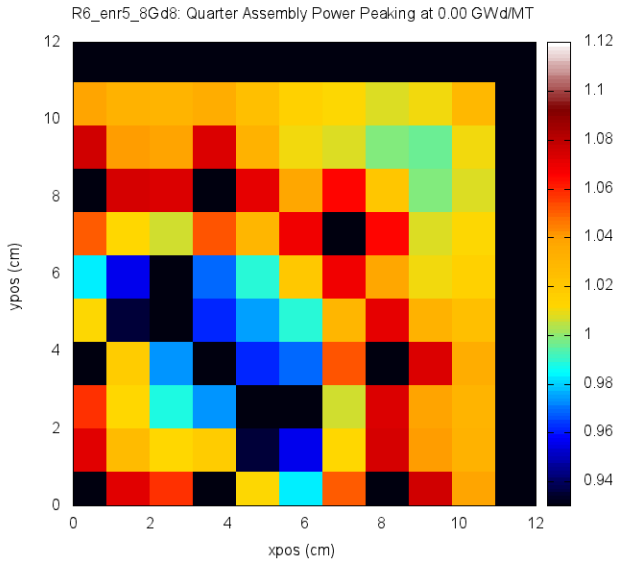

Iteration 6: 16 Gd Pins, 4 w/o

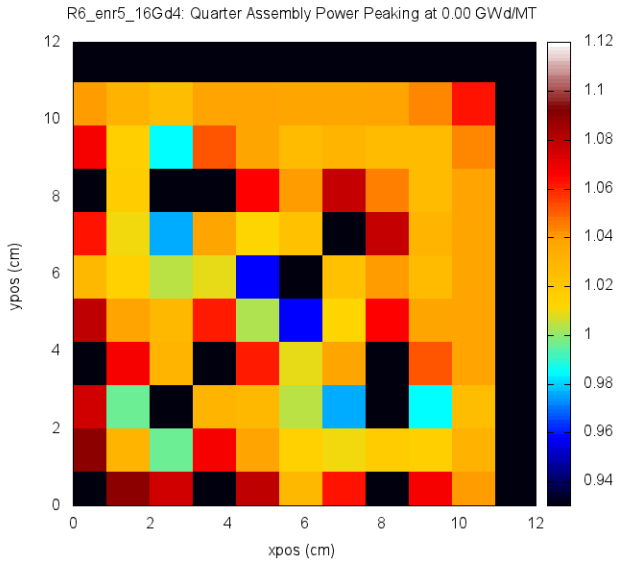

Iteration 6: 16 Gd Pins, 8 w/o

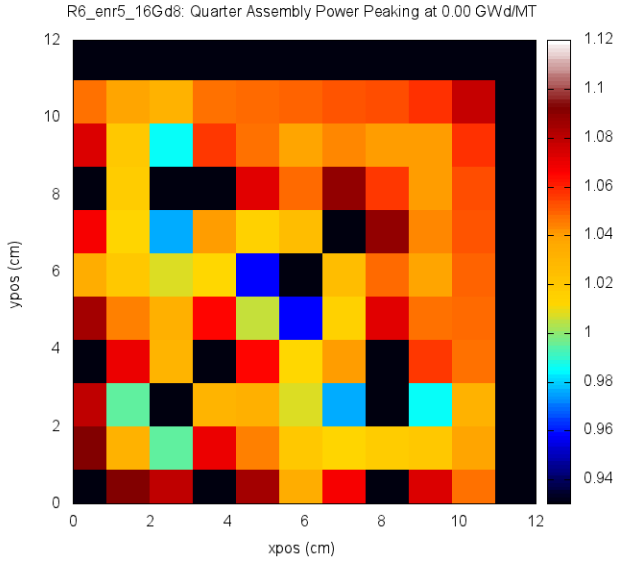

Iteration 6: 80 IFBA Pins

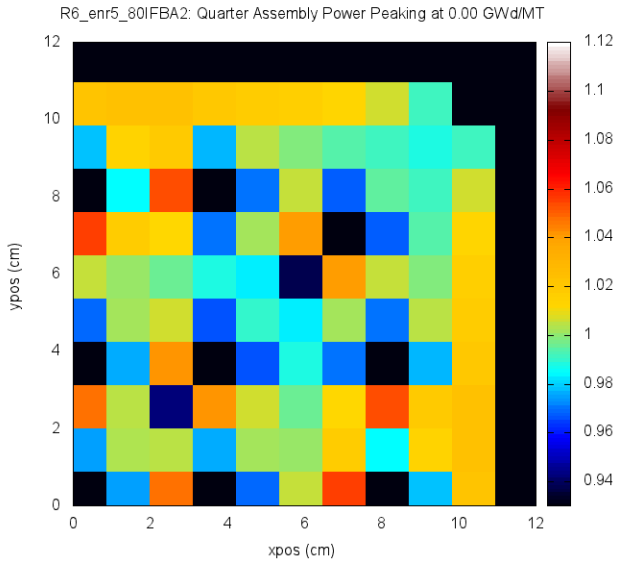

Iteration 6: 160 IFBA Pins

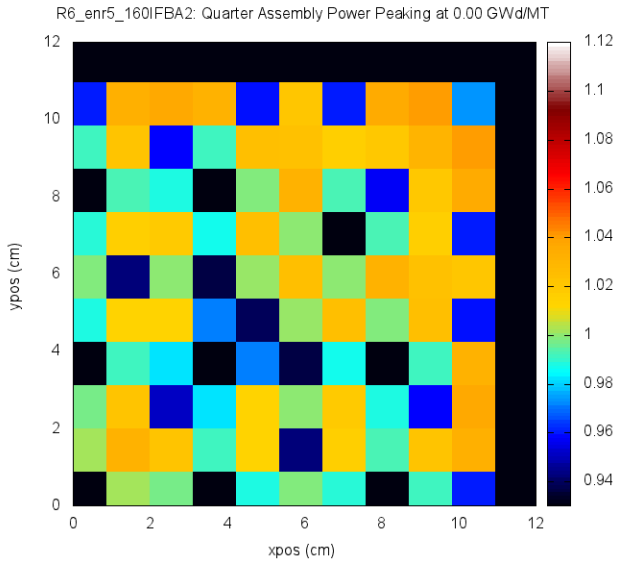

Iteration 7: 8 Gd Pins, 4 w/o

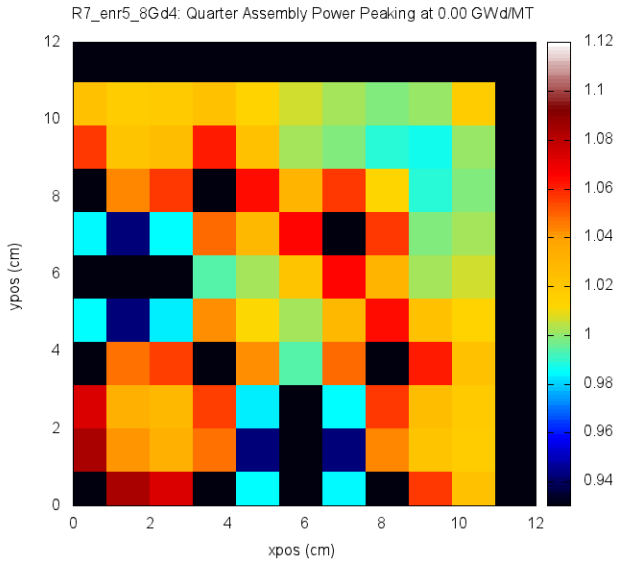

Iteration 7: 8 Gd Pins, 8 w/o

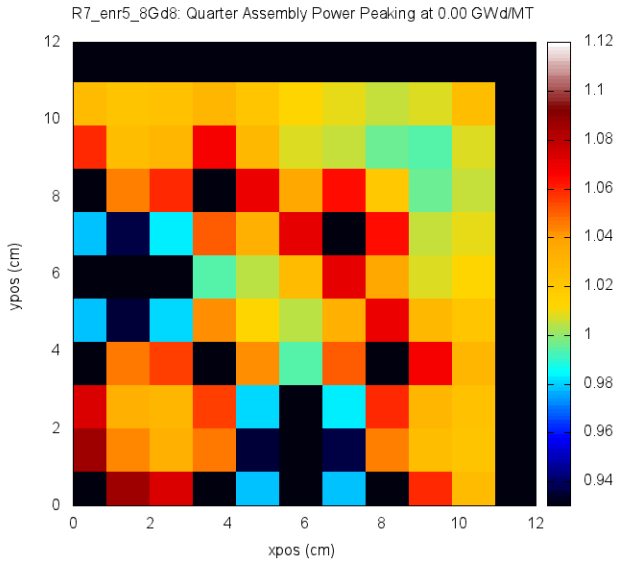

Iteration 7: 16 Gd Pins, 4 w/o

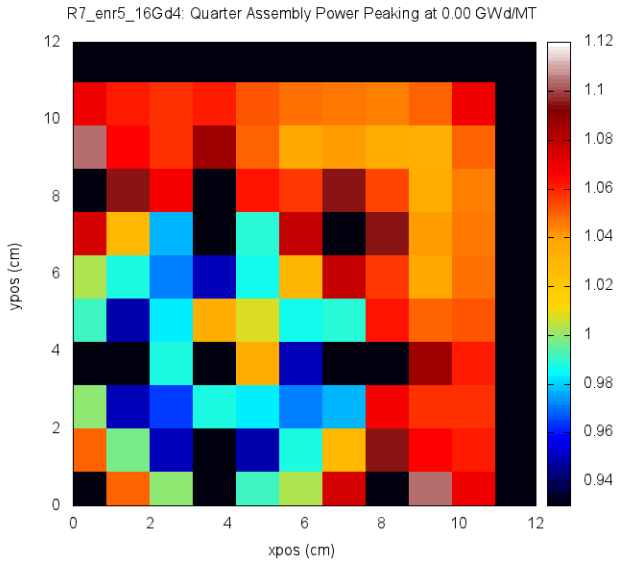

Iteration 7: 16 Gd Pins, 8 w/o

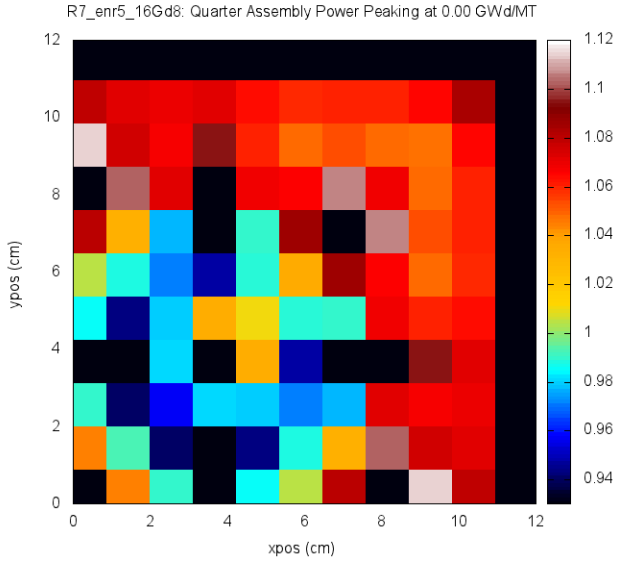

Iteration 7: 80 IFBA Pins

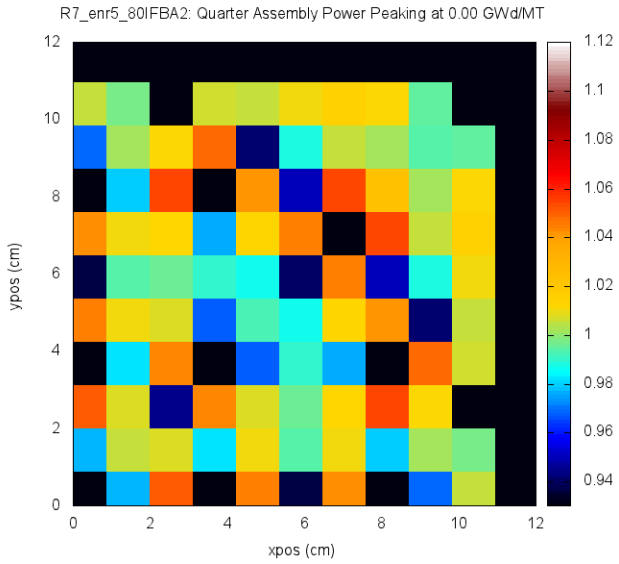

Iteration 7: 160 IFBA Pins

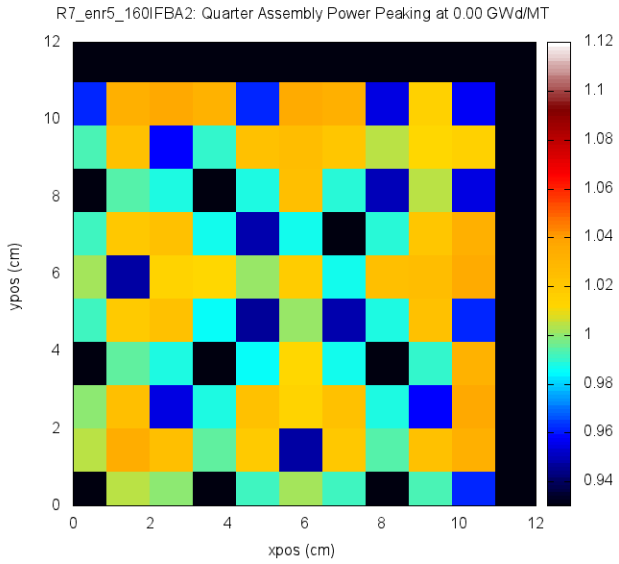

Iteration 8: 8 Gd Pins, 4 w/o

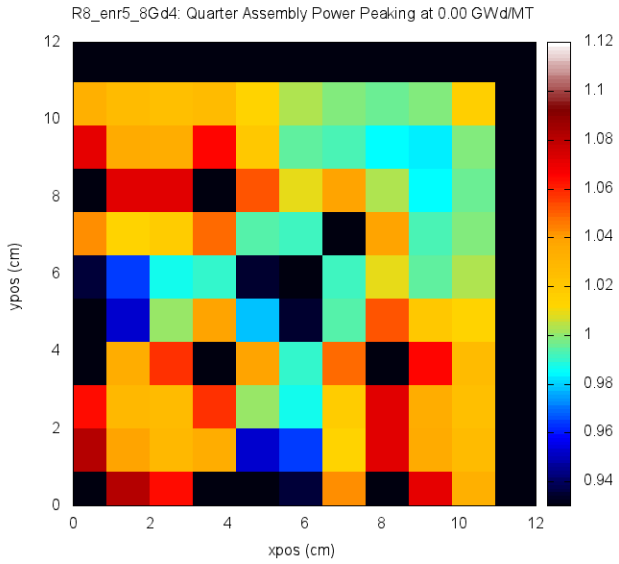

Iteration 8: 8 Gd Pins, 8 w/o

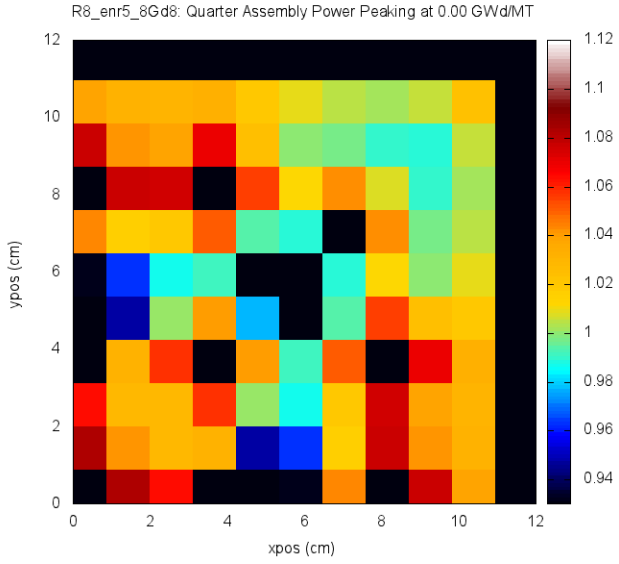

Iteration 8: 16 Gd Pins, 4 w/o

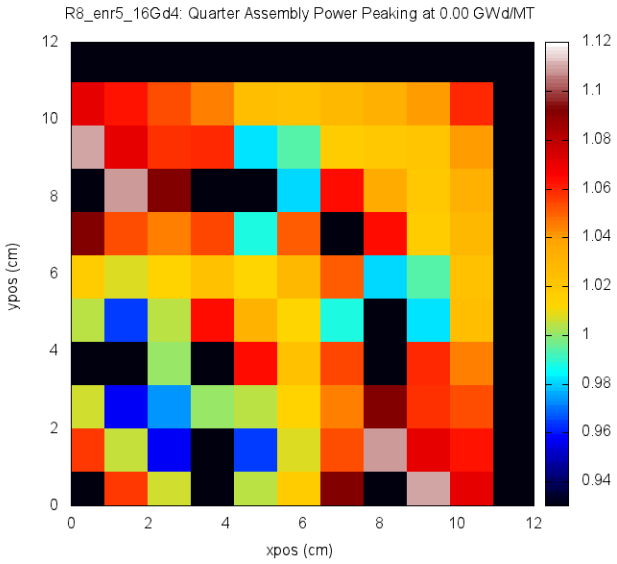

Iteration 8: 16 Gd Pins, 8 w/o

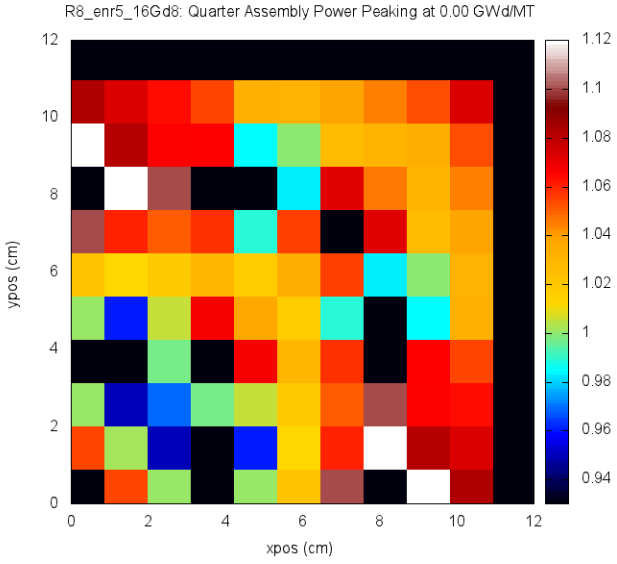

Iteration 8: 80 IFBA Pins

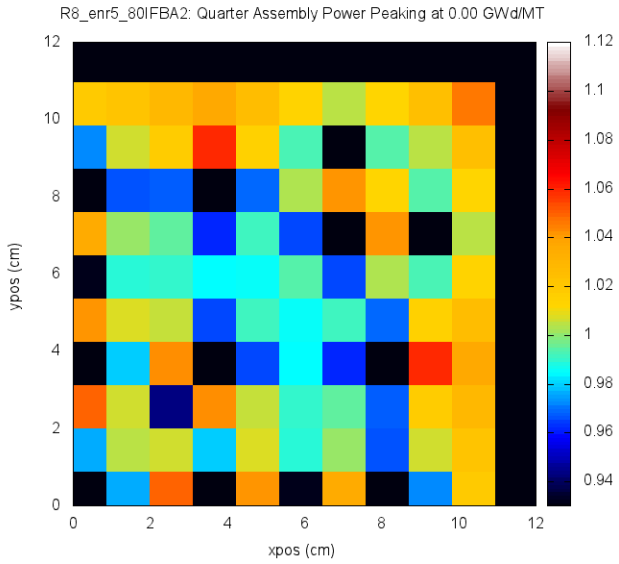

Iteration 8: 160 IFBA Pins

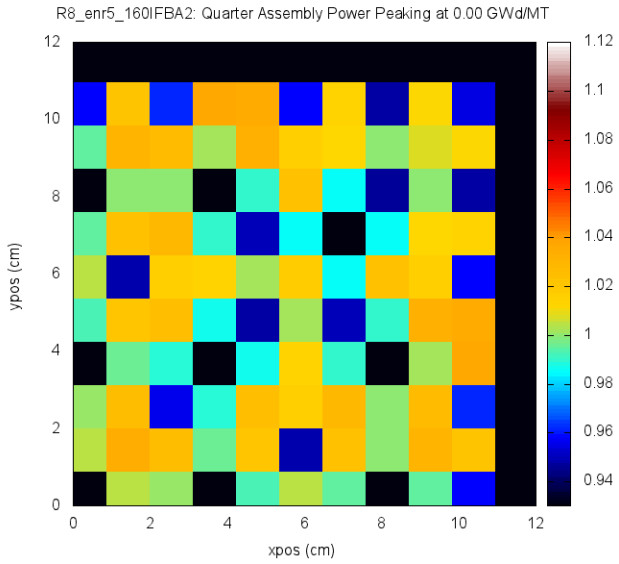

APPENDIX D. ROD INTERNAL PRESSURE

Introduction

Use of IFBA raises concerns regarding the fuel rod internal gas pressure, as helium builds up in the fuel rod free volume due to (n,α) reactions of thermal neutrons with ^{10}B. Excessive rod internal pressure (RIP) would present several reactor safety concerns, including coolant flow restriction due to hypothetical ballooning of the clad and radionuclide release due to clad rupture. These concerns necessitate an investigation involving estimation of the internal fuel rod pressure of the I^2S-LWR and evaluation against performance and safety requirements.

Throughout the course of this study, the I^2S-LWR has undergone design changes. For the sake of comparison, the following analyses shall be applied to both the original and the latest updated designs. The original fuel rod design utilized annular fuel pellets. The design has since been updated to employ solid fuel pellets with an increased plenum length and reduced fuel-clad gap size, thereby improving the fuel cycle length while maintaining sufficient volume for gases contributing to RIP.

Methodology

This calculation of RIP shall account for three pressure contributions: the BOC helium fill gas pressure (pre-pressurization), additional helium generation from IFBA consumption, and fission gas release (FGR). A wide range of values of initial fill gas pressure can be found in the literature, but most are within the range of approximately 300-400 psi at cold temperatures (293 K). As the initial fill gas pressure for the I^2S-LWR has not yet been decided, calculations will be performed for initial fill gas pressures of 330, 360, and 380 psi; each of these pressure values was rounded from initial pressure data found in (3) and (5). Fuel rods containing IFBA will

likely be filled to a lower pressure, so an additional case with an initial pressure of 100 psi will also be analyzed.

The pressure contributions of the helium (from the fill gas and from IFBA consumption) and fission gases are calculated under the assumption that all species behave as ideal gases. Specifically, it is assumed that the ideal gas law holds at all times in the fuel rod free volume:

$$pV = nRT \qquad (1)$$

where p is the gas pressure, V is the fuel rod free volume, n is the total number of moles of all gas species (initial He, He from IFBA, and fission gas), R is the universal gas constant, and T is an average gas temperature. Determination of these variables is discussed under Methodology. With all gas species assumed to exhibit ideal behavior, the RIP may be estimated as:

$$p_2 = \frac{p_1 V_1 n_2 T_2}{n_1 T_1 V_2} \qquad (2)$$

where the subscript 1 refers to variables under cold conditions and the subscript 2 refers to variables under operating conditions at the maximum rod burnup, at which point it is assumed that all IFBA has been depleted and the maximum amount of fission gas has been released.

Helium release from IFBA consumption is determined by assuming that all ^{10}B initially present is completely consumed from (n,α) reactions, so that the number of moles of helium released is equal to the initial number of moles of ^{10}B. ^{10}B concentrations in IFBA are typically given in terms of mass per unit axial length, so that the moles of ^{10}B (and therefore the total moles of He released) may be determined as:

$$n = \frac{xL}{M} \qquad (3)$$

where n is the moles of gas released per fuel pin, x is the linear mass concentration of ^{10}B in IFBA (kg/m), L is the length of the fuel rod along which IFBA is applied (m), and M is the atomic mass of ^{10}B (kg/mol).

Estimation of FGR is a more complicated matter; as the uranium silicide fuel expected to be used in the I^2S-LWR has yet to be employed in commercial reactors, no data is available regarding its FGR. However, experimental data and simple correlations are available for FGR of uranium oxide fuel. Todreas and Kazimi (8) suggest one such correlation:

$$\begin{aligned} f &= 0.05 && T < 1400^oC \\ f &= 0.10 && 1400^oC < T < 1500^oC \\ f &= 0.20 && 1500^oC < T < 1600^oC \\ f &= 0.40 && 1600^oC < T < 1700^oC \\ f &= 0.60 && 1700^oC < T < 1800^oC \\ f &= 0.80 && 1800^oC < T < 2000^oC \\ f &= 0.98 && T > 2000^oC \end{aligned} \qquad (4)$$

where f is the fractional FGR (atoms of fission gas released per atom of fission gas produced) and T is the average fuel operating temperature. For this study, since the FGR of uranium silicide is unknown, calculations are carried out with assumed FGR values of 0, 15, and 30 percent. Depending on the application of this analysis, different (and potentially more stringent) assumptions regarding FGR may be necessary; however, it is hoped that this range will be sufficiently bounding for the time being.

Fission gas production can be determined from yields of xenon and krypton isotopes from thermal fission of ^{235}U available in various databases. The values used in this study are taken from the Berkeley National Laboratory database (2) and are listed in Table 1 below. The yields of short-lived ($t_{1/2}$ < 30 minutes) krypton and xenon isotopes are neglected under the assumption that they decay before escaping from the fuel pellet. These Kr and Xe isotopes (included those neglected in this calculation) decay into Rb (Kr β^- decay) and Cs (Xe β^- decay)

species; thus the decay products do not contribute to RIP. In calculating fission gas production, the fuel is assumed to be fabricated with 96 percent of its theoretical density.

Table 1. Fission Yields for Long-Lived Xe and Kr Isotopes

Isotope	Thermal Fission Yield from ^{235}U (%)
^{83m}Kr	0.536
^{85m}Kr	1.29
^{85}Kr	0.283
^{87}Kr	2.56
^{88}Kr	3.55
^{131m}Xe	0.0405
^{132}Xe	4.31
^{133m}Xe	0.189
^{133}Xe	6.70
^{135}Xe	6.54

The RIP calculation shall be carried out for a single fuel rod with IFBA concentrations of 1.57 and 2.5 mg/in of ^{10}B, assumed to be applied along the entire active fuel rod length. These concentrations are assumed to cover the range of interest for the I^2S-LWR. In Westinghouse PWRs, as well as in the I^2S-LWR core configurations considered thus far, the IFBA coating is generally not applied along the entire fuel rod length; a few inches of fuel are left uncoated at the top and bottom. Thus, the assumption is conservative, but not prohibitively so. As an aside, it is worth noting that if the same amount of boron present in the assumed cases of IFBA applied along the entire active length is only applied along the usual 120 in, the linear concentrations of the low and high IFBA concentrations would be 1.88 and 3.00 mg ^{10}B/in respectively.

Fuel rod geometric dimensions and other relevant thermal data and operating conditions are available from the plant parameters list. The fuel rod of interest is taken as that of the maximum burnup of 64 GWd/MTU (also taken from the plant parameters list). This burnup value yields a conservative estimate for fission gas production, as more recent analyses indicate a discharge burnup of 50 GWd/MTU (P. Ferroni, personal communication, May 4, 2014), which implies less fission gas production than that used in the following calculations. These values are

axial averages of the fuel rod burnup, which are assumed to be suitable for calculating fission gas production. Additional verification of the validity and potential loss of conservatism of this assumption is necessary, as it implies linear dependence of FGR on burnup.

Assumptions

Several assumptions are made to simplify calculations and impose conservatism. As previously mentioned, the gas mixture in the fuel rod is assumed to obey the ideal gas law. Additionally, assuming that IFBA is applied along the entire active length of the fuel rod yields a conservative value for He release. In both design cases (annular and solid fuel pellet), the pellet-clad gap is assumed to be completely closed due to fuel swelling by the end of the cycle. Free volume within the fuel rod at the end of the cycle is therefore assumed to be comprised of the fuel pellet inner void and the plenum in the annular fuel pellet case (under the assumption that the fuel does not swell radially inward), and the plenum only in the solid fuel pellet case. No credit is taken for the potentially available volume of the pellet dish and chamfer. The temperature of the gas within the fuel rod is taken as the axial average of the inner fuel pellet surface temperature in the annular pellet case. This is the hottest radial location in the fuel rod, thereby yielding a conservative estimate of pressure. However, due to the high thermal conductivity of U_3Si_2 fuel, the temperature profile across the radius of the fuel pellet is relatively flat (much more so than for UO_2 fuel), with a temperature change on the order of 100-200 ^oC from the pellet edge; therefore this assumed gas temperature is not excessively conservative. This temperature is applied to the solid pellet case as well. The operating conditions and fuel rod geometry pertinent to the study are specified in Table 2 below. These conditions are then used to determine the fuel rod free volumes given in Table 3.

Table 2. Relevant I^2S-LWR Geometry and Operating Conditions

	Annular Fuel Pellet Design	Solid Fuel Pellet Design
Active Height	365.76 cm	365.76 cm
Plenum Length	19.5 cm	45.7 cm
Fuel Pellet Inner Diameter	0.254 cm	0 cm
Fuel Pellet Outer Diameter	0.803 cm	0.810 cm
Clad Inner Diameter	0.833 cm	0.833 cm
Clad Outer Diameter	0.914 cm	0.914 cm
Coolant Pressure	15.5 MPa	15.5 MPa
Fuel Pellet Average Inner Surface Temperature	728.2 ºC	728.2 ºC

Table 3. Fuel Rod Free Volumes

	Annular Fuel Pellet Design	Solid Fuel Pellet Design
Fuel Pellet Inner Free Volume	18.5 cm^3	0 cm^3
Fuel-Clad Gap Free Volume	14.1 cm^3	10.8 cm^3
Plenum Free Volume	10.6 cm^3	24.9 cm^3
Total Assumed Fuel Rod Free Volume (does not include pellet-clad gap)	29.2 cm^3	24.9 cm^3

It should be noted that though the fuel-clad gap volume was listed, it is only used when calculating the initial fill gas content, as it is assumed that the gap is closed by the end of the cycle due to irradiation swelling. Additionally, the volume occupied by the hold-down spring within the plenum is assumed to be negligible. This assumption is more than compensated by neglecting the dish and chamfer volumes.

RIP Limit

RIP has a significant impact on many interacting criteria which must be satisfied by a given fuel rod design. In the AP1000 fuel rod design, Westinghouse limits RIP so that the cladding yield strength is not exceeded and the gap between the fuel pellet and clad does not grow (9). As calculation of fuel pellet swelling rates is beyond the scope of the present work, the clad material yield strength shall be used to determine an appropriate upper limit on RIP. However, such a simplification neglects other factors leading to various modes of fuel failure related to RIP. The results of this scoping study should therefore be considered only to lay the groundwork for more detailed analyses later. Specifically, calculations with fuel performance

codes such as FRAPCON can account for much more phenomena taking place within the fuel rod.

The specific clad material to be employed in the I2S-LWR has not yet been selected, but the candidate materials are ferritic steels of FeCrAl type. Some temperature-dependent yield strength measurements for such materials are documented in (1); based on this information and I^2S-LWR fuel rod temperature data, a clad yield strength of 500 MPa shall be assumed. The RIP limit is then determined as that which results in a hoop stress on the clad equal to the assumed yield strength. Approximating the clad as a thin-walled cylindrical pressure vessel, the hoop stress is calculated as:

$$\sigma_\theta = \frac{pr}{t} \qquad (5)$$

where σ_θ is the hoop stress, p is the internal gauge pressure (equal to the difference between the absolute RIP and the coolant pressure), r is the clad inner radius, and t is the clad wall thickness. For the following calculations, it is implicitly assumed that the clad wall is perfectly cylindrical with no variation in thickness. Using the geometry and assumed yield strength given previously, Equation 5 gives an RIP limit of 64.1 MPa, or approximately 9300 psi, under operating conditions. This unexpectedly high limit indicates significant gains in safety margins due to use of ferritic steel cladding, which improves in yield strength over Zircaloy by nearly 20 percent (1). It should also be noted that neutron irradiation tends to increase the clad yield strength.

It should be noted that if this limit is achieved during the cycle and then the reactor is shut down and opened for refueling, the RIP falls to 25.8 MPa under cold atmospheric conditions. This pressure yields a clad hoop stress of 914 MPa, which significantly exceeds the room-temperature clad yield strength found in (1). Thus, some capability for venting the accumulated gas from the plenum volume at reactor shutdown should be provided to avoid clad rupture under cold conditions.

While the above calculation evaluates the cladding material integrity, it is anticipated that the welded areas of the fuel rod are more susceptible to failure and would therefore yield a more limiting bound on RIP. It is assumed that the weld can withstand a pressure difference of 3000 psi (20.7 MPa) between the interior of the fuel rod and the surrounding coolant (B. Petrovic, personal communication, May 26, 2015). Using this criterion yields a more conservative RIP limit of 36.2 MPa. This limit shall be applied to the following analyses.

Results

The previously listed volumes and operating conditions are used to determine the RIP for initial fill gas pressures of 100, 330, 360, and 380 psi (0.689, 2.28, 2.48, and 2.62 MPa) for fission gas releases of 0, 15, and 30 percent and for IFBA loadings of 1.57 and 2.5 mg ^{10}B/in. He release is determined from Equation 3, and RIP is calculated using Equation 2. These results are given Tables 4 and 5 below for the annular and solid fuel pellet designs, respectively.

Table 4. RIP Results – Annular Fuel Pellets

Cold Initial Fill Gas Pressure (MPa)	Initial He Content (mol)	IFBA ^{10}B Concentration (mg/in)	Additional He Content (mol)	FGR (%)	Additional Fission Gas Content (mol)	Final RIP (MPa)
0.689	0.0122	1.57	0.0226	0	0	9.95
				15	0.0155	15.7
				30	0.0310	21.5
		2.5	0.0360	0	0	13.8
				15	0.0155	19.5
				30	0.0310	25.3
2.28	0.0404	1.57	0.0226	0	0	18.0
				15	0.0155	23.8
				30	0.0310	29.5
		2.5	0.0360	0	0	21.8
				15	0.0155	27.6
				30	0.0310	33.4
2.48	0.0441	1.57	0.0226	0	0	19.0
				15	0.0155	24.8
				30	0.0310	30.6
		2.5	0.0360	0	0	22.9
				15	0.0155	28.6
				30	0.0310	34.4
2.62	0.0465	1.57	0.0226	0	0	19.7
				15	0.0155	25.5
				30	0.0310	31.3
		2.5	0.0360	0	0	23.5
				15	0.0155	29.3
				30	0.0310	35.1

Table 5. RIP Results – Solid Fuel Pellets

Cold Initial Fill Gas Pressure (MPa)	Initial He Content (mol)	IFBA ^{10}B Concentration (mg/in)	Additional He Content (mol)	FGR (%)	Additional Fission Gas Content (mol)	Final RIP (MPa)
0.689	0.0101	1.57	0.0226	0	0	10.9
				15	0.0175	18.6
				30	0.0351	26.2
		2.5	0.0360	0	0	15.4
				15	0.0175	23.0
				30	0.0351	30.7
2.28	0.0334	1.57	0.0226	0	0	18.7
				15	0.0175	26.3
				30	0.0351	34.0
		2.5	0.0360	0	0	23.2
				15	0.0175	30.8
				30	0.0351	38.4
2.48	0.0364	1.57	0.0226	0	0	19.7
				15	0.0175	27.3
				30	0.0351	35.0
		2.5	0.0360	0	0	24.2
				15	0.0175	31.8
				30	0.0351	39.5
2.62	0.0384	1.57	0.0226	0	0	20.4
				15	0.0175	28.0
				30	0.0351	35.7
		2.5	0.0360	0	0	24.8
				15	0.0175	32.5
				30	0.0351	40.1

Only under the most extreme conditions considered does the RIP exceed the allowable limit set by the weld. It is therefore apparent that the initial pressurization of IFBA-bearing fuel rods should be limited. Some additional studies are carried out to explore fuel rod design space in light of these results, as there appear to be some safety margins in the current design. The assumptions discussed previously are applied to each of these studies.

Initial Pressure

The first study performed keeps the plenum length constant at the value given earlier for each design, and the maximum initial fill gas pressure necessary for remaining below the RIP limit is then solved for over a range of fission gas release values (extending up to 100 percent FGR) by manipulating Equation 2. These results for the both the nominal IFBA content and high

IFBA content are presented in Figures 1 and 2 below for the annular and solid fuel pellet cases respectively.

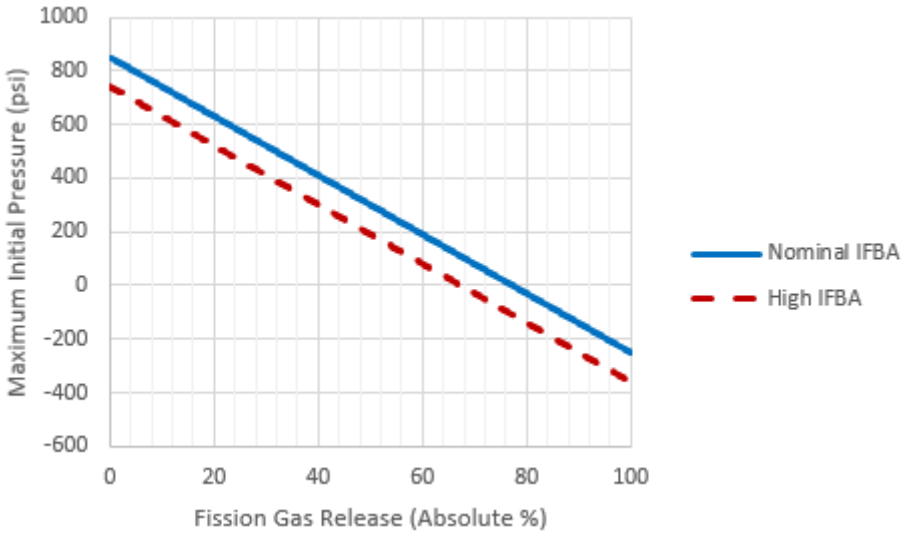

Figure 1. Maximum Initial Fill Gas Pressure – Annular Fuel Pellets

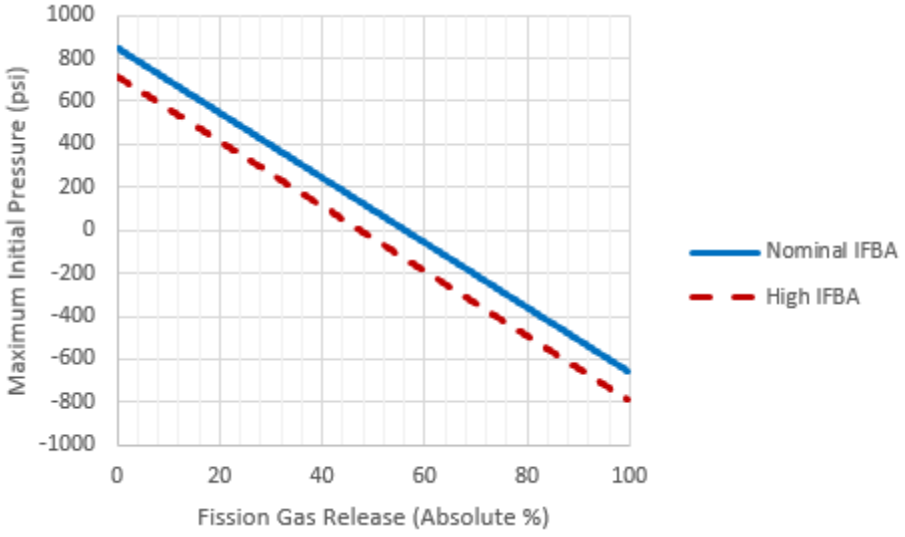

Figure 2. Maximum Initial Fill Gas Pressure – Solid Fuel Pellets

In the case with annular fuel pellets, the fuel pellet inner void provides a substantial volume to accommodate gas buildup, thereby easily containing RIP and allowing some flexibility in selecting initial pressurization. This inner fuel pellet volume is removed in the solid

fuel pellet design, and the RIP limit is reached at lower values of FGR. Even so, it is apparent that the latest I^2S-LWR plenum length can accommodate gas buildup under nominal operating conditions if the initial pressurization is prudently selected.

The curves presented in Figures 3-1 and 3-2 above may be used to inform the selection of the initial fill gas pressure. In addition to accounting for FGR and He release by IFBA consumption, the initial fill gas pressure is typically chosen to delay pellet-clad mechanical interaction (PCMI) and clad flattening (9). PCMI occurs due to the combination of fuel swelling and radially inward clad creep (if the coolant pressure exceeds RIP). If more accurate values of FGR and volumetric swelling of uranium silicide fuel can be determined, the above curves may be used to select an initial fill gas pressure which adequately delays PCMI without exceeding the RIP limit.

Initial Pressure

Next, to assess the magnitude of the impact of the plenum length on RIP, the FGR is varied for several initial fill gas pressures to solve for the minimum plenum length required to keep the RIP below the assumed limit by manipulating Equation 2. Figures 3 and 4 below give the minimum plenum length for the annular fuel pellet case for nominal and high IFBA content, respectively, while Figures 5 and 6 present the same for the solid fuel pellet case. It should be noted that varying the FGR is equivalent to holding the FGR fixed and varying burnup, as burnup directly determines the fission gas production. The results below may therefore be used to gain some insight to the impact of the fuel rod burnup on RIP as well, as burnup will generally not be uniform across all pins in the I^2S-LWR core. The negative plenum lengths would of course be replaced by zero, but they are left here to indicate the amount of margin.

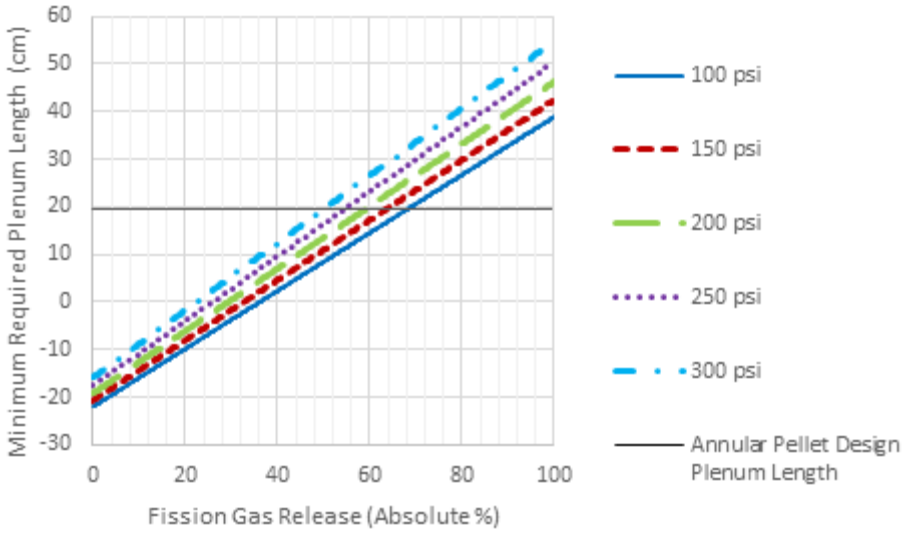

Figure 3. Minimum Plenum Length vs. FGR for Nominal IFBA – Annular Fuel Pellets

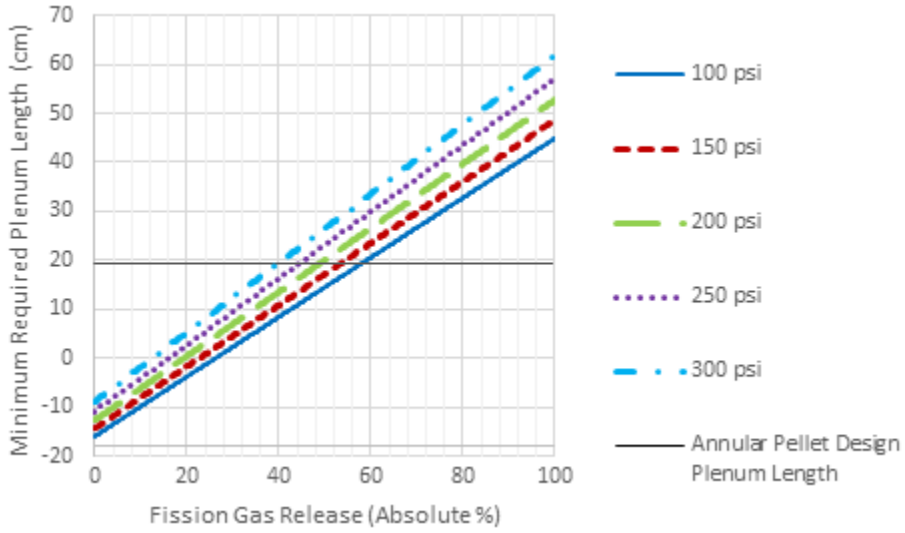

Figure 4. Minimum Plenum Length vs. FGR for High IFBA – Annular Fuel Pellets

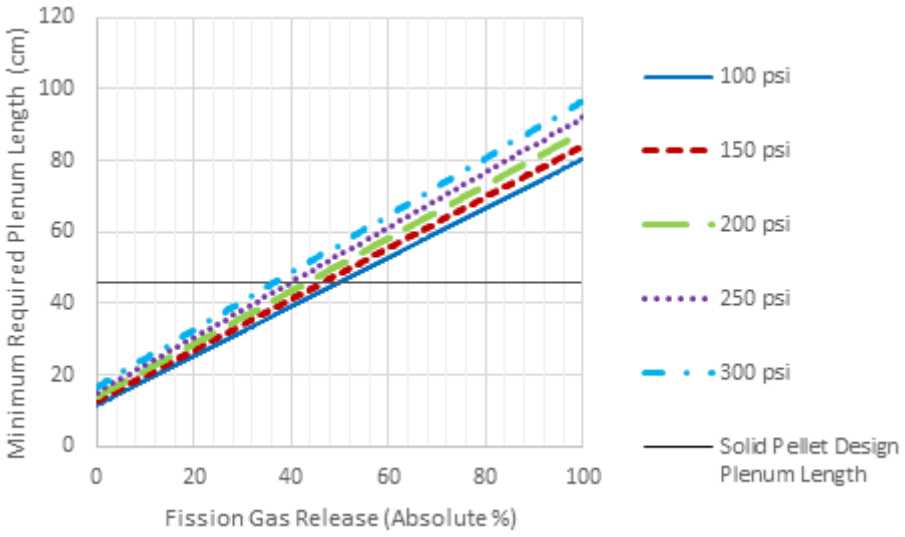

Figure 5. Minimum Plenum Length vs. FGR for Nominal IFBA – Solid Fuel Pellets

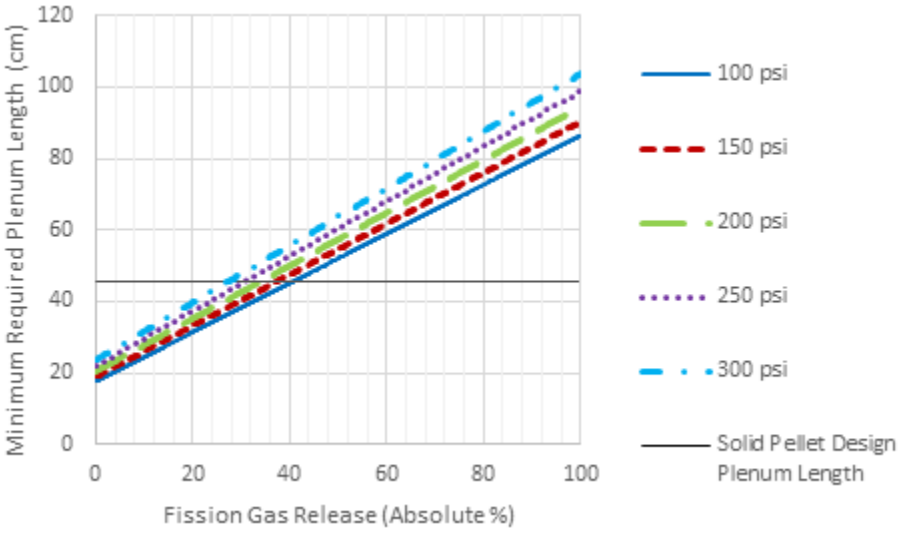

Figure 6. Minimum Plenum Length vs. FGR for High IFBA – Solid Fuel Pellets

Again, the volume provided by the inner fuel pellet void in the annular pellet case significantly reduces the burden on the plenum for withstanding RIP. RIP is still sufficiently contained in the current solid pellet design for nominal operating conditions, but it is challenged at larger values of FGR.

Plenum Length vs. Initial Pressure

The initial fill gas pressure is now varied for the selected FGR values of interest, and the minimum required plenum length is calculated to yield a direct relationship between the plenum length and initial fill gas pressure by manipulating Equation 2 with the final pressure equal to the assumed limit. These results are given for the annular pellet case in Figures 7 and 8 below for the nominal and high IFBA content, respectively, and for the solid pellet case in Figures 9 and 10.

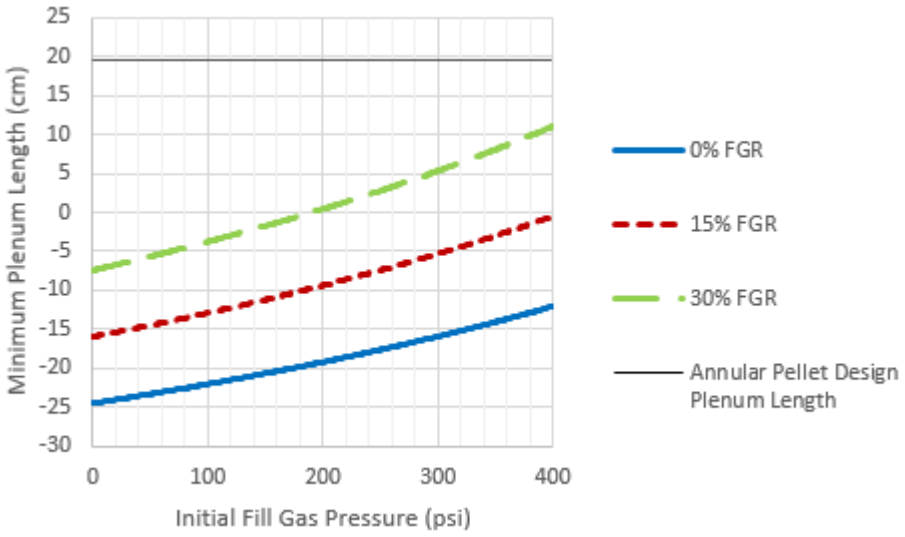

Figure 7. Plenum Length vs. Initial Fill Gas Pressure for Nominal IFBA – Annular Fuel Pellet

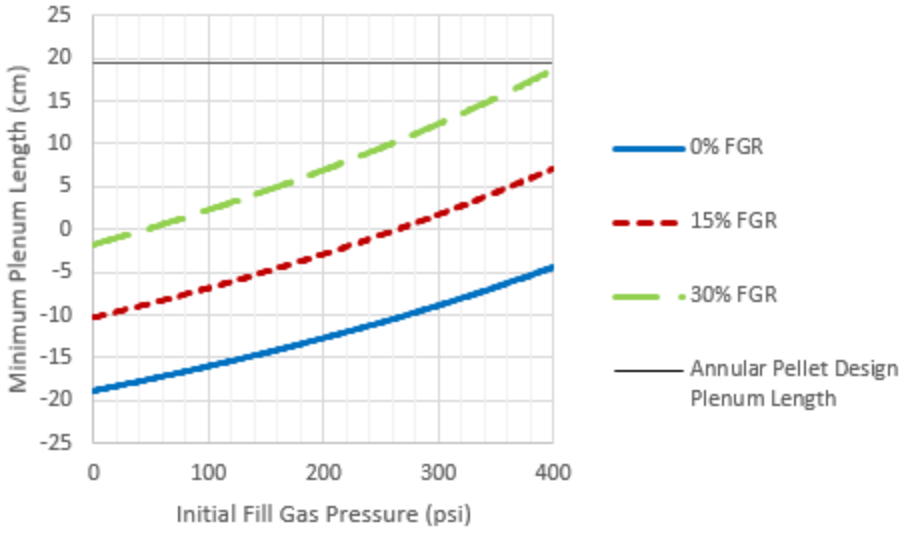

Figure 8. Plenum Length vs. Initial Fill Gas Pressure for High IFBA – Annular Fuel Pellet

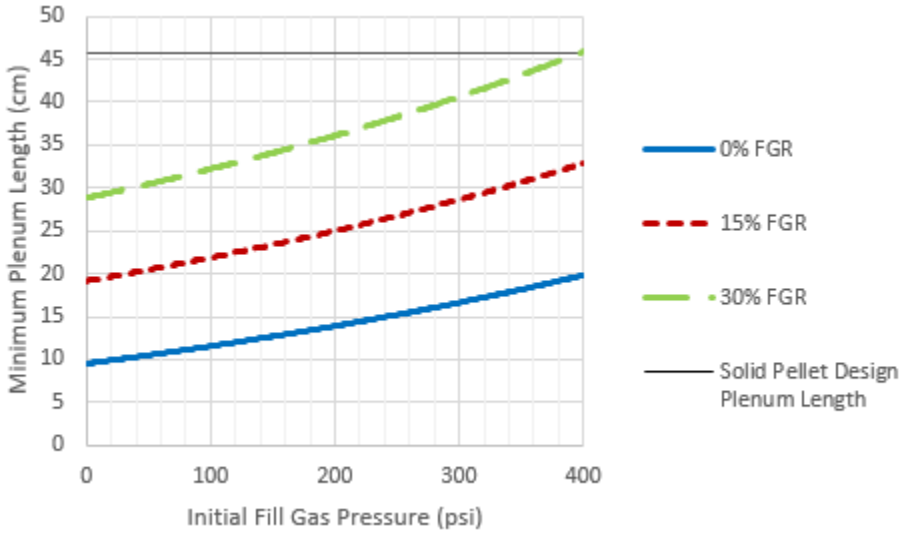

Figure 9. Plenum Length vs. Initial Fill Gas Pressure for Nominal IFBA – Solid Fuel Pellet

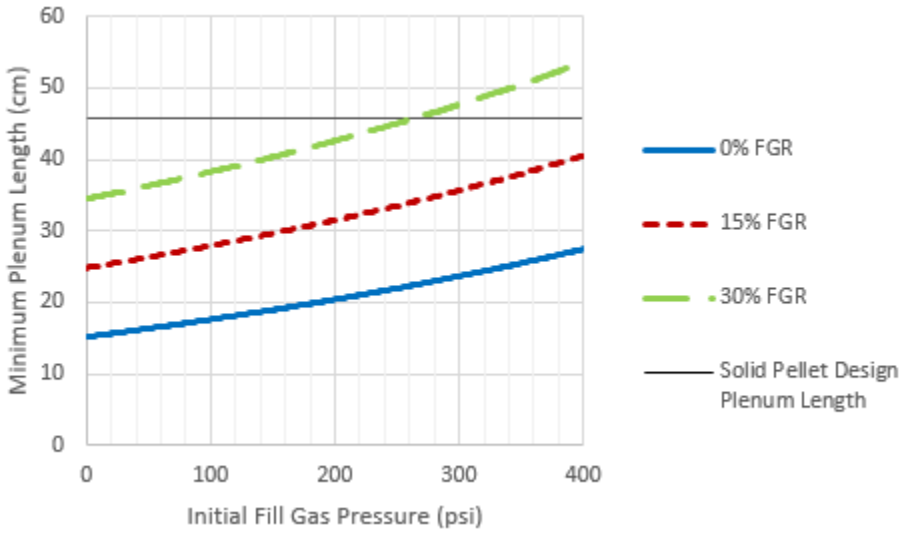

Figure 10. Plenum Length vs. Initial Fill Gas Pressure for High IFBA – Solid Fuel Pellet

Again, the negative plenum length requirements indicate that the fuel pellet inner void in the annular pellet design provides sufficient volume for fission gases and He from IFBA consumption without violating the RIP limit over much the range of initial fill gas pressures and FGR values considered, even with high IFBA content. The plenum length requirements are more stringent in the solid pellet design, but the current plenum length appears to be acceptable over the range of FGR values considered as long as the initial pressurization is kept sufficiently low.

Temperature Sensitivity

The effect of the gas temperature on RIP is now examined by keeping the plenum length constant at the nominal value in each case and determining the maximum allowable initial fill gas pressures for the selected FGR values over a range of gas temperatures by manipulating Equation 2. The gas temperature used in the studies above was chosen as a conservative average value, but realistically, the temperature of the gas inside a fuel rod during the operation of the I^2S-LWR will vary significantly with position in the fuel rod. These results are given for the annular pellet case in Figures 11 and 12 for the nominal and high IFBA content, respectively, and again for the solid pellet case in Figures 13 and 14.

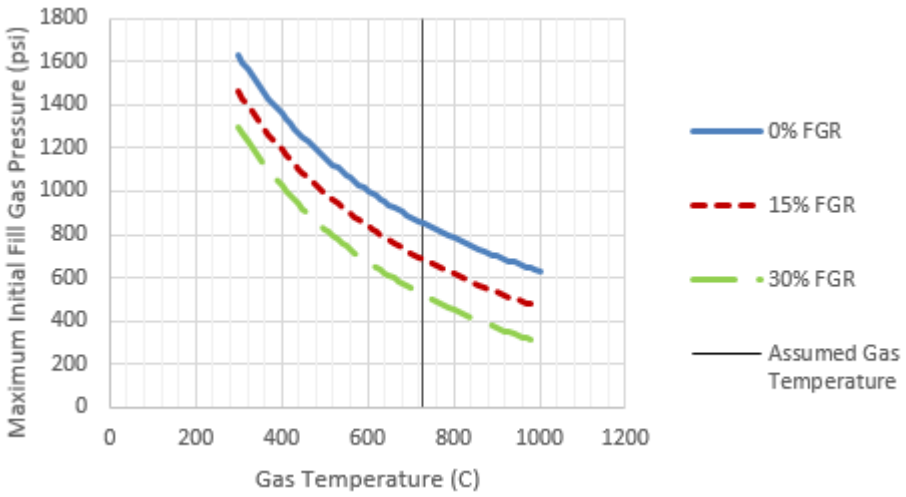

Figure 11. Maximum Initial Fill Gas Pressure vs. Gas Temperature for Nominal IFBA – Annular Fuel Pellet

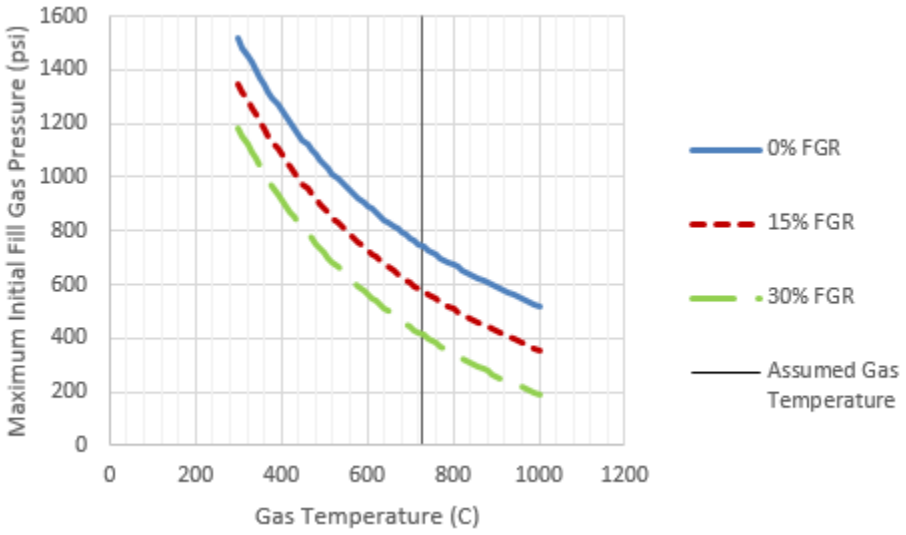

Figure 12. Maximum Initial Fill Gas Pressure vs. Gas Temperature for High IFBA – Annular Fuel Pellet

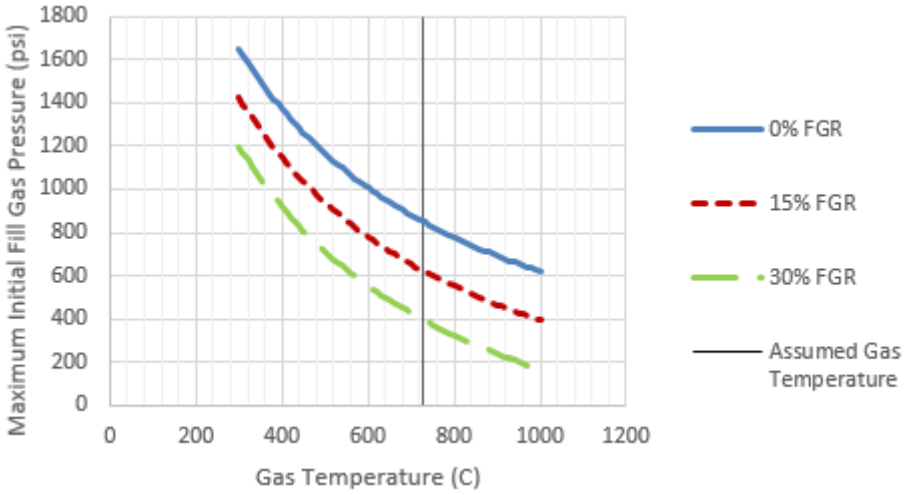

Figure 13. Maximum Initial Fill Gas Pressure vs. Gas Temperature for Nominal IFBA – Solid Fuel Pellet

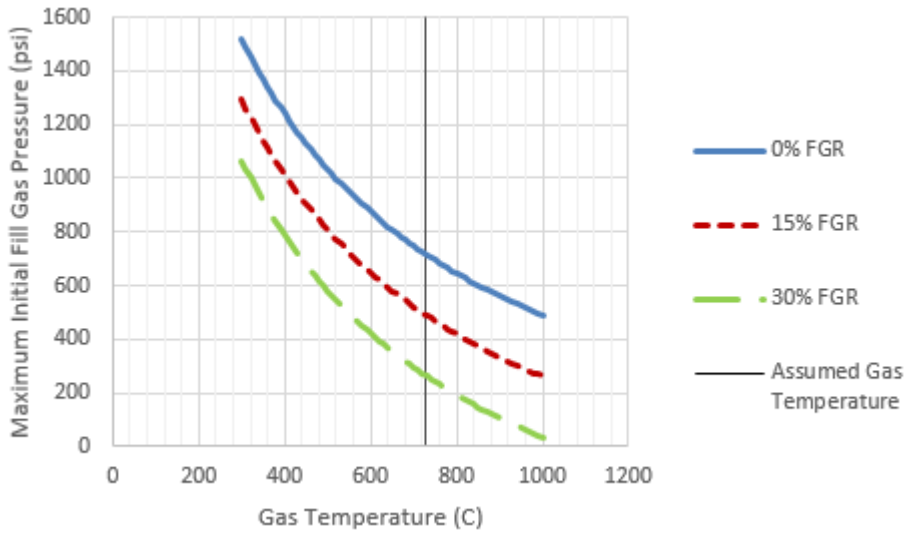

Figure 14. Maximum Initial Fill Gas Pressure vs. Gas Temperature for High IFBA – Solid Fuel Pellet

The above results are promising, as they suggest that the conservative selection of the gas temperature used in previous studies yielded a relatively tight constraint on RIP. It is expected that the actual average gas temperature during operation of the I^2S-LWR will be significantly

lower than the inner fuel pellet surface temperature in the annular pellet case, thereby allowing greater FGR and IFBA consumption without violating the RIP limit. Moreover, the solid pellet cases (with smaller margin) will in reality have most of the gas in the plenum volume at a low temperature (similar to coolant).

Comparison with AP1000

In order to assess the validity of the preceding analysis, the same methodology is applied to a licensed reactor design to determine its RIP characteristics. The design chosen is the Westinghouse AP1000, for which many design specifications are readily available. The relevant geometry and operating conditions are listed in Table 3-3 below; these values were obtained from (9) and (10), except for the gas temperature, which is assumed to be the same as that used in the preceding analysis.

Table 3-3. Relevant AP1000 Geometry and Operating Conditions

Active Height	426.72 cm
Plenum Length	30.8 cm
Fuel Pellet Diameter	0.819 cm
Clad Inner Diameter	0.836 cm
Clad Outer Diameter	0.950 cm
Coolant Pressure	15.5 MPa
Gas Temperature	728.2 ^{o}C

The above geometry gives the free volumes listed in Table 6 below; as the AP1000 employs solid fuel pellets, there is no inner void available for gas release.

Table 6. AP1000 Fuel Rod Free Volumes

Fuel-Clad Gap Free Volume	9.16 cm^3
Plenum Free Volume	16.9 cm^3
Total Fuel Rod Free Volume (including pellet-clad gap)	26.1 cm^3

For estimation of FGR, the same fission yield data as that listed in Table 1 is used. The peak fuel rod burnup is taken from (10) as 62 GWd/MTU. The IFBA content is specified in (10) as well; 0.772 mg ^{10}B/cm is applied along 152 in of the fuel rod. To determine the RIP limit, the

yield strength of the ZIRLO clad is assumed to be comparable to that of Zircaloy; this is taken from (11) as 200 MPa. Applying Equation 5 then yields an RIP limit of 42.8 MPa. It is notable how much margin in this hoop stress limit is lost when using a Zr-based clad as opposed to steel. At operating conditions, the yield strength of the Zr clad is about 40 percent of that of the steel clad, and thus the steel clad can withstand RIP that is about 21 MPa (over 3000 psi) greater than what the Zr clad can withstand.

Regardless, this value is still less limiting than the weld limit assumed previously; therefore, the RIP limit of 36.2 MPa from the previous analyses shall be retained. This information is used to calculate the maximum allowable initial fill gas pressure over a range of FGR; the results are given in Figure 15.

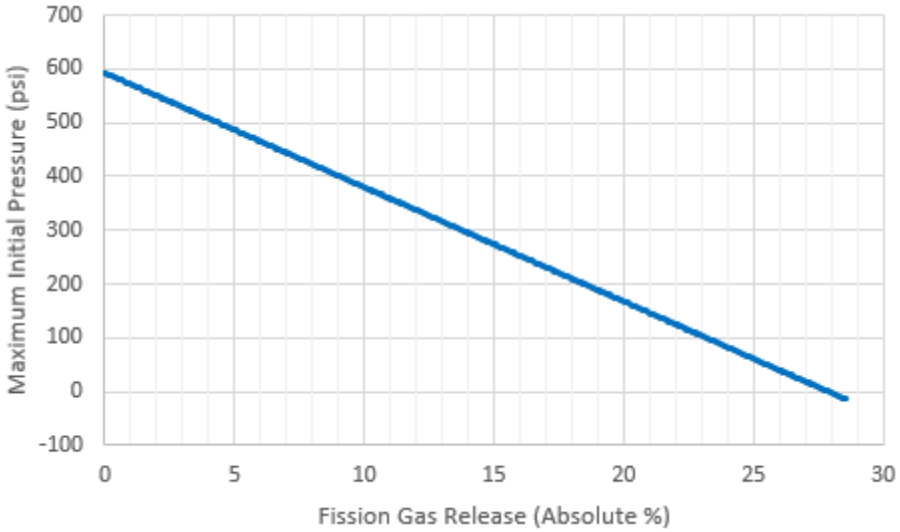

Figure 15. Maximum Initial Pressurization for the AP1000

The initial pressurization for the AP1000 fuel rods varies between 200 and 750 psi (10); the above figure therefore suggests that the methodology followed in this study confirms the design margins of the licensed AP1000 design.

Conclusions

As has already been mentioned, future work must include improved estimates of the fission gas release by uranium silicide fuel. This may take the form of either direct experimental measurements or a more thorough investigation of the physical processes involved in fission gas release and characterization of the fuel microstructure. Additionally, significant uncertainty exists with respect to the pressure limits calculated and assumed in this study. Many assumptions have been made without accounting for various physics phenomena which can impact clad integrity; more detailed analyses may therefore be needed. It may also be necessary to carry out some thermal analyses of the maximum burnup fuel rod, as this may allow some relaxation of the conservative assumptions previously discussed. Transient scenarios must be examined as well; such conditions are likely to necessitate assumptions (regarding temperatures, FGR, etc.) that are significantly more limiting than those employed in this study. The appropriate design basis and acceptable assumptions may then be determined from such considerations. Based on the results only of this scoping study, the inner fuel pellet void of the original design allowed for significant flexibility in the fuel rod design, especially with respect to the plenum length. This justified the design change of switching to the solid fuel pellet, as significant gains in the cycle length were realized with a manageable penalty to RIP alongside a significant increase in the plenum length. However, a review of the methodology employed in this study should be carried out to determine if the results presented are reasonable and sufficiently conservative, and more thorough analyses using industry-standard fuel performance codes may be used to assess the validity of these results.

References

1. Ferroni, P. *Integral Inherently Safe LWR (I^2S-LWR) project material property database*. Westinghouse Electric Company. 30 September 2013.

2. Firestone, R.B. “Thermal Neutron Induced Fission.” Lawrence Berkeley National Laboratory. 1993. Retrieved from http://ie.lbl.gov/fission.html.
3. Geelhood, K.J., W.G. Luscher, and C.E. Beyer. *FRAPCON-3.4: A computer code for the calculation of steady-state thermal-mechanical behavior of oxide fuel rods for high burnup*. Pacific Northwest National Laboratory. March 2011. Retrieved from http://frapcon.labworks.org/Code-documents/NUREG-CR-7022%20Vol1.pdf.
4. Johnson, L., C. Ferry, C. Poinssot, and P. Lovera. *Spent fuel radionuclide source-term model for assessing spent fuel performance in geological disposal. Part I: Assessment of the instant release fraction*. 2005. Retrieved from http://www.sciencedirect.com/science/article/pii/S0022311505003193#.
5. Lanning, D.D. and C.E. Beyer. *Estimated maximum cladding stresses for bounding PWR fuel rods during short term operations for dry cask storage*. Pacific Northwest National Laboratory. January 2004. Retrieved from http://pbadupws.nrc.gov/docs/ML0402/ML040290474.pdf.
6. *Nuclear fuel safety criteria technical review*. Nuclear Energy Agency. 2001. Retrieved from http://books.google.com/books?id=Fne98EZeiZUC&pg=PA25&lpg=PA25&dq=nuclear+fuel+rod+internal+pressure&source=bl&ots=8mkQ-6u5lF&sig=xpJO6vy_F6rgjrKsrK1qSVkKfoI&hl=en&sa=X&ei=5EkfU5GQIoT70wGh44GACA&ved=0CF0Q6AEwCQ#v=onepage&q=nuclear%20fuel%20rod%20internal%20pressure&f=false.
7. Salazar, D. “Updated on I^2S-LWR Nuclear Design.” I^2S-LWR 3rd team meeting, Atlanta, GA, August 4-6, 2014.
8. Todreas, N.E., and M.S. Kazimi. *Nuclear systems*. 2nd ed. Vol. 1. Boca Raton, FL: Taylor & Francis, 2012.
9. *Westinghouse AP1000 design control document rev. 19 – tier 2 chapter 4 – reactor – section 4.2 fuel system design*. Westinghouse Electric Company. 13 June 2011. Retrieved from http://pbadupws.nrc.gov/docs/ML1117/ML11171A444.pdf.
10. *Westinghouse AP1000 design control document rev. 19 – tier 2 chapter 4 – reactor – section 4.3 nuclear design*. Westinghouse Electric Company. 13 June 2011. Retrieved from http://www.nrc.gov/reactors/new-reactors/design-cert/ap1000/dcd/Tier%202/Chapter%204/4-3_r14.pdf.
11. Whitmarsh, C.L. *Review of Zircaloy-2 and Zircaloy-4 properties relevant to N.S. Savannah reactor design*. Oak Ridge National Laboratory. n.d. Retrieved from http://web.ornl.gov/info/reports/1962/3445605716311.pdf.

APPENDIX E. TABULATED DEPLETION DATA

Presented in this section is the tabulated version of the depletion data presented in 4.2.1.1.

Burnup (GWd/MT)	k: Uncontrolled	k: 8 Gd Pins, 4 w/o	k: 8 Gd Pins, 8 w/o	k: 16 Gd Pins, 4 w/o	k: 16 Gd Pins, 8 w/o	k: 80 IFBA Pins	k:160 IFBA Pins
0.000	1.3320	1.2796	1.2710	1.2303	1.2136	1.2297	1.1392
0.109	1.2932	1.2440	1.2356	1.1978	1.1814	1.1981	1.1136
0.328	1.2876	1.2394	1.2308	1.1942	1.1774	1.1957	1.1137
0.546	1.2834	1.2362	1.2274	1.1919	1.1747	1.1944	1.1149
0.765	1.2801	1.2338	1.2248	1.1904	1.1728	1.1937	1.1165
1.07	1.2762	1.2311	1.2218	1.1888	1.1707	1.1933	1.1191
1.48	1.2717	1.2282	1.2185	1.1873	1.1685	1.1932	1.1225
1.88	1.2674	1.2254	1.2153	1.1861	1.1664	1.1929	1.1257
2.28	1.2632	1.2227	1.2121	1.1848	1.1643	1.1925	1.1286
2.88	1.2566	1.2183	1.2072	1.1825	1.1609	1.1914	1.1322
3.68	1.2478	1.2125	1.2005	1.1794	1.1563	1.1893	1.1358
4.48	1.2391	1.2067	1.1939	1.1763	1.1517	1.1865	1.1384
5.28	1.2303	1.2009	1.1873	1.1733	1.1471	1.1833	1.1399
6.44	1.2180	1.1926	1.1779	1.1686	1.1404	1.1780	1.1408
7.96	1.2026	1.1823	1.1662	1.1628	1.1322	1.1703	1.1401
9.48	1.1879	1.1726	1.1552	1.1577	1.1246	1.1619	1.1376
11.0	1.1738	1.1633	1.1448	1.1526	1.1176	1.1531	1.1336
12.5	1.1604	1.1537	1.1350	1.1466	1.1110	1.1440	1.1284
14.0	1.1473	1.1431	1.1253	1.1385	1.1045	1.1345	1.1221
15.5	1.1350	1.1320	1.1164	1.1288	1.0986	1.1249	1.1152
17.1	1.1231	1.1206	1.1079	1.1180	1.0930	1.1153	1.1078
18.6	1.1116	1.1093	1.0997	1.1070	1.0877	1.1057	1.0999
20.1	1.1005	1.0982	1.0916	1.0960	1.0824	1.0960	1.0917
21.6	1.0897	1.0874	1.0833	1.0852	1.0765	1.0864	1.0832
23.1	1.0791	1.0769	1.0743	1.0747	1.0693	1.0768	1.0745
25.2	1.0653	1.0632	1.0614	1.0610	1.0575	1.0640	1.0627
27.8	1.0486	1.0464	1.0450	1.0443	1.0414	1.0481	1.0476
30.3	1.0324	1.0303	1.0288	1.0282	1.0254	1.0325	1.0326
32.9	1.0167	1.0147	1.0132	1.0126	1.0098	1.0173	1.0178
35.5	1.0016	0.9996	0.9982	0.9976	0.9948	1.0024	1.0032
38.1	0.9870	0.9850	0.9836	0.9830	0.9803	0.9880	0.9890
40.7	0.9729	0.9710	0.9696	0.9690	0.9663	0.9740	0.9751
43.2	0.9593	0.9574	0.9560	0.9555	0.9528	0.9605	0.9616
45.8	0.9462	0.9443	0.9430	0.9424	0.9398	0.9474	0.9486
48.4	0.9336	0.9317	0.9304	0.9298	0.9272	0.9348	0.9360
51.0	0.9214	0.9196	0.9183	0.9177	0.9152	0.9226	0.9238
53.6	0.9098	0.9080	0.9067	0.9062	0.9037	0.9110	0.9122
56.1	0.8987	0.8969	0.8956	0.8951	0.8927	0.8999	0.9011
58.7	0.8880	0.8863	0.8851	0.8846	0.8821	0.8892	0.8904

REFERENCES

1. Ade, B.J., 2012. SCALE/TRITON Primer: A Primer for Light Water Reactor Lattice Physics Calculations. Oak Ridge National Laboratory. Retrieved from http://pbadupws.nrc.gov/docs/ML1233/ML12338A215.pdf.
2. Castillo, A. et al., 2014. Comparison of heuristic optimization techniques for the enrichment and gadolinia distribution in BWR fuel lattices and decision analysis. Annals of Nuclear Energy 63, 556-564. Retrieved from http://www.sciencedirect.com/science/article/pii/S0306454913004684.
3. Control Assembly Materials for Water Reactors: Experience, Performance and Perspectives. IAEA-TECDOC-1132. Retrieved from http://www-pub.iaea.org/MTCD/publications/PDF/te_1132_prn.pdf.
4. Espinosa-Paredes, G. and J.R. Guzman, 2011. Reactor physics analysis for the design of nuclear fuel lattices with burnable poisons. Nuclear Engineering and Design 241 (12), 5039-5054. Retrieved from http://www.sciencedirect.com/science/article/pii/S0029549311008193.
5. Ferroni, P., 2013. Integral Inherently Safe LWR (I^2S-LWR) Project Material Property Database. Westinghouse Electric Company.
6. Ferroni, P. et al., 2014. Preliminary thermal-hydraulic feasibility evaluation of the Integral Inherently Safe LWR (I^2S-LWR) high power density core. In: Proceedings of ICAPP 2014, Charlotte, NC, April 6-9.
7. General Design Criteria for Nuclear Power Plants. 10 CFR 50 Appendix A. Nuclear Regulatory Commission. Retrieved from http://www.nrc.gov/reading-rm/doc-collections/cfr/part050/part050-appa.html.

8. Group of authors, 2015. Integral Inherently Safe Light Water Reactor (I^2S-LWR) FY2015_Q2 Quarterly Progress Report to DOE.
9. Haibach, B.V. and M.A. Feltus, 1997. A study on the optimization of integral fuel burnable absorbers using deterministic methods. Annals of Nuclear Energy 24 (11), 835-846. Retrieved from http://www.sciencedirect.com/science/article/pii/S0306454996000552#.
10. Haibach, B.V. and M.A. Feltus, 1997. A study on the optimization of integral fuel burnable absorbers using the genetic algorithm based CIGARO fuel management system. Annals of Nuclear Energy 24 (6), 439-448. Retrieved from http://www.sciencedirect.com/science/article/pii/S0306454996000606.
11. Kalcheva, S. and E. Koonen, 2007. Optimized Control Rods of the BR2 Reactor. Belgian Nuclear Research Centre. Retrieved from http://publications.sckcen.be/dspace/bitstream/10038/814/1/cr_report.pdf.
12. Lawrence Livermore National Laboratory, 2011. ENDF/B-VII.1 Incident-Neutron Data. Retrieved from https://t2.lanl.gov/nis/data/endf/endfvii.1-n.html.
13. Memmot, M.J. et al., 2014. Integral Inherently Safe Light Water Reactor (I^2S-LWR) concept: Integral vessel layout. In: Proceedings of ICAPP 2014, Charlotte, NC, April 6-9.
14. Michalewicz, Z. and D.B. Fogel, 2004. How to Solve It: Modern Heuristics (2^{nd} edition). Springer, Berlin.
15. National Institute of Standards and Technology, 2011. Isobaric Properties of Water. Retrieved from http://webbook.nist.gov/chemistry/fluid/.

16. Petrovic, B., 2014. Integral Inherently Safe Light Water Reactor (I^2S-LWR) concept: Extending SMR safety features to large power output. In: Proceedings of ICAPP 2014, Charlotte, NC, April 6-9.
17. Petrovic, B., 2014. Integral Inherently Safe Light Water Reactor (I^2S-LWR) Trade-Off Studies and Down-Selections. Georgia Institute of Technology.
18. Petrovic, B., 2014. The Integral Inherently Safe Light Water Reactor. Georgia Institute of Technology.
19. Pritchett, J.E. and D.E. Mueller, 1987. Operational Experience with ZrB_2 Integral Fuel Burnable Absorbers. Westinghouse Electric Company. Retrieved from http://web.ornl.gov/sci/nsed/rnsd/staff/Publications/MuellerPubs/OpExpwZrB2IFBAs_1987.pdf.
20. Risovany, V.D. et al., 2000. Dysprosium titanate as an absorber material for control rods. Journal of Nuclear Materials 281 (1), 84-89. Retrieved from http://www.sciencedirect.com/science/article/pii/S002231150000129X.
21. Salazar, D. et al., I^2S-LWR Equilibrium cycle core analyses. In: Proceedings of PHYSOR 2014, Kyoto, Japan, September 28 – October 3.
22. Sanders, C.E. and J.C. Wagner, 2002. Study of the Effect of Integral Burnable Absorbers for PWR Burnup Credit. Oak Ridge National Laboratory. Retrieved from http://web.ornl.gov/~webworks/cppr/y2002/rpt/108945.pdf.
23. Secker, J.R. and J.A. Brown, 2010. Westinghouse PWR burnable absorber evolution and usage. In: Proceedings of the 2010 ANS Winter Meeting and Nuclear Technology Expo, Las Vegas, NV, November 7-11. Retrieved from http://rpd.ans.org/presentations/2010_W/Burnable_Poisons/1-Secker-PWR-Burnable-Absorber-Evolution.pdf.

24. Simmons, R.L. et al., 1988. Integral fuel burnable absorbers with ZrB_2 in pressurized water reactors. Nuclear Technology 80, 343-348. Retrieved from http://web.ornl.gov/sci/nsed/rnsd/staff/Publications/MuellerPubs/IFBAswZrB2inPWRs-NucTech_1988.pdf.

25. Turinsky, P.J. et al., 2005. Evolution of nuclear fuel management and reactor operational aid tools. Nuclear Engineering and Technology 37 (1), 79-90. Retrieved from http://www.kns.org/jknsfile/v37/JK0370079.pdf.

26. Yilmaz, S. et al., 2006. Application of genetic algorithms to optimize burnable poison placement in pressurized water reactors. Annals of Nuclear Energy 33 (5), 446-456. Retrieved from http://www.sciencedirect.com/science/article/pii/S030645490500277X#.

27. Zavaljevski, N., 1990. A model for fuel shuffling and burnable absorbers optimization in low leakage PWRs. Annals of Nuclear Energy 17 (4), 217-220. Retrieved from http://www.sciencedirect.com/science/article/pii/030645499090055I#.